Ecology and Development Series No. 31, 2005

Editor-in-Chief:
Paul L.G.Vlek

Editors:
Manfred Denich
Christopher Martius
Charles Rodgers
Nick van de Giesen

Nathaniel Kwamina Howard

Multiscale analysis of landscape data sets from northern Ghana: Wavelets and pattern metrics

Cuvillier Verlag Göttingen

To Jane, Mawuli and Selasie Howard for their love and support

ABSTRACT

Landscape pattern is spatially correlated and scale-dependent. Thus, multiscale analysis is imperative for understanding the structure, function and dynamics of landscape. In this study, we employed two complementary, yet parallel approaches (the direct and indirect approaches) to multiscale analysis of landscape maps from northern Ghana. First, moving window analysis was conducted to investigate the data sets for heteroscedasticity and proportional effect. In the direct approach, the Maximal Overlap Discrete Wavelet Transform was used for a wavelet-based analysis of variance of the Normalized Difference Vegetation Index (NDVI) and the Digital Elevation Model (DEM). Also, an orthogonal and compactly supported wavelet was applied through seven levels of dyadic decompositions of each data set into large- and small scale features in the horizontal, vertical and diagonal directions. The small-scale features were analyzed with moments and scale plots to investigate statistical self-similarity in the three directions. In the indirect approach, 18 commonly used landscape metrics were used to investigate (1) the effects of changing grain size and (2) the effects of changing extent on the metrics. In case (1), the grain size of each original data set was systematically changed using the majority, mean and median rules through 18 separate aggregation levels; while the extent was kept constant. The values of the 18 metrics were then computed for each resampled data set. In case (2), we systematically increased the extent of the maps (starting from each of the four corners) from 56 km^2 to 5,633 km^2; while keeping the grain size constant.

The results of moving window analysis showed that the local means of the NDVI data sets in some regions were more variable than in others, while their corresponding standard deviations remained fairly constant over the study area. Both local means and standard deviations of DEM remained fairly constant. Thus, estimates from any particular sector of the study area will be as good as estimates elsewhere. No proportional effect was observed between local means and corresponding standard deviations for all three data set. The change in the wavelet variance of the NDVI data sets was not a simple function of resolution. For DEM, however, the wavelet variance varied linearly with its resolution. The dominant scale for the NDVI data sets was found to be 240 meters; however, DEM did not exhibit a dominant scale. The small-scale features of the NDVI data sets were shown to be self-similar over the 120 meter to 3.84 kilometer scales in all the three directions; while those of DEM were self-similar over the 3.6 kilometer to 11.52 kilometer scales in all the three directions. The scaling exponents were different in the three directions for all the data set, indicating the anisotropic nature of the landscapes. Again the scaling exponents were all negative, indicating increasing variability with decreasing scales. The large magnitudes of the slopes indicated long range behavior and may imply a methodology for statistically assimilating remotely sensed data set into large-scale meso and global climate models.

Changing grain size and extent both had significant effects on landscape metrics, and the effects in each case could be grouped into three main types: Type I – simple scaling relationships; Type II – unpredictable behavior and Type III – fixed responses. In general, the effects of changing grain size were more predictable than those of changing map sizes. It was also revealed that the direction of analysis in the case of changing extent had significant effects on landscape pattern analysis, as did the method of aggregation in the case of changing grain size. A comparison of the effects of changing grain size and extent on landscape metrics showed that our results are consistent with the statistical correlations that exist among the metrics. The findings from this study corroborate the general notion: there is no single "correct" or "optimal" scale for characterizing and comparing landscape patterns. Therefore, landscape metric scalograms should be used for characterizing, comparing and monitoring landscape patterns instead of using single value.

Multiskalische Analyse von Landschaftsdaten aus dem Norden Ghanas: Wavelets und Strukturmetrik

KURZFASSUNG

Landschaftsmuster sind räumlich korreliert und maßstabsabhängig. Daher ist die multiskalige Analyse Voraussetzung für das Verständnis von Struktur, Funktionen und Dynamik einer Landschaft. In der vorliegenden Studie wurden zwei komplementäre, jedoch parallele Ansätze zur multiskaligen Analyse von Karten der Landschaft im Norden Ghanas eingesetzt: der direkte bzw. indirekte Ansatz. Zunächst wurde eine „moving window"–Analyse zur Untersuchung der Daten hinsichtlich Heteroskedastizität und proportionaler Wirkung durchgeführt. Beim direkten Ansatz wurde die *Maximal Overlap Discrete Wavelet Transform* für eine auf Wavelet basierende Varianzanalyse des *Normalized Difference Vegetation Index* (NDVI) und des digitalen Höhenmodels (DEM) angewendet. Außerdem wurde eine orthogonale bzw. *compactly supported wavelet* durch sieben Ebenen von dyadischen Zerlegungen für jeden Datensatz in groß- bzw. kleinskalierten Eigenschaften in horizontale, vertikale und diagonale Richtungen angewendet. Die kleinskalierten Eigenschaften wurden mit Momenten und Skalenplots analysiert, um statistische Selbstähnlichkeit in den drei Richtungen zu untersuchen. Beim indirekten Ansatz wurden 18 üblicherweise benutzte Landschaftsmetriken eingesetzt, um (1) die Wirkung von sich verändernde Korngrößen bzw. (2) die Wirkungen von sich verändernden Untersuchungsbereichen auf die Maße zu untersuchen. Im Falle (1) wurde die Korngröße von jedem originären Datensatz systematisch anhand der Regeln für Modal- und Mittelwerte bzw. den Median durch 18 einzelne Aggregationsebenen verändert, wobei die Abgrenzung konstant gehalten wurde. Die Werte der 18 Metriken wurden dann für jeden einzelnen Datensatz berechnet. Im Falle (2) wurden die Untersuchungsbereiche der Karten systematisch vergrößert (beginnend an jeder der vier Ecken der Karten) von 56 km^2 bis 5,633 km^2 unter Beibehaltung einer konstanten Korngröße.

Die Ergebnisse der „moving window"-Analyse zeigen, dass die örtlichen Mittelwerte der NDVI-Daten in manchen Regionen variabler waren als in anderen, während die entsprechenden Standardabweichungen über das Untersuchungsgebiet ziemlich konstant blieben. Sowohl die örtlichen Mittelwerte als auch die Standardabweichungen des DEM blieben ziemlich konstant. Daher werden Werte aus einem zufällig gewählten Abschnitt des Untersuchungsgebiets genauso gut sein wie die aus einem anderen. Eine proportionale Wirkung zwischen den örtlichen Mittelwerten und entsprechenden Standardabweichungen wurde für keine der drei Datengruppen beobachtet. Die Veränderung in der Wavelet-Varianz der NDVI-Daten beruhte nicht auf einer einfachen Funktion der Auflösung. Für das DEM jedoch variierte die Wavelet-Varianz linear mit der Auflösung. Der vorherrschende Maßstab für die NDVI-Daten war 240 m; das DEM zeigte jedoch keinen vorherrschenden Maßstab. Die kleinskalierten Eigenschaften der NDVI-Daten waren selbstähnlich über die 120-m bis 3.84-km Maßstäbe in allen drei Richtungen, während dies beim DEM für die Maßstäbe 3.6 km bis 11.52 km zutraf. Die Skalenexponenten waren in den drei Richtungen für alle Daten unterschiedlich; dies deutet auf die anisotropische Natur der Landschaften hin. Außerdem waren die Skalenexponenten alle negativ; dies deutet auf eine

zunehmende Variabilität mit abnehmenden Skalen hin. Die hohen absoluten Werte der Steigung deuten darauf hin, dass die statistische Selbstähnlichkeit für einen großen Bereich gültig ist, und könnten eine Methode für die statistische Assimilierung von Fernerkundungsdaten in großskalierten meso- bzw. globalen Klimamodellen implizieren. Unterschiedliche Korngrößen bzw. Untersuchungsbereiche zeigten eine signifikante Wirkung auf Landschaftsmetriken. Die Wirkungen konnten in drei Hauptgruppen eingeteilt werden: Typ I - einfache Skalenverhältnisse, Typ II - unvorhersehbares Verhalten und Typ III - feste Reaktionen. Im Allgemeinen waren die Wirkungen der unterschiedlichen Korngrößen besser vorhersagbar als die der unterschiedlichen Kartengrößen. Es zeigte sich ebenfalls, dass die Richtung der Analyse bei den unterschiedlichen Untersuchungsbereichen signifikante Wirkungen auf die Analyse der Landschaftsmuster hatte; dies traf auch bei der Aggregationsmethode bei unterschiedlichen Korngrößen zu. Ein Vergleich der Wirkungen der unterschiedlichen Korngrößen und Untersuchungsbereiche auf Landschaftsmetriken zeigt, dass die Ergebnisse der vorliegenden Studie mit den statistischen Korrelationen, die innerhalb der Metriken existieren, übereinstimmen. Die Ergebnisse untermauern die allgemeine Auffassung: es gibt keinen „korrekten“ bzw. „optimalen“ Maßstab für die Charakterisierung oder für den Vergleich von Landschaftsmustern. Skalogramme von Landschaftsmetriken sollten daher an Stelle von einzelnen Werten für Charakterisierung, Vergleich und Beobachtung von Landschaftsmustern eingesetzt werden.

TABLE OF CONTENTS

LIST OF ACRONYMS AND ABBREVIATIONS

GIS	Geographical information systems
RS	Remote sensing
PET	Potential evapotranspiration
DWT	Discrete wavelet transform
IDWT	Inverse discrete wavelet transform
TA	Total area
NP	Number of patches
PD	Patch density
TE	Total edge
ED	Edge density
LPI	Largest patch index
MPA	Mean patch area
PASD	Patch area standard deviation
PACV	Patch area coefficient of variation
LSI	Landscape shape index
MSI	Mean shape index
AWMSI	Area-weighted mean shape index
MFDI	Mean fractal dimension index
AWMFDI	Area-weighted mean fractal dimension index
CONTAG	Contagion
PR	Patch richness
PRD	Patch richness density
SHDI	Shannon's diversity index
LULC	Land use and land cover
NDVI	Normalized difference vegetation index
DEM	Digital elevation model
MODWT	Maximal overlap discrete wavelet transform
EDOF	Equivalent degrees of freedom
"d6"	Daubechies wavelet with a width of 6
SW	South-west
SE	South-east
NW	North-west
NE	North-east

1 INTRODUCTION

1.1 Background

Spatial heterogeneity is ever-present at all scales and its formation and interactions with ecological processes are central to landscape ecology (Wu *et al*., 2000; Wu, 2004; Shen *et al*., 2004; Wu *et al*., 2002). In order to understand how landscapes affect and are affected by ecological processes, one must be able to quantify spatial heterogeneity and its scale dependence (i.e. how patterns change with scale). The scale dependence of spatial heterogeneity has long been recognized in both ecology and geography. There are two different but related connotations of spatial heterogeneity being scale dependent. The first implies that spatial heterogeneity exhibits various patterns at different scales, or patterns have distinctive "operational" scales (Lam and Quattrochi, 1992) at which they can be best characterized. This connotation is consistent with the concept of characteristic scale and hierarchy that have appeared in ecological literature since the 1980s (Allen and Starr, 1982; Allen *et al*., 1984; O'Neil *et al*., 1986; Urban *et al*., 1987; Wu and Loucks, 1995; Wu, 1999). The second connotation means the dependence of observed spatial heterogeneity on the scale of observation and analysis – often discussed in terms of scale effects on image classification and spatial analysis (Wu, 2004).

Recent studies have shown that an important and universal characteristic of spatial heterogeneity is its scale multiplicity in space (e.g., Miller 1978, Kolasa and Pickett, 1991; Wu and Loucks, 1995; Cullinan *et al*., 1997; Werner, 1999). The scale multiplicity of landscapes has important ecological implications: (1) landscapes may be hierarchically structured; (2) landscapes exhibit distinctive spatial patterns at different scales which may be caused by different processes, and thus the scale of observation significantly influences what is to be observed; (3) understanding landscape functioning requires a multiple-scale characterization of spatial pattern and processes, and single-scale descriptions are highly likely to be partial and misleading; and (4) models developed at one particular scale are not likely to apply at other scales, thus we need to either link models developed at different scales, or develop multiple-scaled or hierarchically structured models.

The process of relating the different observations across scales (or scaling) is a fundamental challenge in both theory and practice in all earth sciences. In particular, scaling is essential for addressing a wide range of ecological and environmental issues concerning biodiversity loss and global change in part because most ecological studies to date have been carried out at very local scales in both time and space (van Gardingen *et al*., 1997; Wu, 1999). Scaling is often a difficult task due primarily to landscape heterogeneity and nonlinearity, and understanding the scale multiplicity in pattern and process is a key to the success of scaling (Wu, 1999). See Chapter 2 for comprehensive discussion of scaling. This study employs two approaches to multiscale analysis of landscape pattern: the direct and indirect approaches. Specifically, we employ wavelets and landscape metrics as methods for detecting and describing multiple-scale or hierarchical structures in landscapes from northern Ghana.

1.2 Motivation

In order to quantify the multiple-scale characteristics of landscapes, a multiscale or hierarchical method must be employed. By definition, a hierarchical method is multiple-scale. However, a multiple-scale method may not necessarily be hierarchical in the sense of a nested hierarchy (Wu 1999). There are two general approaches to multiscale analyses: (1) the direct approach which involves inherent multiple-scale methods, and (2) the indirect approach which involves repeated use of single-scale methods at different scales. Commonly used multiscale methods in landscape ecology include semivariance analysis (Robertson and Gross, 1994; Burrough, 1995), spectral analysis (Platt and Denman, 1975; Ripley, 1978), fractal analysis (Krummel *et al*., 1987; Milne, 1991; Nikora *et al*., 1999), lacunarity analysis (Plotnick *et al*., 1993; Henebry and Kux, 1995), blocking quadrat variance analysis (Greig-Smith, 1983; Dale, 1999), scale variance analysis (Townshend and Justice, 1988, 1990; Wu *et al*., 2000) and wavelet analysis (Bradshaw and Spies, 1992; Saunders *et al*., 1998; Brunsell and Gillies, 2003; Hu *et al*., 1998; Kumar and Foufoula-Georgiou, 1993a,b). The mathematical formulation or processes of each of these methods involve multiple-scale components, and are therefore either hierarchical or multiscaled. The indirect approach to multiscale analyses, on the other hand, involves methods that are designed for single-scale analysis. Appropriate methods are used to estimate a wide variety of landscape

metrics (e.g., diversity, contagion, edge density, relative richness) as well as statistical measures (e.g., mean, variance, variance-mean ratio, and coefficient of variation). The scale multiplicity in the indirect approach is realized when a landscape data set is resampled at different scales according to grain size or extent, and then the landscape metrics or statistical measures computed for the resampled data at the different scales. A common way to resample data is to systematically aggregate the original fine resolution data set to produce a hierarchically nested data set.

There are two related, yet distinct goals for conducting a multiscale analysis of an ecological landscape. The first goal involves characterizing the multiple-scale structure of a landscape, while the second involves detecting or identifying "scale breaks" or hierarchical levels in a landscape. In both cases, the researcher obtains a better understanding of how spatial heterogeneity changes with scale. However, a description of landscape pattern at different scales may be necessary or desirable even if scale breaks do not exist or the landscape is not hierarchical. On the other hand, scale breaks often lead to the identification of characteristic scales of patterns which may frequently facilitate understanding underlying processes. Thus, one may view the two goals as complementing each other. This is one of the researcher's motivations for employing both approaches to multiscale analysis of landscape data sets.

Recent research (e.g. Bradshaw and Spies, 1992; Kumar and Foufoula-Georgiou, 1993a, 1993b; Hu *et al*., 1998; Saunders *et al*., 1998; Brunsell and Gillies, 2003) suggests that wavelet transforms are powerful tools for analyzing the scaling behavior of remotely sensed and other geophysical data sets. Like Fourier transforms, wavelet transforms are series of expansions of a function using orthonormal basis. The rational and motivation for choosing wavelets over other inherent multiscale methods lies in the fact that wavelet transforms possess the following remarkable and unique properties (among others) that make them most attractive for this research. Wavelet transforms are based on multi-resolution analysis. In other words, wavelet multiresolution decomposition allows the separation of functions into multiresolution components: large-scale and small-scale components. This property allows for the separate study of both large-scale behavior and small-scale behavior. Wavelets are localized in both time/space and scale/frequency domains. They have compact support (they are zero everywhere outside the domain of finite size) which enables their

localization in time or space. Also, the wavelet basis are dilates and translates of a "mother wavelet" which enable their localization in frequency or scale such that the size of the support is proportional to the "size of the feature" it represents. There is small support for high-frequency features and large support for low-frequency features. These properties allow for zooming into the irregularities of a function and characterize them locally. Furthermore, fluctuations at different scales can be obtained due to the multiscale transform properties of wavelets. Another property of wavelets which is useful for this research is that, two-dimensional wavelet transforms enable the decomposition of a process into spatially oriented frequency components. Thus, features with dominant frequencies in different directions are extracted as separate components. This property is exploited to study the anisotropic behavior of our data.

Scale effects have been studied using landscape metrics in ecology, remote sensing, and geography in the past two decades (Meentemeyer and Box, 1987; Turner *et al*., 1989, 2001; Bian and Walsh, 1993; Moody and Woodcock, 1994; Benson and Mackenzie, 1995; Wickham and Riitters, 1995; Jelinski and Wu, 1996; O'Neill *et al*., 1996; Qi and Wu, 1996; Wu *et al*., 2002). Scale effects on spatial pattern analysis may be observed in each of the following three situations: (1) changing the size of the smallest observable measurement (grain) within the landscape data only, (2) changing the size of the study area (extent) only, and (3) changing both the grain size and extent. In the first situation, scale effects may occur as a result of the effect of changed grain size as well as the method employed to effect the change. The extent may also be changed in different ways: e.g. by carving out from the center of a map or by starting from one corner and moving in along a diagonal. Studies have shed new light on the problems of scale effects in pattern analysis as well as the multiscale nature of spatial heterogeneity. However, most studies considered only a few landscape metrics over a narrow range of scales. Also, the landscape data sets used in all of these studies emanated from Europe and North America. In this study, the researcher will consider several commonly used landscape metrics over a very wide range of scales. It is also the researcher's belief that differences in composition and configuration of landscape data sets could affect the outcome. The researcher, therefore, wishes to investigate the scaling relations exhibited by the landscape data from northern Ghana and compare the results with those from related studies.

1.3 Objectives

The main objective of this research is to employ direct and indirect approaches to multiscale analysis of landscape data from northern Ghana. In particular, we shall use the wavelet transform as a direct approach to detecting and describing the multiple-scale nature of landscape data sets from northern Ghana. In the indirect approach, several landscape metrics will be computed over a wide range of grain sizes (with different aggregation methods) and spatial extents (with different direction of analysis). Scaling relations would then be constructed for the landscape metrics whose change with grain size or extent is consistent among different landscape data sets.

The specific objectives include:

1. To investigate the land use and land cover maps for heteroscedasticity and proportional effect.
2. To determine the dominant scales of NDVI and DEM through wavelet-based analysis of variance.
3. To employ orthogonal wavelets in detecting and describing multiple-scale patterns in landscape data sets.
4. To investigate how commonly used landscape metrics change over broad ranges of grain sizes or spatial extents, and assess how these changes differ among distinctive landscapes.
5. To formulate general scaling relations for landscape metrics whose change with grain size or extent are consistent across landscapes.
6. To compare the effects of changing grain size and extent in respect of statistical correlations that exists among landscape metrics.

1.4 Organization of thesis

The entire thesis is partitioned into five broad chapters under the headings: 1. Introduction, 2. Literature Review, 3. Datasets and Methods, 4. Results and Discussion and 5. Summary and Conclusion.

The introduction chapter gives a brief background to the study – discusses what the problems are and the attempts that have been made at solving them. It also mentions the researcher's motivation for outlining his research objectives and describes how he hopes to achieve them. Chapter 2 is a detailed review of the term scale and

associated issues, the theory of wavelets, and a description of landscape pattern metrics. The chapter discusses the sources of ambiguity of the term scale and explains its meaning as used in this thesis. Relevant scaling issues are also mentioned and discussed. The chapter also describes the theories behind wavelet analysis, and highlights the strengths and weaknesses of other direct multiscaling methods. Finally, the chapter describes the 18 metrics selected for this study.

The source of the landscape data sets used in the research, the data sets, the problems associated with the data sets and how the problems are resolved are discussed in chapter 3. The chapter also discusses the theories behind the methods used in the various analyses and gives detailed descriptions of the important steps involved. Chapter 4 is on results and discussion. In this chapter, summaries of results of all the analyses conducted in this study are presented in the form of tables and/or graphs. The major findings in the study are then discussed in relation to result from similar and related research. Chapter 5 is the final chapter of this thesis. It summarizes all the major findings and discusses them concisely vis-à-vis the set objectives of the research. Conclusions that may be derived from the findings of the study are outlined. Recommendations are also made on issues that require further study.

2 LITERATURE REVIEW

2.1 Scale and scaling effects

With modern advances in spatial information technologies which include geographical information systems (GIS) and remote sensing (RS), enormous amounts of data set on the earth's surface exist in local, regional and global scales. The existence of abundant RS and related GIS data at various scales offers new potential and challenges in the development and implementation of techniques for dealing explicitly with scale (Goodchild and Quattrochi, 1997). Literature shows that data measurements and models of most phenomena are scale-dependent. Thus the evaluation of errors related to scale and the validation of models require particular attention (Arbia, 1989; Ehleringer and Field, 1993; Foody and Curran, 1994). In other words, the issue of scale plays an important role in RS and GIS research (Cao and Lam, 1997). In this section, we shall explain the term scale and outline the issues associated with scaling that may be relevant to this study. We shall also outline and briefly discuss some of the well-known methods for scaling. We begin with an explanation of our adopted meaning of scale.

2.1.1 The meaning of scale

The term scale is used by several different specialists including remote sensing specialists, ecologists, cartographers, mathematicians, geographers, spatial and geostatisticians. Its various and often conflicting meanings depend on the context and the disciplinary perspective of the user. The different definitions of scale are often used interchangeably and it is not always clear which one is being used. To avoid ambiguity in its usage, it is prudent and helpful to clarify the meaning of scale and other related terms in any scale-oriented research work like ours.

One definition which can be applied to all forms of scale namely spatial, temporal, quantitative and analytical is that "scale denotes the resolution within the range of a measured quantity" (Schneider, 1994). This is an effective definition because it encompasses two interacting and very important facets of scale: *resolution* and *range*. Resolution (also known as grain) refers to the finest distinction that can be made in an observation set. In raster lattice data, the resolution is represented by the cell size; in

field sample data, it is represented by the quadrat size; in imagery, by the pixel size and in vector GIS data, by the minimum mapping unit. On the other hand range, which is also known as extent, refers to the scope or domain of the data set. Typically, it is defined as the size of the study area (Allen and Hoekstra, 1991). It is worth mentioning that as a result of logistical constraints in measurements, resolution and extent are negatively correlated. Thus, in sampling we sacrifice fine resolution for large extent or we narrow the extent of our data set when we require fine resolution. Nature itself, of course, has fine resolution and large extent. Another important point to note is that more detailed information is obtained at finer resolutions.

Another potential source of confusion in terminology associated with scale is the various meanings of the adjectives *small* and *large*. To remote sensing specialists, small and large scales refer to the relative relationship between the dimensions of a map or an image and their correspondence on the earth's surface. To them, small scale infers relatively larger extent (and therefore less detail) than large scale. We shall, however, adopt the usages by ecologists and other scientists which have reversed meanings. That is, a small scale study relates to an analysis performed in relatively great spatial detail (usually over a small area). Similarly, a large scale analysis relates to a large area (usually with less spatial detail). Note also that by our adopted definition, *high* (or *fine*) resolution is associated with relatively small scales, while *low* (or coarse) resolution is related to analysis performed at large scales.

2.1.2 Scaling issues

Scaling is different from scale. Scaling focuses on what happens to the characteristics of an object when its scale (size/dimension) is changed. To explain the scaling issue, consider a side of length 1 meter and use it to build up a square and a cube. Then the square will have a surface area of 1 square meter and cube will have a volume of 1 cubic meter. When we double the length of the side, the square will have a surface area of 4 square meters and the cube will have a volume of 8 cubic meters. This clearly shows that when the scale of the side changes by a factor of 2, the surface area changes by a factor of 4 and the volume by a factor of 8. It portrays a nonlinear scaling among the length of the side, the surface area of the square and the volume of the cube. Research has shown that reducing the resolution of a raster land cover map (going to

larger cells) can increase the dominance of the contiguous classes, but decrease the amount of small and scattered classes in the representation (Turner *et al*., 1989). Faced with scaling issue in hydrology, for example, we have to find out how topographic attributes change if we change the spatial resolution of a topographic map, or how the drainage area changes if we change the length of a stream (Dodds and Rothman, 2000). In a broad context, scaling requires the identification of process nonlinearities with change in scale, the range of scales for which linearity may hold, and the properties that may be coherent between scales (Wessman, 1992). While it is inaccurate to state that a process is restricted to any particular scale, it is possible to point to specific time and space scales at which one process prevails over another (Schneider, 1994).

There are two forms of scaling: *upscaling* and *downscaling*. Upscaling refers to any resampling techniques that are designed to transform an image data set collected at a high spatial resolution to a lower spatial resolution representation of the same image. Downscaling is the direct opposite and refers to any techniques that transform image data sets from a lower spatial resolution to a higher spatial representation of the same image (Strahler *et al.*, 1986). Figure 2.1 illustrates the concepts of upscaling and downscaling.

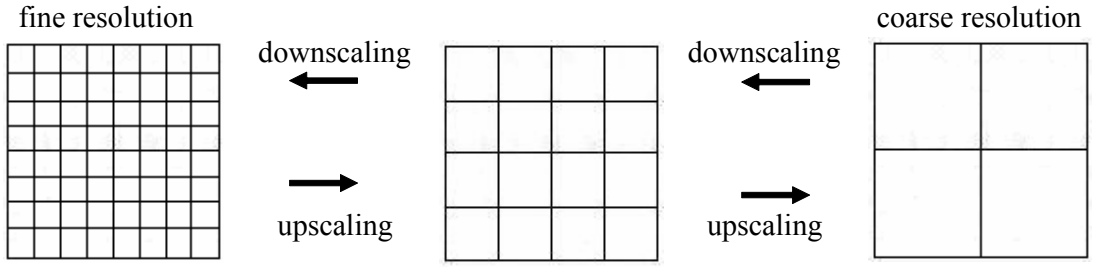

Figure 2.1 An illustration of upscaling and downscaling

From this point on, we shall dwell on upscaling issues which are the main focus of this study. Ideally, an upscaling technique is intended to reduce the size of a data set of a high resolution image while maintaining its inherent information contents at a lower spatial resolution. Unfortunately, this goal is somewhat contradictory as upscaling involves generalization techniques which tend to produce more homogeneous, variance reduced, thus inherently lower information content data sets (Wieczorek, 1992).

Why scaling?

It is commonly acknowledged that the only way to capture scale dependent spatial processes is to make correct observations at the scales at which the processes and physical laws are taking place (Wood and Lakshmi, 1993; Harvey, 1997). However, for the majority of cases, available databases are limited to much smaller spatial scales than those at which the actual processes occur. Despite rapid advances in data extraction methods, the acquisition of spatial data sets at large scales and in great details still remains the most expensive and difficult part of any GIS (Burrough and McDonnell, 1998). Upscaling has become a topical issue in environmental science in recent years because

1. it has become evident that most environmental and resource management problems can only be dealt with effectively at broad scales;
2. ecologists are now acutely aware that in order to unravel how nature works, they must have an understanding of broad-scale patterns and processes; and
3. transfer of information between scales is indispensable. There is the need to integrate data from various sources and at different scales for problem solving.

Consequences of scaling

The effects of scale on the analysis of spatial pattern may occur in each of the following three situations: (1) changing the size of the grain (or resolution) only, (2) changing the extent only, and (3) changing both grain and extent. In general, much more research has been done into the effects of changing the size of the grain than those of changing the extent. A quantitative understanding of these two kinds of scale effects across different systems and methods is still lacking. Scale effects do not necessarily have to be considered as problems because they can be used for understanding the multiple-scale characteristics of landscapes (Jelinski and Wu, 1996; Wu *et al*., 2000 & 2002). In principle, the relevant pattern is revealed only when the scale of analysis approaches the operational scale of the phenomenon under study (Allen *et al*., 1984; Wu and Loucks, 1995; Wu, 1999). In practice, however, not all scale breaks revealed in multiscale analysis by resampling data correspond to actual operational scales or hierarchical levels due to inaccuracies caused by the methods of data aggregation and analysis (Wu *et al*., 2000; Hay *et al*., 2001).

As one increases the scale of a system, fine scale processes may average away and become constants. For example, at the scale of a forest sample quadrat (say, 0.01 ha), it is reasonable to ignore larger-scale variability in soil parent material: the trees on the quadrat all see the same type of soil. Similarly, from the time-scale of years to decades, long-term trends in the climate may not be apparent even though fluctuations in the weather might have occurred. Another consequence of scaling is that as we increase the extent of our analysis, parameters that were constant now become variable. For example, if we were to extend the forest sampling to cover a large watershed or basin, soil types would indeed vary. Also, new interactions may arise as one increases the extent of inquiry. At the scale of a landscape mosaic, interactions among forest stands, such as via dispersal of plant or animal species, emerge as new phenomena for study. Statistical relationships may change. The magnitude and/or sign of correlations may change with spatial extent. At the scale of a single habitat patch, abundances of different species might be negatively correlated due to interspecific interactions; but if one considers a set of these habitat patches in a heterogeneous landscape, any species inhabiting similar habitat types will be positively correlated.

Variability relationships may change dramatically with a change in resolution or extent. Prediction may change. Important variables come and go with changes in scale. Potential evapotranspiration (PET) depends on physical parameters such as temperature, vapor pressure deficit, wind speed, and soil moisture status as well as biological parameters such as stomatal conductance and surface roughness. At very fine scales, one might include many of these factors to predict PET or actual evapotranspiration (Monteith, 1965). At sub-continental scales, PET can be predicted adequately by temperature and latitude (Thornthwaite and Mather, 1955). The nature of the process does not change with scale, but the relative contribution of explanatory variables does, and so does our ability to measure all the variables over a large extent.

2.1.3 Methods of scaling

While a host of different scaling techniques exists in the literature (Meentemeyer and Box, 1987; Turner *et al.*, 1991), only a few are readily available to probable users, and very little instructions regarding the appropriateness of these techniques to different types of data sets exist. For instance, the only available resampling algorithms for

remotely sensed data have been directly copied from classic image processing interpolation techniques and included in commercial remote sensing image analysis packages, even though they are not theoretically developed for remotely sensed imagery (Moreno and Melia, 1994). This often leads to an inappropriate use of these routines by inexperienced users. In fact, as no proven theory of spatial scaling exists (Schneider, 1994), the tendency to produce large volumes of non-representative data sets is enormous. A typical example is the upscaling which is routinely performed on Advanced Very High Resolution Radiometer data, where pixels representing an integrated spectral response from a nominal one square kilometer area extent are aggregated to 20 km^2 pixels, for weekly use as a global vegetation index (Justice *et al.*, 1989).

The commonly used aggregation techniques include the scale variance, local variance, the local Gi*(d) statistic, Fourier analysis, variogram analysis, simple and multi-fractal dimension and spectral analysis. Among these, multiscale variance, local variance and local Gi*(d) statistic methods were suggested and used much earlier in scale related research. The Fourier analysis has become a routine method in image processing (Jansen 1996), while the local Gi*(d) is a distance based measure of spatial association (Getis and Ord, 1992). The variogram method which is the core of geostatistics (Cressie, 1991) is the most popular method used to identify the effective range of spatial scales within which image variations are spatially dependent. The use of the fractal techniques in analyzing remotely sensed images has been explored by several authors (De Cola, 1994; Cao and Lam, 1997; Quattochi *et al*., 1997). We shall review some of these methods and discuss their strengths and limitations.

The scale variance method

Scale variance analysis is a hierarchical analysis that was first developed by Moellering and Tobler (1972). To conduct scale variance analysis, one needs to systematically aggregate spatial data set by increasing the size of the grain progressively so that a nested data hierarchy is formed. The size of each grain is called the *scale level* (Moellering & Tobler, 1972). The statistical model of scale variance is expressed as:

$$X_{ijk\ldots z} = \mu + \alpha_i + \beta_{ij} + \gamma_{ijk} + \ldots + \omega_{ijk\ldots z},$$

where $X_{ijk\ldots z}$ is the value of a spatial unit (e.g., a pixel) at the hierarchical level that corresponds to the finest grain size; μ is the mean of the entire data set; α_i is the effect of level α, β_{ij} is the effect of level β, γ_{ijk} is the effect of level γ and $\omega_{ijk\ldots z}$ is the effect of level ω. From the above model, the total variance of the landscape can be partitioned hierarchically at different grain sizes. For example, the scale variance components for a 3-level (α, β, γ) hierarchy will be as follows. The total variation of the system is expressed as the total sum of squares:

$$SS_{\text{Total}} = \sum_{i=1}^{I}\sum_{j=1}^{J_i}\sum_{k=1}^{K_{ij}}\left(X_{ijk} - \bar{X}_{\bullet\bullet\bullet}\right)^2,$$

where I is the number of α level units, J_i is the number of β level units in each i^{th} α level unit, and K_{ij} is the number of γ level units in each ij^{th} β level unit. The total sum of squares can then be partitioned into parts attributable to the scale levels $\alpha, \beta,$ and $\gamma,$ so that the total sum of squares will be the sum total of the sum of squares due to α and β and γ. That is $SS_{Total} = SS_{\alpha} + SS_{\beta} + SS_{\gamma}$. The formulae for the various sums of squares are

$$SS_{\alpha} = \sum_{i=1}^{I}\sum_{j=1}^{J_i}\sum_{k=1}^{K_{ij}}\left(\bar{X}_{i\bullet\bullet} - \bar{X}_{\bullet\bullet\bullet}\right)^2,$$

$$SS_{\beta} = \sum_{i=1}^{I}\sum_{j=1}^{J_i}\sum_{k=1}^{K_{ij}}\left(\bar{X}_{ij\bullet} - \bar{X}_{i\bullet\bullet}\right)^2 \text{ and}$$

$$SS_{\gamma} = \sum_{i=1}^{I}\sum_{j=1}^{J_i}\sum_{k=1}^{K_{ij}}\left(X_{ijk} - \bar{X}_{ij\bullet}\right)^2$$

Dividing the partitioned sums of squares by their respective degrees of freedom, we obtain the corresponding estimators for mean sum of squares.

Thus

$$MS_\alpha = \frac{SS_\alpha}{I-1},\quad MS_\beta = \frac{SS_\beta}{\sum_{i=1}^{I} J_i - 1} \quad \text{and} \quad MS_\gamma = \frac{SS_\gamma}{\sum_{i=1}^{I}\sum_{j=1}^{J_i}(K_{ij}-1)}.$$

For regular lattice data sets, the scale variance components are simply given by

$$SV_\alpha = \frac{MS_\alpha}{JK},\quad SV_\beta = \frac{MS_\beta}{K} \quad \text{and} \quad SV_\gamma = MS_\gamma.$$

Scale variance analysis starts with the construction of nested data hierarchies after which the above equations are used to compute the total sum of squares, partitioned sums of squares, mean sum of squares and scale variance at each scale level. Finally, the percent total sum of squares is plotted against scale levels to give the scale variance graph. From this graph, one can readily visualize the presence of peaks or the lack of them. A peak implies that high variability occurs at the corresponding scale level, which is indicative of the average size of dominant patches in the landscape. The height of the peak reflects the relative contribution of that particular scale level to the total variability of the landscape. This method is a simple and easy to understand. But as Cao and Lam (1997) pointed out, the validity of the assumption that the operational scale of geographical processes coincides with the level of maximum variability is not clear. The decomposition of variance is based on the averaging and other aggregation methods which may bring change in the performance of the model. Also, the requirement of hierarchical data limits its application in remote sensing applications.

The local variance method

The local variance method was first suggested by Woodcock and Strahler (1987) to measure the relationship between the size of the objects in the scene and spatial resolution. The local variance calculates the mean value of the standard deviation by passing an *n* pixel by *n* pixel moving window for each pixel, and then takes the mean of all local variance over the entire image as an indication of the local variability in an

image. Woodcock and Strahler (1987) used a 3×3 window and upscaled the images to coarser scales to examine the change in local variance with pixel size. Pixel sizes were plotted on the *x*-axis and local variance on the *y*-axis, depicting the change in variance with pixel size. By examining a single image, several window sizes and orientations could be utilized to establish the scale and form of autocorrelation based on changes in variance levels. Instead of changing pixel sizes, window sizes could be changed. The local variance method is similar to the covariance portion of traditional measures of autocorrelation for short distances (Cliff and Ord, 1981). A serious limitation of this method is that it is dependent on the global variance in the image, so the values of local variance for one image can only be compared with those from the same images upscaled to different resolutions.

The Gi*(d) statistic method

Since the ground scene is not random, the brightness value of one pixel carries some information about its neighborhood. In this sense, the Gi*(*d*) statistic was designed to establish if clusters of high or low data values occur around a pixel within the specified distance (Anselin, 1995). The local Gi*(*d*) could be computed for an image at progressively increasing values of *d* or by defining a set of neighbors for each pixel. Resulting values of the Gi*(*d*) statistic at varying distances of *d* may be presented in the form of a spatial correlogram, a positive peak indicates spatial clustering of high values, whereas a negative troughs indicates clusters of low pixel values. Getis and Ord (1992) have applied Gi*(*d*) in high resolution image analysis and the result showed the Gi*(*d*) map had a good match with the patch clustering. Unlike the local variance, the Gi*(*d*) method considers the local spatial association, and is a good added information component compared to the variogram and local variance windows. Also it can be compared among different images. But it is a complicated measurement and requires a large amount of computation time even for a moderate image.

The variogram analysis method

Since Jupp *et al*. (1988a, 1988b) and Curran (1988) introduced the theory of autocorrelation and regularization in digital images, variogram analysis has widely been adopted for modeling the scale variation in remote sensing application, such as

soil mapping (Dubayah *et al*., 1997), biomass estimation (Atkinson and Curran, 1995) and landscape pattern (Turner *et al*., 1991). The variogram for lag distance *h* is defined as the average square difference of values separated approximately by *h*:

$$\gamma(h) = \frac{\sum_{i=1}^{n-k} \sum (X(i) - X(i+h))^2}{2(n-h)},$$

where n is the number of pixel pairs separated at distance h. The terms $X(i)$ and $X(i+h)$ represent the pixel values at i and $i+h$, respectively. Empirically in some plots, the semivariance is normalized by the global variance. The shape of a semivariogram may be fitted with a model (such as linear/sill, exponential, spherical and Gaussian). Typically the range and sill are two parameters of semivariograms used to describe data. If there is no nugget effect, which, when it occurs, is expressed as a finite limit for the variogram at the distance of zero, the semivariance is zero when lag is zero. With the distance increasing, the difference between the compared pixels becomes larger. At some distance, the semivariogram develops a flat region called sill. The distance (or lag) at which the sill is reached is called range. The range generally indicates the extent to which values sampled from spatial process are similar. The height of sill often infers the variability of images.

Variogram analysis is the core of Geostatistics, and more detailed theoretical and mathematical exploration of variogram is presented in Geostatistic (Cressie, 1991). It is regarded to provide "a concise and unbiased description of the scale and pattern of variability in a data set" (Curran, 1988). But mathematically, two assumptions are required to use variogram: spatial stationarity, that assumes the mean and variance do not vary with spatial location, and ergodicity, which assumes that spatial statistics taken over the area of the images as a whole are unbiased estimates of those parameters. If these assumptions are broken, semivariogram can't be used.

Fractal analysis

Fractal analysis was developed mainly because of the difficulty in analyzing spatial forms and processes by classic geometry. The key concept underlying fractals is self-similarity (Lam and Quattrochi, 1992), that means the curve or surface is made up of

copies of itself in a reduced scale. This simulation capability of fractals makes it a promising tool for detecting scale tendency embedded in remotely sensed images. It has been used to characterize surface shapes (Rees, 1992), land cover patterns (De Cola, 1989), image texture (Henebry and Kux, 1995), and scaling properties of terrain feature (Xia and Clarke, 1997). Xia and Clarke (1997) have given a detail review on the application of fractals. There are several algorithms to measure fractal dimension. Xia and Clarke (1997) summarized seven most commonly used algorithms including the *walking division* method, *variogram* method, *box-counting* method, *power spectrum* method, *area-perimeter* method, *size-frequency* method and the *stream number-stream length* method.

The selection of these methods differs among geographical features and subjects of interest, and often involves many subjective decisions, which often have significant effect on the final results of fractal computation. It is often common that different researchers would produce quite different results for the same data sets (Klinkenberg and Goodchild, 1992). Since the true fractal with self-similarity at all scales is infrequent, the simple fractal model was limited in a certain range of scales. Instead of the simple fractal model, multifractal model can be thought of as a hierarchy of sets each with its own fractal dimension, so the scaling properties of data is a scaling exponent function (Pecknold *et al*., 1997). Pecknold *et al*., (1997) used multifractal model to illustrate the scaling properties of landscape topography, cloud radiance and aeromagnetic anomaly, their results shows that multifractal model provide a more realistic framework and is seen to hold great promise for systematic treatment of scale issue. But the present techniques of multifractal model are insufficient to deal with multiple satellite images, and remain inaccessible to the average researcher.

Spectrum analysis

Similar to semivariogram, the spectrum analysis also concerns itself with pixels at constant intervals. It has been used to describe pattern (Cullinan and Thomas, 1992). To use this method, image intersections lengths collected along transect are expressed as linear equations of sine and cosine functions known as Fourier transform. Smoothed periograms are generated by plotting the information

$$G(f) = (C(f)^2 + Q(f)^2) * m/8\pi)$$

as a function of the sine and cosine coefficients $C(f)$ and $Q(f)$ with neighbors averaged against the block size $(m/2f)$,

$$C(f) = \frac{2}{m}\sum_{i=1}^{m} X(i)\cos\left(\frac{2\pi * i * f}{m}\right) \text{ and } Q(f) = \frac{2}{m}\sum_{i=1}^{m} X(i)\sin\left(\frac{2\pi * i * f}{m}\right),$$

where m is the total number of block units (or periodgrams), f is the period. $C(f)$ is proportional to the reduction in the sum of squares associated with fitting the sine and cosine waves of period (m/f). Depending on whether plots are against the period or block size, the result is an estimate of scales of pattern, or patch size for one or more scales of heterogeneity (Ripley, 1978). The period is defined by the length of transect required to complete a full cycle of wave, and the pattern size is estimated as one half of the period. If plots are made against the period, the location of the resulting peaks should indicate the scale of pattern. Alternatively, if plots are made against the block size, the location of the resulting peaks can be multiplied by two to estimate the period. Spectrum analysis is sensitive to the block size; often the spectrum plots have spurious peaks that make interpretation difficult. It is argued whether it should be used widely. Also, many software packages do not provide the spectrum function to estimate confidence levels, which also largely limits its use (Cullinan and Thomas, 1992).

Recent research (Kumar and Foufoula-Georgiou, 1993a & 1993b; Hu *et al*., 1998) suggests that wavelet decompositions are powerful tools in analyzing the variation in signal properties across different resolutions of geophysical variables. Due to the preservation qualities of wavelet transforms, they allow for the analysis of the fluctuations between spatial resolutions within data sets. A key advantage of wavelet transforms over other forms of analysis is that they allow for the breakdown of a signal into a scale frequency space. This permits the determination of the relative contributions of the different spatial scales present within an image. An additional benefit of wavelet analysis is that, if a process exhibits self-similar scaling behavior, the wavelet coefficients obtained through a wavelet transform preserve that self-similarity (Kumar and Foufoula-Georgiou, 1993a & 1993b). If a process does not show self-similar behavior, this methodology still permits analysis of the actual scaling behavior through a multi-scaling framework. Hu *et al*., (1998) used multiresolution wavelet

analysis to study the scale variation of soil moisture. In that study, soil moisture images were decomposed into large scale and small scale wavelet coefficients. The results suggested that the variation in soil moisture could be analyzed at large- and small-scales, independent of each other. The small-scale coefficients were analyzed with moments and scale plots. A surprising result of the research was that small-scale coefficients exhibited simple scaling, while the large-scale coefficients exhibited multiscale characteristics. Kumar and Foufoula-Georgiou (1993a, b) used multiresolution wavelets to analyze the spatial characteristics of precipitation. Their results were consistent with those of Hu *et al*., (1998): that the small scale coefficients exhibited simple scaling over a small range of scales, while large scale coefficients exhibited multiscale.

The application of wavelet transforms to the study of scaling effects, this researcher believes, will produce results the will complement those from indirect multiscale analysis of landscape pattern. In the following section, we shall describe what wavelets are, how they work and why they are useful for upscaling.

2.2 The theory of wavelets

It is well known from Fourier theory that a signal can be expressed as a Fourier series expansion, which is the sum of a series of sines and cosines. A major disadvantage of a Fourier expansion, however, is that it has only frequency resolution and no time resolution (Misiti *et al*., 2001; Daubechies, 1992). This means that although we might be able to determine all the frequencies present in a signal, we do not know when exactly they occur. To overcome this problem, several solutions were developed which are able to represent a signal in the time and frequency domain at the same time. The idea behind these time-frequency joint representations is to cut the signal of interest into several parts and analyze them separately. Although analyzing a signal in this way will give more information about the location of different frequency components and when they occur, we are faced with a fundamental problem: how do we cut the signal?

Wavelet analysis is probably the most recent solution to overcome the shortcomings of the Fourier transform. In wavelet analysis, the use of a fully scalable modulated window solves the signal-cutting problem. The window is shifted along the signal and for every position the spectrum is calculated. This process is repeated many

times with a slightly shorter (or longer) window for every new cycle. In the end the result will be a collection of time-frequency representations of the signal, all with different resolutions. If we look at a signal with a large "window," we would notice gross features. Similarly, if we look at a signal with a small "window," we would notice small features. Because of this collection of representations, we can speak of a multiresolution analysis. In the case of wavelets, we normally do not speak about time-frequency representations but about time-scale representations.

2.2.1 What are wavelets?

Wavelets are functions that are defined over a finite interval. Within an interval, they *wave* above and below the horizontal axis, integrate to zero and are square integrable. Wavelets are alternatives to other basis functions like sine and cosine, orthogonal polynomials, Walsh functions, etc., Morretin (1997). Therefore, the basic idea in wavelet analysis is to represent any arbitrary function by a linear combination of a set of wavelets or basis functions. These basis functions or wavelets are obtained from a single prototype wavelet called the *mother wavelet*, by dilations or contractions (scaling) and translations (shifts). The wavelet transform carves up functions, operators, or data into various components at different scales, allowing one to study each component separately.

2.2.2 A brief history of wavelets

Wavelets were developed from concepts and theories that already existed in various fields and also from a couple of bright discoveries. The first known connection to modern wavelets dates back to Jean Baptiste Joseph Fourier, 1768-1830 (Vidakovic, 1999). In 1807, Fourier's study of frequency analyses led to what we now call Fourier analysis. He decomposed a continuous and periodic function $f(x)$ defined on the interval $[-\pi, \pi]$ into the series

$$\frac{a_0}{2} + \sum_{n=1}^{\infty} a_n \cos nx + b_n \sin nx,$$

where the coefficients a_n, and b_n are defined, respectively, as

$$a_n = \frac{1}{\pi}\int_{-\pi}^{\pi} f(x)\cos nx\,dx, \quad n = 0, 1, 2, \ldots$$

and

$$b_n = \frac{1}{\pi}\int_{-\pi}^{\pi} f(x)\sin nx\,dx, \quad n = 1, 2, 3, \ldots.$$

By this, a signal is decomposed into complex exponential functions of different frequencies and a frequency versus amplitude plot is obtained. The plot indicates how much of each frequency exists in a signal. Although the Fourier transform provides how much of each frequency exists in a signal, it does not indicate when in time these frequency components exist. This is a major obstacle because most signals, especially in the areas of biomedicine are non-stationary as the frequency content of the signal changes with time. The electroactivity of the heart, brain and muscles, for example, are all non-stationary signals.

According to Vidakovic (1999), the first mention of wavelets appeared in an appendix to the thesis of Alfred Haar in 1909. In 1910, Alfred Haar discovered the first *wavelet basis* when he showed that any continuous function *f(x)* on $[0,1]$ can be approximated by

$$f_n(x) = \langle \xi_0, f \rangle \xi_0(x) + \langle \xi_1, f \rangle \xi_1(x) + \ldots + \langle \xi_n, f \rangle \xi_n(x),$$

and that when $n \to \infty$, f_n converges to *f* uniformly (Haar, 1910). The approximation above is equivalent to an approximation by step functions whose values are the mean values of the function over appropriate dyadic intervals. One property of the Haar wavelet is that it has *compact support*, which means that it vanishes outside of a finite interval. Unfortunately, it does not have good time-frequency localization and the resulting wavelet basis functions have the additional disadvantage of being discontinuous which makes them unsuitable as a basis for smoother functions.

In the 1930s, several independent researches continued on the representation of functions using *scale-varying* basis functions. By using scale-varying basis functions, a 1930s physicist called Paul Levy investigated Brownian motion (Meyer, 1993). He found that the Haar basis function is superior to the Fourier basis functions for studying small complicated details in the Brownian motion. Fifty years later,

Grossman and Morlet defined wavelets in the context of quantum physics. They stated that by the Heisenburg Uncertainty Principle, one could not know the exact time-frequency representations of a signal. The only information one can obtain is the time intervals in which certain band frequencies exist. This assertion provided a way of thinking about wavelets based on physical intuition. In 1985, Stephane Mallat made a huge leap in the field of wavelet analysis by discovering the relationship between pyramid algorithms and orthonormal wavelet bases. Soon after Mallat's work, Yves Meyer constructed the first non-trivial wavelets. Unlike the Haar wavelets, the Meyer wavelets are continuously differentiable; however they do not have compact support. A couple of years later, Ingrid Daubechies used Mallat's work to construct a set of wavelet orthonormal basis functions that are perhaps the most elegant, and have become the cornerstone of wavelet application today.

2.2.3 Why do we employ wavelet methods?

Wavelet transforms are so remarkable and useful due to certain peculiar characteristics. We list and explain some of the characteristics below.

1. Wavelets are based on multi-resolution analysis. Functions, operators, or data are separated into multiresolution components. The fine resolution components capture the fine scale features in the signal, while the coarse resolution components capture the coarse scale features in the signal. This characteristic allows for the separate study of the various components at different scales.

2. Wavelets are localized in both space/time and scale/frequency domains. Hence they are good building blocks for a variety of signals. They can easily detect and preserve important local structural features such as discontinuity, trends, etc., in data sets. A Fourier series approximation is not well suited to these types of signals.

3. Wavelets are smooth, which is a necessary condition for efficient representation of the characteristics of data for many applications. This smoothness can be measured by the number of derivatives and/or the number of vanishing moments that exist for that wavelet. A function defined on the interval $[a, b]$ has n vanishing moments if

$$\int_a^b f(x)x^i dx = 0, \quad \text{for} \quad i = 0, 1, 2, \ldots, n\text{-}1.$$

The higher the number of vanishing moments, the better smooth signals can be approximated in a wavelet basis.

4. The wavelet approximation can compact the energy of a signal into a relatively small number of wavelet functions. This data compression feature of wavelets is valuable for applications such as nonparametric statistical estimation and classification.
5. There exists fast $(O(n))$ and stable algorithms to calculate the discrete wavelet transform and the inverse discrete wavelet transform.

2.2.4 Wavelets and multiresolution analysis

The Haar basis functions (see Example 2) are discontinuous and therefore unsuitable for representing smooth functions. However, it is possible to construct a variety of wavelet bases with better approximating properties such as good time-frequency localization, various degrees of smoothness and larger vanishing moments which enable parsimonious representation of different classes of functions. The concept of multiresolution analysis provides the mathematical framework for the construction of such orthonormal basis functions.

Multiresolution analysis

Multiresolution analysis is the process of decomposing a complex function to lower level resolutions. Consider the space L^2, the vector space of square integrable functions in $\Re$:

$$L^2 = \left\{ f : \int_{-\infty}^{\infty} f^2(x)dx < \infty \right\}.$$

In a multiresolution analysis (Mallat, 1989), we decompose L^2, in nested subspaces V_j

$$\ldots V_{-2} \subset V_{-1} \subset V_0 \subset V_1 \subset V_2 \ldots$$

such that closure of their union is L^2,

$$\text{i.e. } \overline{\bigcup_{j=-\infty}^{\infty} V_j} = L^2,$$

and their intersection contains only the zero function

$$\bigcap_{j=-\infty}^{\infty} V_j = \{\mathbf{0}\}.$$

[Note: $\overline{A}$ denotes the closure of the set A]. In the dyadic case, that is when each subspace $\mathbf{V}_j$ is twice as large as $\mathbf{V}_{j-1}$, a function $f(x)$ that belongs to one of these subspaces $\mathbf{V}_j$ has the following properties:

$$f(x) \in \mathbf{V}_j \Leftrightarrow \text{ dilation } f(2x) \in \mathbf{V}_{j-1}, \tag{2.1}$$

$$f(x) \in \mathbf{V}_0 \Leftrightarrow \text{ translation } f(x+1) \in \mathbf{V}_0. \tag{2.2}$$

If we can find a function $\phi(x) \in \mathbf{V}_0$ such that the set of functions consisting of $\phi(x)$ and its integers translates

$$\{\phi(x-k)\}_{k \in \mathbf{Z}}$$

form basis for the space $\mathbf{V}_0$, we call it a scaling function or father function. For the other subspaces $\mathbf{V}_j$ (with $j \neq 0$) we define: $\phi_{j,k}(x) = 2^{j/2}\phi(2^j x - k)$.

Wavelet functions

Because the subspaces $\mathbf{V}_j$ are nested:

$$\mathbf{V}_j \subset \mathbf{V}_{j+1},$$

we can decompose $\mathbf{V}_{j+1}$ in $\mathbf{V}_j$ and $\mathbf{W}_j$ (the orthogonal complement of $\mathbf{V}_j$ in $\mathbf{V}_{j+1}$):

$$\begin{aligned} \mathbf{V}_j \otimes \mathbf{W}_j &= \mathbf{V}_{j+1} \\ \mathbf{W}_j &\perp \mathbf{V}_j \end{aligned} .$$

The direct sum of the subspaces $\mathbf{W}_j$ is equal to L^2, :

$$\overline{\bigcup_{j=-\infty}^{\infty} \mathbf{V}_j} = \overline{\bigoplus_{j=-\infty}^{\infty} \mathbf{W}_j} = L^2.$$

This means that $\mathbf{V}_j$ is a *coarse resolution* representation of $\mathbf{V}_{j+1}$, while $\mathbf{W}_j$ carries the high-resolution difference information between $\mathbf{V}_{j+1}$ and $\mathbf{V}_j$. If we can find a function $\psi(x) \in \mathbf{W}_0$ that obeys the translation property

$$\psi(x) \in \mathbf{W}_0 \Leftrightarrow \text{translation } \psi(x+1) \in \mathbf{W}_0,$$

and such that the set of functions consisting of $\psi(x)$ and its integer translates

$$\{\psi(x-k)\}_{k \in \mathbf{Z}}$$

form a basis for the subspace $\mathbf{W}_0$, we call it a *wavelet function* or *mother function*. For the other subspaces $\mathbf{W}_j$ (with $j \neq 0$) we define:

$$\psi_{j,k}(x) = 2^{j/2} \psi(2^j x - k).$$

2.2.5 The Wavelet transform

The wavelet transform is a form of a frequency transform. The transform uses wavelets as basis functions. The transformation of a function into its wavelet components has common background with the transformation of a function into its Fourier components. We shall begin the discussion of wavelets with a brief overview of Fourier transforms, highlighting only the concepts that are important to the development of wavelets.

The Fourier series expansion

Here, we adopt the approach by Ogden (1997), and only consider functions defined on the interval $[-\pi, \pi]$. If a function *g*, say, is defined instead on a different finite interval $[a, b]$, then it can be transformed via

$$f(t) = g\left(\frac{2\pi t}{(b-a)} - \frac{(a+b)\pi}{(b-a)} \right).$$

Let $L^2[a, b]$ be the space of all square-integrable functions:

$$\int_a^b f^2(t)dt < \infty.$$

Then any function $f \in L^2[a, b]$ of period 2π can be written as a linear combination of dilated sine and cosine functions:

$$f(t) = \frac{1}{2}a_0 + \sum_{n=1}^{\infty} \left(a_n \cos nt + b_n \sin nt \right), \tag{2.3}$$

where a_n and b_n are the Fourier coefficients given by

$$a_n = \frac{1}{\pi} \int_{-\pi}^{\pi} f(t) \cos ntdt \quad n \geq 0, \tag{2.4}$$

and

$$b_n = \frac{1}{\pi} \int_{-\pi}^{\pi} f(t) \sin ntdt \quad n \geq 1. \tag{2.5}$$

The coefficients are said to measure the *frequency content* of the function *f* at the resolution level *n*. The equality in Equation (2.3) is understood to mean

$$\int_{-\pi}^{\pi} \left[f(t) - \left(\frac{1}{2}a_0 + \sum_{n=1}^{\infty} \left(a_n \cos nt + b_n \sin nt \right) \right) \right]^2 dt = 0,$$

and the summation can well be approximated by the finite sum with limit index *N*:

$$S_N(t) = \frac{1}{2}a_0 + \sum_{n=1}^{\infty}\left(a_n \cos nt + b_n \sin nt\right). \tag{2.6}$$

Equation (2.6) is called the Fourier series expansion of $f(x)$. Note that the set of functions

$$\{\sin(n\cdot),\ \cos(n\cdot);\ \ n = 1, 2, 3, \ldots\},$$

form an orthogonal basis for the space $L^2[-\pi, \pi]$. Thus the Fourier series is the expansion of a function in terms of sine and cosine functions of differing frequencies, which form a set of orthogonal basis functions.

Suppose f is a periodic linear function defined on the interval $[-\pi, \pi]$ by

$$f(t) = \begin{cases} t + \pi, & -\pi \le t \le -\dfrac{\pi}{2}, \\ \dfrac{\pi}{2}, & -\dfrac{\pi}{2} \le t \le \dfrac{\pi}{2}, \\ \pi - t, & \dfrac{\pi}{2} < t \le \pi. \end{cases}$$

Then the Fourier coefficients for $f(t)$ computed from Equations (2.4) and (2.5) are summarized in Table 2.1.

Table 2.1 Fourier coefficients for f(t) in Example 1

n	0	1	2	3	4	5	6	7	8	9
a_n	$\frac{3\pi}{4}$	$\frac{2}{\pi}$	$\frac{-1}{\pi}$	$\frac{2}{9\pi}$	0	$\frac{2}{25\pi}$	0	$\frac{2}{49\pi}$	0	$\frac{2}{81\pi}$
b_n	-	0	0	0	0	0	0	0	0	0

It is observed from Table 2.1 that all the b_n's corresponding to the sine basis functions are zero, and in general, a_n decreases as n increases. This indicates that most of the frequency contents are concentrated at low frequencies. The graph of $f(t)$ and its representations by Equation (2.6) for $N = 1, 2,$ and 3 are shown in Figure 2.2.

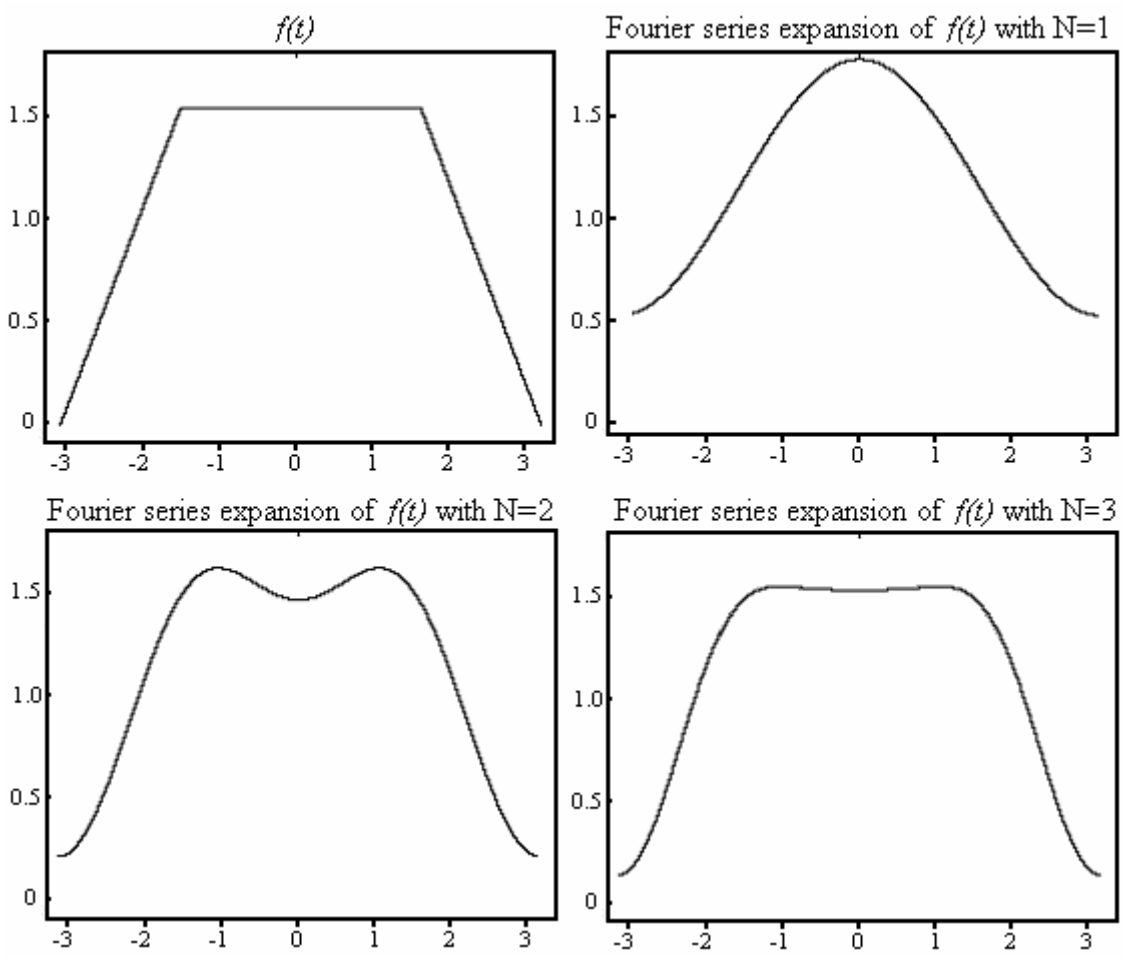

Figure 2.2 Graph of f(t) in Example 1 and its Fourier series expansion for $N = 1,2,3$

It can be observed from the graph that as the summation limit N gets larger, the resulting Fourier sum approximates $f(t)$ better. Infact, the approximation of $f(t)$ is fairly good using the first 3 pairs $(\text{i.e. } N = 3)$ of basis functions.

The wavelet series expansion

The Fourier series expansion is a tool widely used for many scientific purposes, but it is best suited to the study of stationary signals where all frequencies have an infinite coherence time. The Fourier analysis brings only global information which is not sufficient to detect compact patterns. In 1993, Gabor introduced a local Fourier analysis, taking into account a sliding window which leads to a time frequency-analysis. This method is only applicable to situations where the coherence time is independent of the frequency. Morlet introduced the wavelet transform in order to have a coherence time proportional to the period (Meyer, 1993).

By analogy with Fourier analysis, let us consider the space $L^2(\Re)$ of all square-integrable functions on $\Re$. In this case, the basis functions that generate $L^2(\Re)$ must not be only orthonormal, but must decay rapidly to zero as $|t| \to \infty$. The wavelet series expansion for any continuous time function $f \in L^2(\Re)$ can be written as a linear combination:

$$f(t) \approx \sum_k s_{J,k}\phi_{J,k}(t) + \sum_k d_{J,k}\psi_{J,k}(t) + \sum_k d_{J-1,k}\psi_{J-1,k}(t) + \ldots + \sum_k d_{1,k}\phi_{1,k}(t), \quad (2.7)$$

where J is the number of multiresolution components (scales) and k ranges from 1 to the number of coefficients in the specified component. The terms $s_{J,k}, d_{J,k}, \ldots, d_{1,k}$ are the wavelet coefficients and are given approximately by the integrals

$$s_{J,k} \approx \int f(t)\phi_{J,k}(t)dt \quad (2.8)$$

$$d_{j,k} \approx \int f(t)\psi_{j,k}(t)dt \qquad j = 1, 2, \ldots, J. \quad (2.9)$$

Their magnitude gives a measure of the contribution of the corresponding wavelet function to the approximating sum. The functions $\phi_{j,k}(t)$ and $\psi_{j,k}(t)$ are the approximating wavelet functions and are generated from ϕ and ψ through scaling and translation as follows:

$$\phi_{j,k}(t) = 2^{-j/2}\phi(2^{-j}t - k) = 2^{-j/2}\phi\left(\frac{t - 2^j k}{2^j}\right), \quad (2.10)$$

$$\psi_{j,k}(t) = 2^{-j/2}\psi(2^{-j}t - k) = 2^{-j/2}\psi\left(\frac{t - 2^j k}{2^j}\right). \quad (2.11)$$

The wavelet series expansion in Equation (2.7) is orthogonal since the basis functions $\phi_{j,k}(t)$ and $\psi_{j,k}(t)$ are orthogonal:

$$\left.\begin{aligned} \int \phi_{J,k}(t)\phi_{J,k'}(t)dt &= \delta_{k,k'} \\ \int \psi_{j,k}(t)\phi_{J,k'}(t)dt &= 0 \\ \int \psi_{j,k}(t)\psi_{j',t'}(t)dt &= \delta_{j,j'}\delta_{k,k'} \end{aligned}\right\}, \text{ where } \delta_{i,j} = \begin{cases} 1 & \text{if } i = j \\ 0 & \text{if } i \neq j. \end{cases} \quad (2.12)$$

The simplest and oldest example of a wavelet is the Haar function, a piecewise function defined on the interval $[0,1]$ by

$$\psi^{(H)}(t) = \begin{cases} 1 & 0 \le t < \frac{1}{2}, \\ -1 & \frac{1}{2} \le t < 1, \\ 0 & \text{otherwise.} \end{cases}$$

For this wavelet function, the scaling function is

$$\phi(t) = 1, \quad 0 \le t < \frac{1}{2};$$

and the wavelet basis functions are given by

$$\psi_{j,k}^{(H}(t) = \begin{cases} 2^{j/2} & 2^{-j}k \le t < 2^{-j}\left(k + \frac{1}{2}\right), \\ -2^{j/2} & 2^{-j}\left(k + \frac{1}{2}\right) \le t < 2^{-j}\left(k + \frac{1}{2}\right), \\ 0 & \text{otherwise.} \end{cases}$$

The graph of the Haar wavelet function is shown in Figure 2.3.

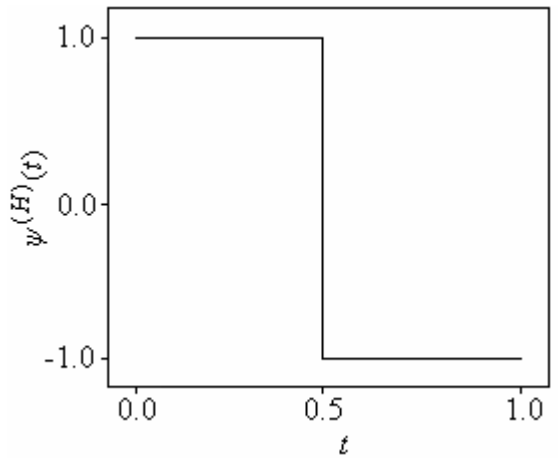

Figure 2.3 Graph of the Haar wavelet function

The 2-D wavelet series expansion

We have so far discussed the wavelet representation of one-dimensional (1-D) functions (see Equation (2.5)). The 2-D wavelet series expansion is a straight forward generalization of the 1-D expansion. A 2-D function $F(x,y)$ can be written as a sum of 2-D wavelets at different scales and locations:

$$\begin{aligned} F(x,y) \approx & \sum_{m,n} s_{J,m,n}\Phi_{J,m,n}(x,y) + \sum_{j=1}^{J}\sum_{m,n} d^{v}_{j,m,n}\Psi^{v}_{j,m,n}(x,y) \\ & + \sum_{j=1}^{J}\sum_{m,n} d^{h}_{j,m,n}\Psi^{h}_{j,m,n}(x,y) \\ & + \sum_{j=1}^{J}\sum_{m,n} d^{d}_{j,m,n}\Psi^{d}_{j,m,n}(x,y). \end{aligned} \tag{2.13}$$

Analogous to the 1-D series, $F(x,y)$ is decomposed into a sum of coarse resolution (level *J*) smooth coefficients and a sum of fine to coarse resolution (levels 1 to *J*) detail coefficients. However, there are three types of detail coefficients in the 2-D series: the vertical detail, horizontal detail and diagonal detail. There are three types of 2-D basis functions which are generated from the father wavelet Φ and the mother wavelets Ψ^{v}, Ψ^{h}, Ψ^{d} by scaling and translation as follows:

$$\begin{aligned} \Phi_{J,m,n}(x,y) &= 2^{-J}\Phi(2^{-J}x-m, 2^{-J}y-n) \\ \Psi^{v}_{j,m,n}(x,y) &= 2^{-j}\Psi^{v}(2^{-j}x-m, 2^{-j}y-n) \\ \Psi^{h}_{j,m,n}(x,y) &= 2^{-j}\Psi^{h}(2^{-j}x-m, 2^{-j}y-n) \\ \Psi^{d}_{j,m,n}(x,y) &= 2^{-j}\Psi^{d}(2^{-j}x-m, 2^{-j}y-n). \end{aligned}$$

The 2-D wavelet transform coefficients are given approximately by the integrals

$$\begin{aligned} s_{J,m,n} &\approx \iint \Phi_{J,m,n}(x,y)F(x,y)dxdy \\ d^{v}_{j,m,n} &\approx \iint \Psi^{v}_{j,m,n}(x,y)F(x,y)dxdy \\ d^{h}_{j,m,n} &\approx \iint \Psi^{h}_{j,m,n}(x,y)F(x,y)dxdy \\ d^{d}_{j,m,n} &\approx \iint \Psi^{d}_{j,m,n}(x,y)F(x,y)dxdy \end{aligned}. \tag{2.14}$$

The discrete wavelet transform

The task of calculating wavelet coefficients at every possible scale is an arduous one, and results in enormous amounts of data. It has been established that if scale and positions are chosen based on powers of 2, then the analysis is much more efficient and as accurate as using the entire data. This is what the *discrete wavelet transform* (DWT) does. The DWT calculates the coefficients of the wavelet series expansion (Equation 2.7) for a discrete signal $f_1, f_2, f_3, \ldots, f_n$ of a finite extent. The DWT maps the vector

$$\mathbf{f} = \left(f_1, f_2, f_3, \ldots, f_n\right)^{\mathrm{T}}$$

to a vector of *n* wavelet coefficients

$$\mathbf{w} = \left(w_0, w_1, w_2, \ldots, w_{n-1}\right)^{\mathrm{T}}.$$

The vector $\mathbf{w}$ contains the wavelet coefficients $s_{J,k}$ and $d_{j,k}$, $j = 1, 2, \ldots, J$ the wavelet series expansion. The $s_{J,k}$ are called the *smooth* coefficients and are thought to represent the underlying smooth behavior of the data set at the coarse scale 2^J. The $d_{J,k}$ are called the *detail* coefficients and represent progressively finer scale deviations from the smooth behavior. Mathematically, the DWT is equivalent to $\mathbf{w} = \mathbf{W}\mathbf{f}$, where $\mathbf{w}$ is an $n \times 1$ vector of length $n = 2^J$ comprising both the discrete scaling coefficients $s_{J,k}$ and the discrete wavelet coefficients $d_{J,k}$. The term $\mathbf{W}$ is an $n \times n$ real-valued orthogonal matrix defining the DWT and satisfying $\mathbf{W}^{\mathrm{T}}\mathbf{W} = \mathbf{I_n}$. The orthogonality of $\mathbf{W}$ implies that $\mathbf{f} = \mathbf{W}^{\mathrm{T}}\mathbf{w}$ and $\|\mathbf{w}\|^2 = \|\mathbf{f}\|^2$. Hence $\mathbf{w}_n^2$ represents the contribution to the energy attributable to the DWT coefficients with index *n*.

In practice, the DWT is implemented using filters which were developed by Mallat (Mallat, 1998). This practical filtering algorithm yields a fast wavelet transform – a process through which a signal (data set) passes, and out of which wavelet coefficients quickly emerge. This algorithm consists of a sequence of low-pass and high-pass filters, and requires only order *n* operations. An outline of Mallat's algorithm is given in the sections following.

The inverse discrete wavelet transform

An original signal vector $\mathbf{f}$ can be recovered from the DWT coefficients by applying the inverse discrete wavelet transform (IDWT). Because of the orthogonality of the matrix $\mathbf{W}$ associated with the chosen wavelet basis, the IDWT is given mathematically by $\mathbf{f} = \mathbf{W}^{-\mathrm{T}}\mathbf{w}$. Often, the reconstructed signal is not identically equal to the original signal. This is due to round-off error. To assess the round-off error of the reconstructed signal vector $\hat{\mathbf{f}}$, we compute the L^2 relative error, which is given by

$$relative\ error = \frac{\left(\sum_{i=1}^{n}\left(f_i - \hat{f}_i\right)^2\right)^{1/2}}{\left(\sum_{i=1}^{n} f_i^2\right)^{1/2}}.$$

The IDWT is achieved through the inverse fast wavelet transform.

Mallat's pyramid algorithm

The DWT and IDWT are computed through Mallat's forward and backward pyramid algorithms, which are remarkably fast algorithms. Each algorithm uses low-pass and high-pass filters, along with a *down-sampling* (decimation) or *up-sampling* (zero-padding) operator.

The forward algorithm

The DWT algorithm is shown in Figure 2.4. There are two analysis filters – a low-pass filter and a high-pass filter – at each stage of the pyramid as well as a decimation-by-two operation.

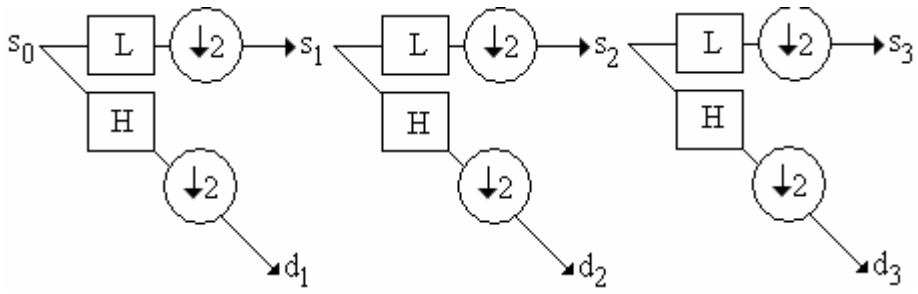

Figure 2.4 A 3-level DWT pyramid algorithm for 1-D data

The decimation operation is indicated by the symbol ↓2 and consists of deleting every other value of the filter output, thereby reducing the length of each component by half. The input signal $s_0 = (s_{0,1}, s_{0,2}, \ldots, s_{0,n})^{\mathrm{T}}$, consists of the values of the discrete signal: $s_{0,i} = f_i \quad i = 1, 2, \ldots, n.$ Suppose

$$n_j = \frac{n}{2^j}.$$

Then the output of the algorithm is the set of DWT detail coefficients

$$\mathbf{d}_j = (d_{j,1}, d_{j,2}, \ldots, d_{j,n_j})^{\mathrm{T}}$$

at levels $i = 1, 2, \ldots, J,$ which corresponds to scales $2, 4, 8, \ldots, 2^J$, along with the DWT smooth coefficients

$$\mathbf{s}_J = (s_{J,1}, s_{J,2}, \ldots, s_{J,n_J})^{\mathrm{T}}.$$

The algorithm can be iterated, using successive smooth coefficients as input signals at subsequent levels. In practice, one has to decide on the number of iterations needed. This is usually referred to as the number of *levels*, depending on the nature of the signal, or on any suitable criterion such as the *entropy*. Given a signal of length *N*, the algorithm consists of a maximum of $\log_2 N$ levels. By performing a number of iterations, the original signal is broken down into many lower components. For example, Figure 2.4 shows a 3-level iteration algorithm for 1-D signal.

The backward algorithm

The backward algorithm shown in Figure 2.5 inverts the forward algorithm to reconstruct the original signal.

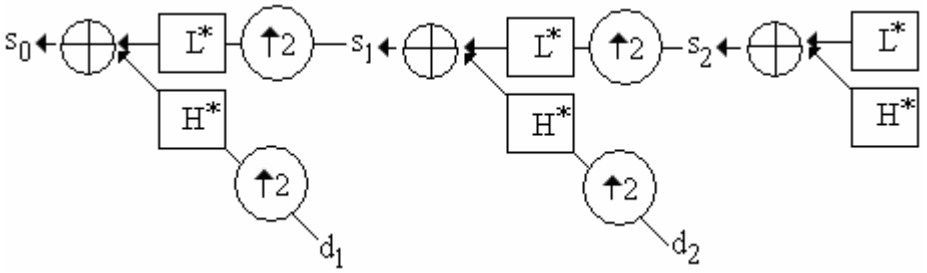

Figure 2.5 A 3-level IDWT pyramid algorithm for 1-D data

As in the case of the forward algorithm, there are two synthesis filters – a low-pass filter and a high-pass filter $\left(\mathrm{L}^{*} \text{ and } \mathrm{H}^{*}\right)$ at each stage of the pyramid as well as an *up-sample-by-two* operation, indicated by the symbol ⑫ The up-sample operation consists of inserting zeros between every other value of the filter input, thereby doubling the length of each component.

The 2-D discrete wavelet transform

The properties which make wavelets attractive for analyzing 1-D data sets also hold for images, matrices and other 2-D data sets. In particular, wavelets have proven very effective and efficient for image analysis. In order to apply wavelets to images, an extension is made to the DWT to obtain the 2-D DWT. The 2-D DWT computes the coefficients of the 2-D wavelet series expansion (Equation 2.13) for an $m \times n$ image $\mathbf{F}_{m,n}$. The 2-D DWT maps the image $\mathbf{F}_{m,n}$ to an $m \times n$ matrix of wavelet coefficients $\mathbf{w}_{m,n}$. The 2-D DWT is implemented by an extension of Mallat's forward pyramid algorithm. This algorithm consists of passing the 1-D low-pass and high-pass filters through the rows of the image data set, while retaining every other column. The same filters are then passed through the columns of the resulting data set, while retaining every other row. Figure 2.6 illustrates an S-PLUS output of a 3-level 2-D DWT indicating the various wavelet coefficients.

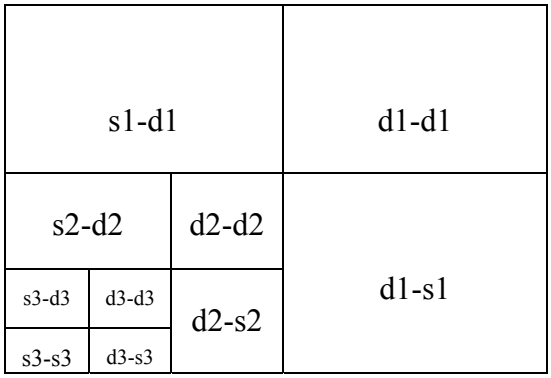

Figure 2.6 Wavelet coefficient matrices of a 3-level 2-D DWT

The coefficient matrix ($s_{3,m,n}$), located in the lower left-hand corner shows the smooth wavelet coefficients which approximates the original image. The coefficients $d3-s3$, $d2-s2$, and $d1-s1$ (representing $d^{v}_{j,m,n}$ for $j=1, 2, 3,$ see Equation (2.14)), located along the $x-$axis, corresponds to the vertical edges of the image. The coefficients $s3-d3$, $s2-d2$ and $s1-d1$ (representing $d^{h}_{j,m,n}$), located along the y-axis, corresponds to the horizontal edges. The coefficients $d3-d3$, $d2-d2$ and $d1-d1$ (representing $d^{d}_{j,m,n}$), located along the diagonal, corresponds to diagonal edges.

The 2-D inverse discrete wavelet transform

Analogous to reversing the DWT to obtain an original signal from its wavelet coefficients, the 2-D DWT algorithm can be reversed to obtain an original image from its wavelet coefficients. This process is called the 2-D inverse discrete wavelet transform (2-D IDWT). To assess the round-off error of the reconstructed image $\mathbf{F}_{m,n}$, we compute the L^2 relative error which is given by

$$relative\ error = \frac{\left(\sum_{j=1}^{n}\sum_{i=1}^{m}\left(f_{i,j}-\hat{f}_{i,j}\right)^2\right)^{1/2}}{\left(\sum_{j=1}^{n}\sum_{i=1}^{m} f_{i,j}^2\right)^{1/2}}.$$

Orthogonal wavelet families

Only very special pairs or families of functions ϕ and ψ can produce an orthogonal wavelet series expansion. Here, we discuss briefly the four commonly used types of orthogonal wavelet families.

Haar: The Haar wavelet is the first known wavelet and was proposed in 1909 by Alfred Haar. It is the simplest possible wavelet. The Haar wavelet has compact support, that is, it is zero outside a finite interval. It is a square wave and the only compact orthogonal wavelet which is symmetric. The Haar wavelet is not continuous and therefore not differentiable, thus it is unsuitable as a basis for classes of smoother functions.

Daublets: The daublets or Daubechies wavelet were the first continuous orthogonal wavelets with compact support. They were constructed by and are named after Ingrid Daubechies who is one of the pioneers in wavelet research. It has varying widths

Symmlets: The symmlets also have compact support and were also constructed by Daubechies. While the daublets are quite asymmetric, the symmlets were specifically constructed to be as nearly symmetric (least asymmetric) as possible.

Coiflets: The coiflets were also constructed by Daubechies to be nearly symmetric and also have vanishing moments for both the mother and father wavelets.

2.2.6 Summary of properties of wavelet families

Although the wavelet families described above have different characteristics and varying functionality, there are no hard and fast rules for selecting one for a given analysis (Bruce and Gao, 1996). In selecting a wavelet for an analysis, it is reasonable to examine its properties against the data to be analyzed and the overall aims of the study. Wavelet families have many different properties such as smoothness, temporal/spatial localization, vanishing moments, frequency localization, symmetry and orthogonality. The properties are described below:

- Smoothness – The smoothness of a wavelet approximation is generally inversely related to the support width of the wavelet – very compact wavelets are less smooth. Another measure of smoothness for a wavelet is given by the number derivatives which exist for that wavelet. For many applications, the wavelet function must be sufficiently smooth to efficiently represent the characteristics of the underlying data.
- Temporal/Spatial Localization – The most important feature of wavelet analysis is the ability to localize data features in time and space. The support width of a wavelet is directly related to its ability to localize features in time and space. Very compact wavelets, such as the Haar, are very well localized in time and in space.

- Vanishing Moments – A wavelet with higher number of vanishing moments can better represent higher degree polynomial signals. The number of vanishing moments is also closely related to the smoothness of a wavelet. A mother wavelet ψ with M vanishing moments satisfies

$$\int t^m \psi(t) dt = 0 \quad m = 1, 2, \ldots, M-1.$$

- Frequency Localization – Wavelets localize features not only in time and space, but also in frequency. Smoother wavelets have better frequency localization properties.
- Symmetry – Symmetric wavelets have the advantage of avoiding any phase shifts; the wavelet coefficients do not *drift* relative to the original signal. With the exception of the Haar wavelet, the orthogonal wavelets which have compact support are not symmetric; the daublets are highly asymmetric and the symmlets and coiflets are nearly symmetric.
- Orthogonality – The orthogonality of the wavelet transform is central for most applications of wavelets.

Comparison of wavelet families

Table 2.2 shows a summary of the comparison of three kinds of wavelets. The Daubechies and Haar wavelets have orthogonality, which has some nice features. For example, the scaling and wavelet functions are the same for both forward and inverse transform. Also, the correlations in the signal between subspaces are removed.

Table 2.2 Comparison of properties of three kinds of wavelets

Property	Haar	Daubechies	Biorthogonal Spline
Explicit function	yes	no	yes
Orthogonal	yes	yes	no
Symmetric	yes	no	yes
Continuous	no	yes	yes
Compacted support	yes	yes	yes
Vanishing moments	no	yes	yes
Fast algorithm	yes	yes	yes

Among the three wavelets, the Haar wavelet transform is the simplest and fastest to implement. The major disadvantage of the Haar wavelet is that it is discontinuous,

which makes it difficult to simulate a continuous signal. It is also noteworthy that both the Haar wavelet and the biorthogonal spline are symmetric, while Daubechies is not. The advantage of symmetry is that the corresponding wavelet transform can be implemented using mirror boundary conditions that reduce boundary artifacts. The scaling function of the biorthogonal spline is a B-spline. The B-spline of degree N is the shortest possible scaling function of order $N-1$ and B-splines are smoothest scaling functions for a filter of a given length. Because splines are piece-wise polynomials, they are easy to manipulate. For example, it is very easy to obtain derivatives and integrals of splines.

2.3 Description of landscape metrics

Several landscape metrics will be studied in this research. They include total area, number of patches, patch density, total edge, edge density, largest patch index, mean patch area, patch area standard deviation, patch area coefficient of variation and landscape shape index. The rest are mean shape index, area-weighted mean shape index, mean fractal dimension index, area-weighted mean fractal dimension index, contagion, patch richness, patch richness density and Shannon's diversity index. For each metric we provide a mathematically definition, its unit of measurement and a range of values for which it is defined. The description of all these metrics is based on the notations and formulations by McGarigal and Marks (2002).

2.3.1 Total area

Total area (*TA*) equals the total area (in square meters) of the landscape, divided by 10,000 to convert to hectares. That is,

$$TA = A\left(\frac{1}{10{,}000}\right),$$

where A is the total area minus the area of any background patches within the landscape. It is measured in hectares and has range $TA > 0$ with no upper limit.

2.3.2 Largest patch index

Largest patch index (*LPI*) equals the area (in square meters) of the largest patch in the landscape divided by total landscape area, multiplied by 100%. In other words, *LPI* equals the percent of the landscape that the largest patch represents. Mathematically, *LPI* is given by

$$LPI = \frac{\max_{j=1}^{n}(a_{ij})}{TA}(100\%),$$

where a_{ij} is the area of patch *ij*, $i = 1,\ldots,m$ is the number of patch types and $j = 1,\ldots,n$ is the number of patches. It is expressed as a percentage and therefore lies between 0 and 100%. *LPI* approaches 0% when the largest patch in the landscape is increasingly small. It approaches 100% when the entire landscape consists of a single patch; that is, when the largest patch comprises 100% of the landscape.

2.3.3 Number of patches

Number of patches (*NP*) equals the number of patches in the landscape. It, however, does not include any background patches within the landscape or patches in the landscape border. *NP* is computed as

$$NP = N,$$

where *N* is the total number of patches in the landscape, excluding any background patches. *NP* has no unit of measurement and $NP \geq 1$.

2.3.4 Patch density

Patch density (*PD*) is equal to the number of patches in the landscape divided by total landscape area. It is given as

$$PD = \frac{N}{TA}(10{,}000)(100),$$

where *N* is the total number of patches and *TA* is the total area of the landscape. It is measured in number per 100 hectares and $PD > 0$ without an upper limit.

2.3.5 Mean patch area

Mean patch area (*MPA*) is equal to the total area of the landscape divided by the total number of patches, and divided by 10,000 to convert to hectares. It is given by the equation

$$MPA = \frac{TA}{N}\left(\frac{1}{10{,}000}\right),$$

where *TA* and *N* are the total area and total number of patch respectively, in the landscape. It is measured in hectares and has range of $MPA > 0$ without an upper limit.

2.3.6 Patch area standard deviation

Patch area standard deviation (*PASD*) equals the square root of the sum of the squared deviations of each patch area from the mean patch area, divided by the total number of patches, divided by 10,000 to convert to hectares. Note that this is the population standard deviation, not the sample standard deviation. Mathematically,

$$PASD = \sqrt{\frac{\sum_{i=1}^{m}\sum_{j=1}^{n}\left[a_{ij} - \frac{TA}{N}\right]^2}{N}}\left(\frac{1}{10{,}000}\right),$$

where a_{ij} is the area of patch ij, $i = 1,\ldots,m$ is the number of patch types and $j = 1,\ldots,n$ is the number of patches, *TA* is the total area of the landscape and *N* is the total number of patches in the landscape. It is measured in hectares and $PASD > 0$ with no upper bound. $PASD = 0$ when all patches in the landscape are of the same size or when there is only one patch, in which case there is no variability.

2.3.7 Patch area coefficient of variation

Patch area coefficient of variation (*PACV*) is given by the standard deviation of the patch area (*PASD*) divided by the mean patch size (*MPA*), multiplied by 100 to convert to percent. That is, the variability in patch area relative to the mean patch area. This is the population coefficient of variation and not the sample coefficient of variation. Mathematically, it is given by

$$PACV = \frac{PASD}{MPA}(100\%).$$

It is measured in percent and so $0 \le PACV \le 100$. It is 0 when all patches in the landscape are of the same size or when there is only one patch.

2.3.8 Total edge

Total edge (*TE*) equals the sum of the lengths of all edge segments in the landscape. If a landscape border is present, *TE* includes landscape boundary segments representing true edge only. If a landscape border is absent, *TE* includes a user-specified proportion of the landscape boundary. Regardless of whether a landscape border is present or not, *TE* includes a user-specified proportion of background edge. It is given by

$$TE = E,$$

where *E* is total length of edge in landscape. The unit of measurement is meters and has range of values greater or equal to 0. *TE* is 0 when there is no edge in the landscape; that is, when the entire landscape and landscape border, if present, consists of a single patch and the user specifies that none of the landscape boundary and background edge be treated as edge.

2.3.9 Edge density

Edge density (*ED*) equals the sum of the lengths of all edge segments in the landscape, divided by the total landscape area multiplied by 10,000 to convert to hectares. If a landscape border is present, *ED* includes landscape boundary segments representing true edge only. If a landscape border is absent, *ED* includes a user-specified proportion of the landscape boundary. Regardless of whether a landscape border is present or not, *ED* includes a user-specified proportion of background edge. Mathematically, it is given by

$$ED = \frac{E}{TA}(10{,}000),$$

where *E* is total length of edge in landscape and *TA* is the total area of the landscape. It is measured in meters per hectare and has values ranging from 0 and above. $ED = 0$ when there is no edge in the landscape.

2.3.10 Landscape shape index

Landscape shape index (*LSI*) equals the sum of the landscape boundary (regardless of whether it represents true edge or not) and all edge segments within the landscape boundary, divided by the square root of the total landscape area, adjusted by a constant for a square standard. It is given by

$$LSI = \frac{(0.25)E}{\sqrt{TA}},$$

where E is total length of edge in landscape and TA is the total area of the landscape. LSI has no units and has range of $LSI \geq 1$; it is 1 when the landscape consists of a single square patch. LSI increases without limit as landscape shape becomes more irregular and/or as the length of edge within the landscape increases.

2.3.11 Mean shape index

Mean shape index (*MSI*) is given by the sum of the patch perimeter divided by the square root of patch area for each patch in the landscape, adjusted by a constant for a square standard, divided by the number of patches. In other words, *MSI* equals the average shape index of patches in the landscape. Mathematically, it is given by

$$MSI = \frac{\sum_{i=1}^{m}\sum_{j=1}^{n}\left(\frac{0.25\mathrm{p_{ij}}}{\sqrt{a_{ij}}}\right)}{NP},$$

where p_{ij} is the perimeter of patch *ij* in meters, a_{ij} is the area of patch *ij*, $i = 1,\ldots,m$ is the number of patch types, $j = 1,\ldots,n$ is the number of patches and *NP* is the total number of patches in the landscape. *MSI* has values greater or equal to 1; it is 1 when all patches in the landscape are square. *MSI* increases without limit as the patch shapes become more irregular.

2.3.12 Area-weighted mean shape index

The area-weighted mean shape index (*AWMSI*) equals the sum, across all patches, of each patch perimeter divided by the square root of patch area, adjusted by a constant to adjust for a square standard, multiplied by the patch area and divided by the total

landscape area. In other words, *AWMSI* equals the average shape index of patches, weighted by patch area so that larger patches weigh more than smaller ones. It is given by the equation

$$AWMSI = \sum_{i=1}^{m}\sum_{j=1}^{n}\left[\left(\frac{0.25\mathrm{p_{ij}}}{\sqrt{a_{ij}}}\right)\left(\frac{a_{ij}}{TA}\right)\right],$$

where p_{ij} is the perimeter of patch *ij*, a_{ij} is the area of patch *ij* , $i = 1,\ldots,m$ is the number of patch types , $j = 1,\ldots,n$ is the number of patches and *TA* is the total area of the landscape. *AWMSI* is without units and have values greater or equal to 1. $AWMSI = 1$ when all patches in the landscape are square. It increases without limit as the patch shapes become more irregular.

2.3.13 Mean fractal dimension index

Mean fractal dimension index (*MFDI*) equals the sum of two times the logarithm of patch perimeter, divided by the logarithm of patch area for each patch in the landscape, divided by the number of patches. *MFDI* is given by the equation

$$MFDI = \frac{\sum_{i=1}^{m}\sum_{j=1}^{n}\left(\frac{2\ln\left(0.25\mathrm{p_{ij}}\right)}{\ln a_{ij}}\right)}{NP},$$

where p_{ij} is the perimeter of patch *ij* and *i*, *j*, and *N* have their usual meanings. It has a range of $1 \le MFDI \le 2$ but no units. A fractal dimension greater than 1 for a 2-dimensional landscape mosaic indicates a departure from a Euclidean geometry. The value of *MFDI* approaches 1 for shapes with very simple perimeters such as circles or squares, and approaches 2 for shapes with highly convoluted, plane-filling perimeters.

2.3.14 Area-weighted mean fractal dimension index

Area-weighted mean fractal dimension index (*AWMFDI*) equals the sum, across all patches, of two times the logarithm of patch perimeter divided by the logarithm of patch area, multiplied by the patch area divided by total landscape area. In other words, *AWMFDI* equals the average patch fractal dimension of patches in the landscape, weighted by patch area. Mathematically, it given by

$$AWMFDI = \sum_{i=1}^{m}\sum_{j=1}^{n}\left[\left(\frac{2\ln(0.25p_{ij})}{\ln a_{ij}}\right)\left(\frac{a_{ij}}{TA}\right)\right].$$

Its range of values is given as $1 \le AWMFDI \le 2$ and has no units of measurement. Estimated values of *AWMFDI* share similar characteristics as those of *MFDI*.

2.3.15 Shannon's diversity index

Shannon's diversity index (*SHDI*) equals the negative of the sum, across all patch types, of the proportional abundance of each patch type multiplied by that proportion. It is given by

$$SHDI = -\sum_{i=1}^{m}(P_i \cdot \ln P_i),$$

where P_i is the proportion of the landscape occupied by patch type *i* and $i = 1,\ldots,m$ is the number of patch types. *SHDI* is greater or equal to 0 with no units. It is 0 when the landscape contains only one patch (or no diversity). *SHDI* increases as the number of different patch types increases and/or the proportional distribution of area among patch types becomes more equitable.

2.3.16 Patch richness

Patch richness (*PR*) equals the number of different patch types present within the landscape boundary. That is,

$$PR = m,$$

where *m* is the number of patch types present in the landscape, excluding the landscape border if present. The range of values is given as $PR \ge 1$ with no units.

2.3.17 Patch richness density

Patch richness density (*PRD*) equals the number of different patch types present within the landscape boundary divided by total landscape area, multiplied by 10,000 and 100 to convert to 100 hectares. It is given by the mathematical expression

$$PRD = \frac{m}{TA}(10{,}000)(100).$$

Unit of measurement is number per 100 hectares and has positive values with no upper bound.

2.3.18 Contagion

The contagion index (*CONTAG*) equals the negative of the sum of the proportional abundance of each patch type multiplied by the number of adjacencies between cells of that patch type and all other patch types, multiplied by the logarithm of the same quantity, summed over each patch type; divided by 2 times the logarithm of the number of patch types; multiplied by 100. Note, *CONTAG* considers all patch types present on an image and considers like adjacencies. All background edge segments are ignored, as are landscape boundary segments if a border is not provided, because adjacency information for these edge segments is not available. It is given by the equation

$$CONTAG = \left[1 + \frac{\sum_{i=1}^{m}\sum_{k=1}^{m}\left[(P_i)\left(\frac{g_{ik}}{\sum_{k=1}^{m} g_{ik}}\right)\right]\left[\ln(P_i)\left(\frac{g_{ik}}{\sum_{k=1}^{m} g_{ik}}\right)\right]}{2\ln(m)}\right](100)$$

where P_i is the proportion of the landscape occupied by patch type i, g_{ik} is the number of adjacencies between pixels of patch types i and k, and $i,k = 1,\ldots,\mathrm{m}$ is the number of patch types. It has values $0 \le CONTAG \le 100$ and has % as its unit of measurement. It approaches 0 when the distribution of adjacencies among unique patch types becomes increasingly uneven. It is 100% when all patch types are equally adjacent to all other patch types. *CONTAG* is undefined if the number of patch types is less than 2.

3 DATA SETS AND METHODS

3.1 Description of data sets

In this section, we shall briefly describe the study area and the data sets used in this research. Data summaries will be computed and discussed. Also, problems associated with the data sets as well as their solutions will be explained.

3.1.1 The study area

The study covers an area of about $100\ \text{km} \times 100\ \text{km}$ (or approximately $10,000\ \text{km}^2$) in the Northern Region of Ghana. It lies between latitudes $8°\ 50'$ and $10°\ \text{N}$, and between longitudes $0°\ 30'$ and $1°\ 30'\ \text{W}$. The Northern Region is one of the ten administrative regions, and has 18 of the 138 districts in Ghana. It is bounded on the north by the Upper East and Upper West regions of Ghana, on the west by Cote D'Ivoire, on the east by Togo and on the south by Brong Ahafo and Volta regions of Ghana. Although the Northern Region covers about 31% of the total size of Ghana, its population in 2000 was about 1.8 million which is equivalent to only about 10% of the total population of Ghana. The population density in northern Ghana ranges from the lowest of 10 persons/km^2 to the highest of 150 persons/km^2, with an average of 26 persons/km^2. The rate of growth of the population is about 2.5% (Ghana Statistical Service, 2002). The main ethnic groups are Dagomba, Nanumba, Mamprusi, Gonja and Komkomba.

The geographical features of the Northern Region are mostly low lying, except in the north- eastern corner which has the Gambaga escarpment. The land is drained by the tributaries of the Volta Lake: rivers Nasia, Daka, Oti, the Black Volta and the White Volta; covering over a third of the total land mass. There are two main seasons in the study area: rainy and dry seasons. The rainy season is between May and October each year, followed by a dry season from November to April. The dry season peaks in December and January with dry harmattan winds from the Sahara Desert. Year round temperatures are generally high, averaging about $27°\ \text{C}$. Maximum temperatures of around $38°\text{C}$ occur between March and April each year, while minimum temperatures of about $19°\text{C}$ occur in January (Fact File, 2003). Between April and

October, relative humidity is highest in the night (about 95%), dropping to about 70% during day time (Overseas Development Institute, 1999). At other times of the year, relative humidity in the night is less than 80% and drops to as low 25% in January.

Latest characterization of the soils in northern Ghana shows the following: soil pH values range between 4.5 and 6.7, organic matter content range from 0.6% to 2.0%, total nitrogen ranges from 0.02% to 0.05%, available phosphorous varies between 2.5 and 10.0 mg P/kg of soil, and available calcium ranges between 45 and 90 mg/kg of soil (Soil Research Institute, 2001). Soil fertility in the study area has declined in the last two decades (Abatania and Albert, 1993; Gordon and Amatekpor, 1999). The causes are attributed mainly to bush burning, continuous cropping, mono cropping and overgrazing. The consequence of the decline in soil fertility is lower yields in maize, sorghum and groundnuts which are the crops commonly grown in the area. The tropical climate sustains the Guinea Savanna vegetation made up of grassland, clusters of shrubs, short trees and such big trees as mahogany, Shea butter, *Dawadawa*, Mango and Baobab (Kipo, 1993). The main land use changes are intensification of land use and the expansion of agricultural land into previously forested areas.

3.1.2 The data sets

Five large secondary data sets were used in this research. They included two land use and land cover (LULC) maps, two normalized differential vegetation index (NDVI) maps and one digital elevation model (DEM) data set. The LULC maps were acquired in November 1984 and November 1999; they are therefore called LULC84 and LULC99 respectively in this study. The NDVI maps were produced from the LULC maps, and are consequently named NDVI84 and NDVI99. Each of the LULC and NDVI data sets is stored in 3114×2010 pixels with a grain size of $30\,\text{m} \times 30\,\text{m}$ and covers an area of about $93\,\text{km} \times 60\,\text{km}$ (approximately $5{,}600\,\text{km}^2$). The DEM data set is of lower detail and stored in 1202×1202 pixels with a grain size of $90\,\text{m} \times 90\,\text{m}$ and covers an area of approximately $108\,\text{km} \times 108\,\text{km}$. Classification of the LULC maps was carried out using the maximum likelihood algorithm (Braimoh, 2004). The map was classified into six land use and land cover types based on the scheme in Table 3.1.

Table 3.1 Classification scheme for assigning codes to land use and land cover types

Code	Land use and land cover type	
	LULC84	LULC99
1	Cropland	Built-up area
2	Built-up area	Water
3	Closed woodland	Cropland
4	Water	Closed woodland
5	Open woodland	Grassland
6	Grassland	Open woodland

A brief description of each land use and land cover type is given below:

Land cover type	Description
Closed woodland	Mainly trees over 5 m high, riparian vegetation (>150 trees/ha)
Open woodland	Mainly trees (75-150 trees/ha) with shrub undergrowth
Grassland	Mainly combination of grasses and shrubs with or without scattered tress (<10 trees/ha)
Cropland	Agricultural land with crops, harvested agricultural land
Built-up area	Settlements, airports and roads
Water	Rivers, inland waters, reservoirs

Figure 3.1 shows the LULC maps for 1984 and 1999.

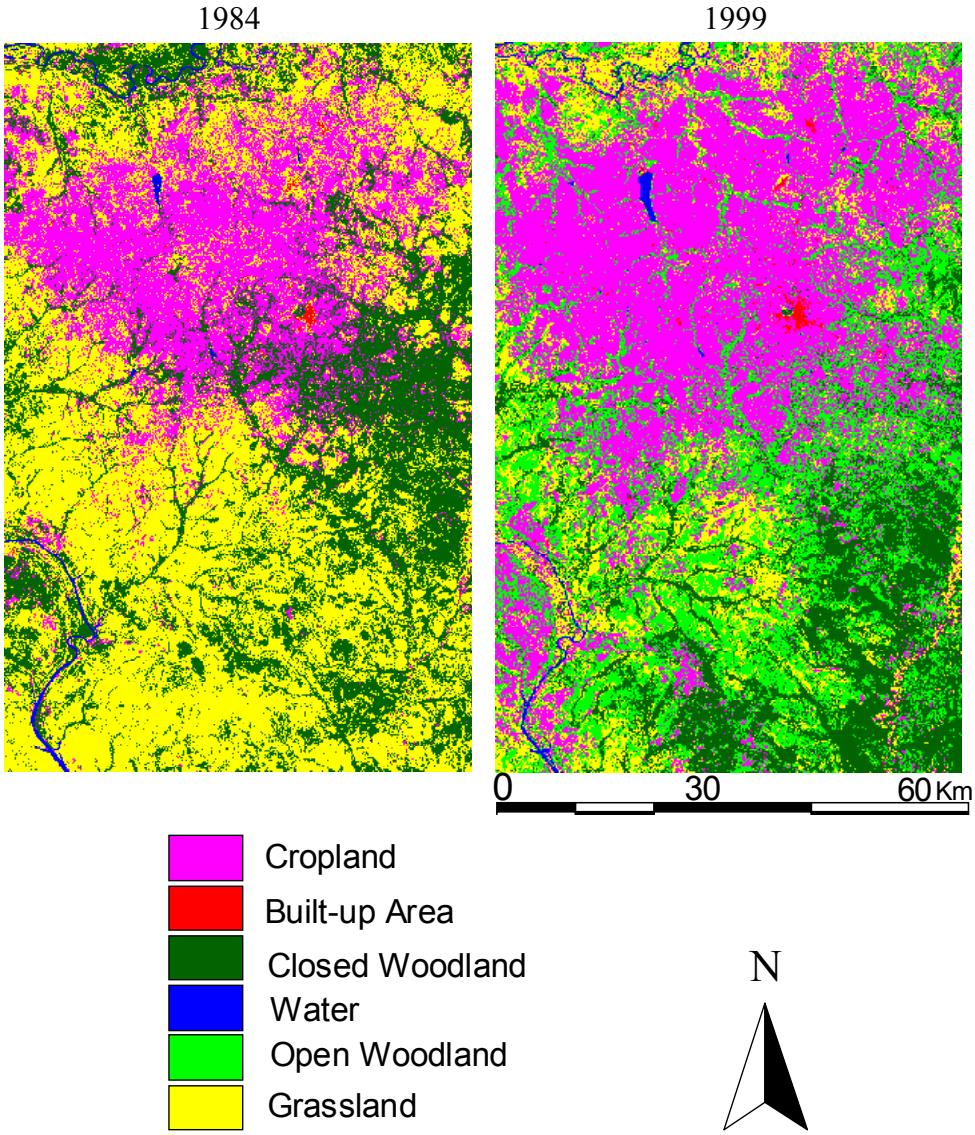

Figure 3.1 Land use and land cover maps of the study area in 1984 and 1999

The NDVI maps are a measure of biomass distribution over the study area. They are continuous data sets with each value indicating the relative amount of vegetation present per pixel. NDVI is calculated by subtracting the red from the near-infrared surface reflectance values to generate a vegetation index, and then dividing by their sum to normalize the values. Thus

$$\mathrm{NDVI} = \frac{\rho_{\mathrm{nir}} - \rho_{\mathrm{red}}}{\rho_{\mathrm{nir}} + \rho_{\mathrm{red}}},$$

where ρ_{red} and ρ_{nir} corresponds to red and near-infrared surface reflectance values, respectively. NDVI data values range between -1 and 1; with 0.5 indicating dense

vegetation and values less than zero indicating absence of vegetation. Water, typically, has NDVI value of less than zero; bare soils have values between 0 and 0.1; and vegetation has values over 0.1 (Grimes *et al*., 2003). Table 3.2 shows typical red and near-infrared reflectance values and corresponding NDVI for certain land cover types.

Table 3.2 Typical red and near-infrared reflectance values and corresponding NDVI values for certain land cover types

Land cover type	Red	Near-infrared	NDVI
Dense vegetation	0.100	0.500	0.667
Dry bare soil	0.269	0.283	0.025
Clouds	0.227	0.228	0.002
Snow and ice	0.375	0.342	-0.046
Water	0.022	0.013	-0.257

Source: Holben, 1986

Figure 3.2 shows the NDVI maps for 1984 and 1999.

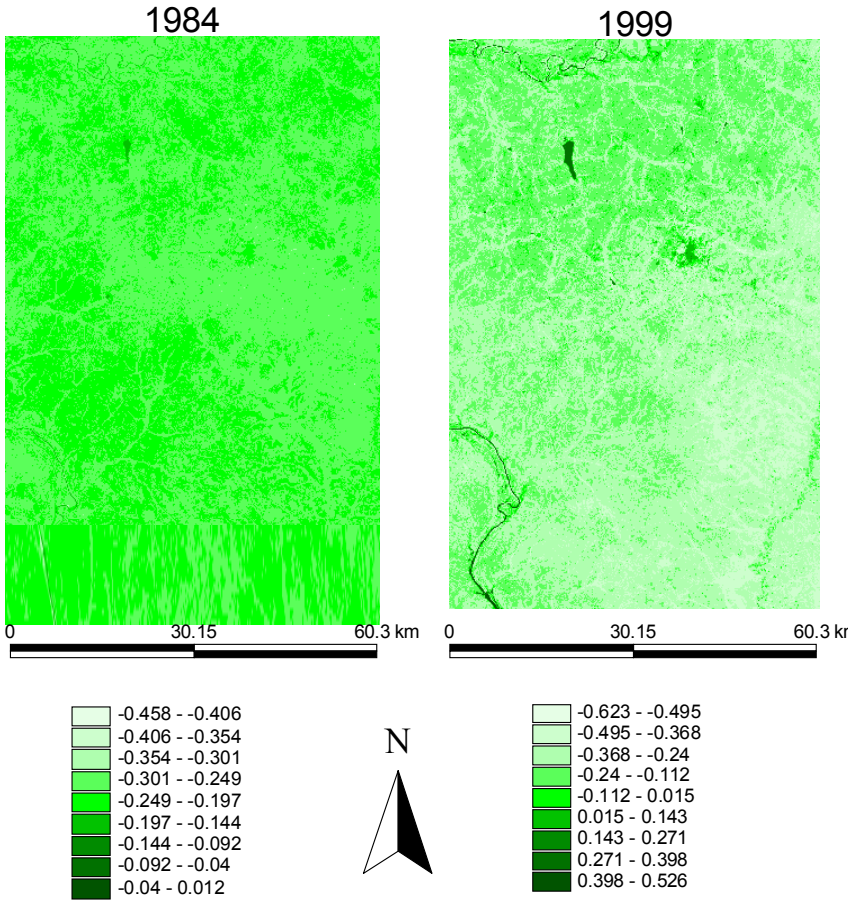

Figure 3.2 Normalized difference vegetation index maps of the study area

The DEM data set was processed by the Shuttle Radar Topography Mission global processor. It consists of terrain elevations in meters for ground positions at regularly spaced horizontal intervals of the study area. The DEM data set is shown in Figure 3.3.

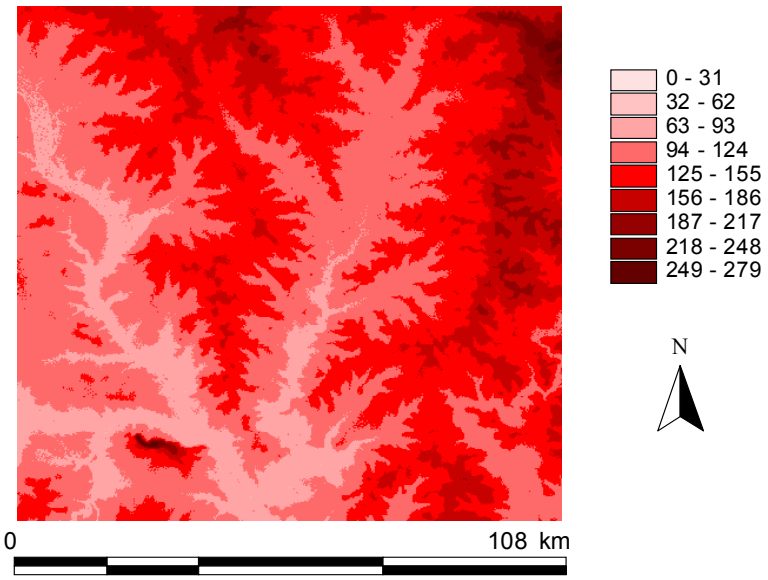

Figure 3.3 Digital elevation model of the study area

3.1.3 Data summaries

In this section, we compute summary statistics and construct descriptive graphs for members of each group of data set. These statistics will inform us about the central values, the spread and the shape of each of our research data sets. Table 3.3 shows summary statistics for the two NDVI data sets. For example, the minimum and maximum pixel values of NDVI84 are -0.4583 and 0.0124, respectively. NDVI84 has a mean value of -0.2507, with a standard deviation of 0.0109. Fifty percent of the pixel values lie between -0.2571 and -0.2437; while 25% lie below -0.2571 and another 25% above -0.2437. The kurtosis value of 7.6757 indicates that the distribution of the pixel values of NDVI84 is more outlier prone than the normal distribution (kurtosis of a normal distribution is 3). The skewness value of 0.2059 indicates that the distribution of NDVI84 is skewed to the right of the mean value of -0.2507 (skewness for a normal distribution is 0). NDVI99 is also more outlier prone than the normal distribution. However, it is more spread out than NDVI84.

Table 3.3 Summary statistics of the pixel values of the NDVI and DEM data sets

Statistic	NDVI84	NDVI99	DEM
Minimum value	−0.4583	−0.6230	0
First quartile	−0.2571	−0.3210	107
Median	−0.2498	−0.2667	125
Mean	−0.2507	−0.2623	128
Third quartile	−0.2437	−0.2111	145
Maximum value	0.0124	0.5259	279
Standard deviation	0.0109	0.0909	28
Coefficient of variation	−0.0435	−0.3465	0.2215
Skewness	0.2059	1.5034	0.6243
Kurtosis	7.6757	8.5559	0.7087

It was observed from scatter plots of NDVI84 and NDVI99 that most of the values of NDVI84 lie between -0.35 and -0.15, with only a few lying outside this range. NDVI99 appeared to have fewer outliers compared to NDVI84. The minimum value as well as larger values (> 200 m) of DEM appears to be outliers as shown in box plot in Figure 3.4. The mean elevation is 128 meters with a standard deviation of 28. The distribution of DEM is slightly skewed to the right of the mean and less outlier prone compared to the normal distribution.

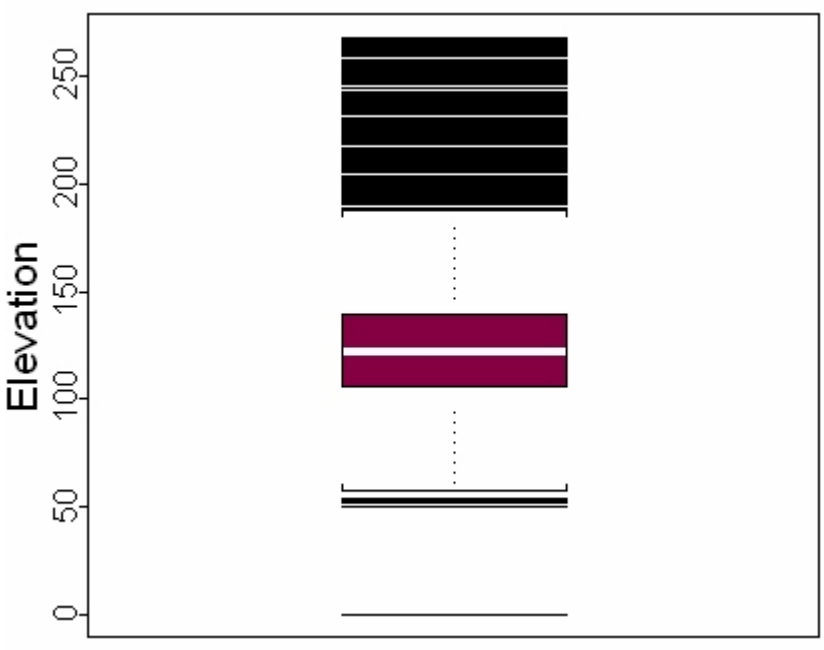

Figure 3.4 Box plot of the digital elevation model data set

Table 3.4 is a frequency table of the LULC data. It shows the number of cells of each land cover type and the percentage of the total number of cells in each data it represent.

Table 3.4 Frequency of classes in the land use and land cover maps

Land use land cover type	Frequency in LULC84		Frequency in LULC99	
	Count	%	Count	%
Closed Woodland	1,765,008	28.20	1,106,936	17.69
Open Woodland	1,565,005	25.00	1,702,071	27.19
Grassland	1,449,563	23.16	899,604	14.37
Cropland	1,407,994	22.50	2,473,423	39.52
Built-up Area	32,224	0.51	35,680	0.57
Water	39,346	0.63	41,426	0.66

For both LULC84 and LULC99, Built-up Area is the least abundant class. It represents less than 1% of the total number of cells. Water also represents less than 1% of the cells in both LULC84 and LULC99. Closed Woodland is the most abundant in the LULC84, representing over 28% of the total number of cells; whilst Cropland is the most abundant in the LULC99, representing almost 40% of the total number of cells. From Figure 3.5, we observe that the proportions of Closed Woodland and Grassland in LULC84 exceed those in LULC99; while the proportions of Open Woodland and Cropland in LULC99 exceed those in LULC84. The differences in the portions of Built-up Area and Water in the two data are not significant.

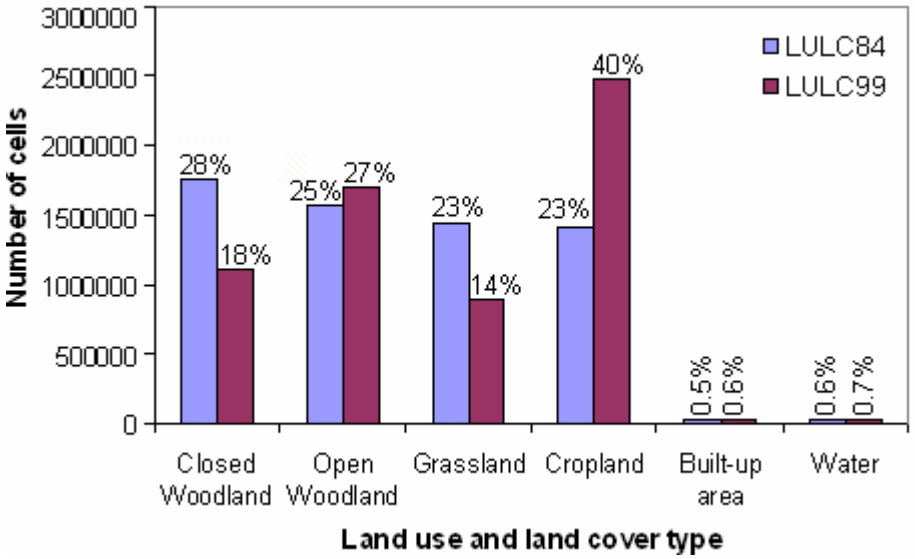

Figure 3.5 Bar chat of land use and land cover types of LULC84 and LULC99

3.1.4 Problems with the data sets

Though very large, the volume of each data set did not pose much problems in the research; rather it is their dimensions that posed problems in the sections on wavelet analysis. By definition, an orthogonal wavelet transform requires that the size N of the data is a power of two: $N = 2^J$ for some integer $J > 0$ (Vidakovic and Mueller, 1994; Ogden, 1997). To employ the orthogonal wavelet transform, therefore, requires that each data set is a square matrix whose side is a power of two. Unfortunately, the size of our data sets did not meet this requirement; they are either 3114×2010 data matrices (in the case of LULC and NDVI maps), or 1202×1202 data matrix (in the case of DEM).

In practice, a common way to precondition data sets to meet the orthogonal wavelet transform requirement is to "pad with zeros", that is, to increase the size of the data set to the next larger power of two (Ogden, 1997). This would mean that each of the 3114×2010 data sets would now become 4096×4096, with several row and column entries all being zeros. Though some researchers prefer this remedy, we shall not use it for the following reasons:

1. To some extent the scheme "dilutes" the data sets near its boundaries, since wavelet coefficients will have zeros averaged into their computations.
2. Orthogonality of the wavelet transform is not strictly maintained; because the filters are not applied evenly (multiplying a signal element of magnitude zero is equivalent to omitting the filter coefficient).

Rather than padding the original data sets with zeros, some rows and columns at the edges were "cut off" to obtain 1024×1024 (i.e. $2^{10} \times 2^{10}$) dimension data sets. Thus, throughout the sections on wavelet analysis, the term data set is used to mean 1024×1024 portion of an original data set.

3.2 Analysis of moving window statistics of NDVI and DEM data sets

It is common with large environmental data sets such as ours, that data values in some regions are more variable than in others. Statistically, such an anomaly in the variability of a data set is called *heteroscedasticity* (Isaaks and Srivastava, 1989). Such anomalies may have serious implications on estimations from the data sets, and so need to be

identified. The computation of summary statistics within moving windows is frequently used to investigate anomalies both in the average value and in variability. The area under study was divided into several local neighborhoods of equal sizes and then summary statistics within each local neighborhood were computed for analysis.

3.2.1 Size of the moving window

The size of the moving window depends on the coefficient of variation of the data set. If the coefficient of variation is very large, more data points will be required to obtain reliable statistics. For example, if the coefficient of variation is greater than 1, then perhaps as many as 20 to 50 data points per window may be required to compute reliable statistics. The size of the moving window also depends on the average spacing between data points and on the overall dimensions of the study area. There is the need to have relatively large windows to allow enough data points within each window to facilitate computation of reliable statistics. On the other hand, if the size of the windows is too large then there will not be enough of them to identify anomalous localities (Isaaks and Srivastava, 1989). There is, therefore, the need to find a compromise between the need for large windows (to ensure reliable statistics) and the need for enough number of windows (to help identify local anomalies). This compromise is usually found in overlapping the windows so that two adjacent neighborhoods have some data values in common. Overlapping is useful for small data sets or data sets which do not have uniform spacing; however, it is not necessary for large and regular grid data sets such as ours.

To determine the appropriate size of moving windows for investigating heteroscedasticity, the coefficient of variation for each data set was computed. The magnitude of the coefficient of variation for both NDVI data sets was greater than 1, indicating the need for several data points for the estimation of reliable statistics. By experimenting with different sizes, we decided on moving windows of size 5 km long and 5 km wide in a 19×12 grid data layout. This dimension allows for an average of approximately 27,452 data points in each window, enough for the computation of reliable statistics. The dimension also leads to 228 moving windows, enough for the identification of local anomalies.

3.2.2 Proportional effect

Anomalies in the local variability have an impact on the accuracy of estimates from the entire data set. The prospects for accurate estimates are quite good if the data points in the study area are uniform. On the other hand, local estimates are likely to be poor if the data points fluctuate wildly in the study area. This will be the case irrespective of the estimation method one chooses; estimates from any reasonable method will benefit from low data variability and suffer from high data variability. There are four possible relationships that can occur between the local average and the local variability.

1. The local average and the local variability are both constant.
2. The local average changes while the local variability remains constant.
3. The local average remains constant while the local variability changes.
4. The local average and the local variability both change together.

For purposes of estimation, the first two cases are ideal. Estimates from any particular locality will be as good as estimates from elsewhere, if the local variability remains constant. In most environmental data sets, however, variability changes from one locality to the other. It is therefore preferable to have the fourth scenario; where the local variability is related to the local average and is, therefore predictable. If a relationship exists between the local average and the local variability, it is generally referred to as a *proportional effect*. In this section, we wish to investigate anomalies in the average value and in the variability, as well as the presence or absence of a proportional effect in the study area. To investigate the data sets for heteroscedasticity and proportional effects, the mean and standard deviation of the pixel values in each of the 228 local windows were computed for analysis. The results and discussion of the analysis are presented in Section 4.1.

3.3 Analysis of wavelet variance

In many areas of scientific research, investigators determine to a large extent how research data sets are collected. However, in the field of satellite remote sensing the resolution of a given sensor is fixed *a priori*; thereby making the scale of measurement inflexible (Brunsell and Gillies, 2003). This poses some difficulty when the dominant scales for a given process are not known. It is, therefore, necessary and important to

estimate and investigate what the dominant scales within an image are. Also, the first step toward examining the scaling characteristics of a data set is to calculate the length scale, which is defined as the scale with the highest wavelet variance (Kumar and Foufoula-Georgiou, 1997). These reasons warrant wavelet variance analysis of the data sets.

Wavelet variance analysis is a method for the partitioning of the sample variance of an image data set into portions that are associated with the different scales of the image. This type of analysis tells us what scales are important contributors to the overall variability of an image data set (Constantine and Percival, 2002). The wavelet variance is of interest for the following reasons.

1. The wavelet variance offers a scale-by-scale decomposition of the variability in a data set, therefore, it has considerable appeal for researchers studying processes that exhibit fluctuations over a range of different scales. The square root of the wavelet variance has the same units as the original data, which make its more easily interpretable.

2. For certain stationary processes, the sample variance of a time series, namely,

$$\hat{\sigma}_X^2 \equiv \frac{1}{N}\sum_{t=0}^{N-1}\left(X_t - \overline{X}\right)^2, \quad \text{where } \overline{X} \equiv \frac{1}{N}\sum_{t=0}^{N-1} X_t ,$$

can grossly underestimate the process variance σ_X^2 even when the sample size N is quite large. For such processes, the wavelet variance is a useful substitute because it replaces the problematic notion of a 'global' variance with a sequence of variances over particular scales, for which we can readily formulate unbiased estimators. In addition, the wavelet variance is well-defined and can be easily estimated for certain nonstationary processes for which the variance is either infinite or an ever increasing function of the sample size. In this section, we explore this wavelet-based analysis of variance of the NDVI and DEM data sets by estimating and investigating their wavelet variances. We begin with a formal definition and a brief review of the background theories for the estimation of wavelet variance.

3.3.1 Definition of wavelet variance

We adopt the definition by Percival and Walden, 2000. Let

$$\{\widetilde{h}_{j,l} : l = 0,\ldots, L_j - 1\}$$

be the *j*th level maximal overlap discrete wavelet transform (MODWT) filter associated with scale $\tau_j = 2^{j-1}$, where $L_j \equiv (2^j - 1)(L-1) + 1$ is the width of the filter and $j = 1, 2, 3, \ldots$. Let

$$\{X_t : t = \ldots, -2, -1, 0, 1, 2, \ldots\}$$

represent a discrete parameter real-valued stochastic process, that is, a collection of random variables indexed by the set of all integers. Define the level *j* MODWT wavelet coefficients for this process as

$$\overline{W}_{j,t} \equiv \sum_{l=0}^{L_l - 1} \widetilde{h}_{j,l} X_{t-l}, \qquad t = \ldots, -2, -1, 0, 1, 2, \ldots.$$

If it exists and is finite, the time-dependent wavelet variance for scale τ_j is defined to be the variance of $\overline{W}_{j,t}$; i.e.,

$$v^2_{X,t}(\tau_j) \equiv \mathrm{var}\{\overline{W}_{j,t}\}.$$

If we assume that the width of the wavelet filter is $L \geq 2d$, where *L* is its width and *d* is its number of backward differences, then $v^2_{X,t}(\tau_j)$ will be finite and independent of time. If *L* is large enough we will have $E\{\overline{W}_{j,t}\} = 0$, so that

$$v^2_X(\tau_j) = \mathrm{var}\{\overline{W}_{j,t}\} = E\left\{(\overline{W}_{j,t} - E\{\overline{W}_{j,t}\})^2\right\} = E\left\{\overline{W}^2_{j,t}\right\}.$$

3.3.2 Estimation of wavelet variance

Suppose the series $X_0, X_1, \ldots, X_{N-1}$ is a portion of a stochastic process $\{X_t\}$. Let $\{\widetilde{h}_l\}$ be a MODWT wavelet filter of width *L*, and assume that $\{X_t\}$ satisfies conditions such that the wavelet variance $v^2_X(\tau_j)$ for scale $\tau_j = 2^{j-1}$ based upon this filter is finite and

independent of time. Let $L_j \equiv (2^j - 1)(L-1) + 1$ be the width of the equivalent MODWT filter $\{\widetilde{h}_{j,l}\}$ for level j. Then the unbiased MODWT estimator of the wavelet variance is defined as

$$\hat{\nu}_X^2(\tau_j) \equiv \frac{1}{M_j} \sum_{t=L_j-1}^{N-1} \widetilde{W}_{j,t}^2 ,$$

where $\widetilde{W}_{j,t}$ is the MODWT wavelet coefficient at level j and time index t, and $M_j \equiv N - L_j + 1$, with $M_j \geq 1$ (Percival and Walden, 2000). The unbiased wavelet variance estimator uses only the last M_j and avoids the first $L_j - 1$ coefficients on each level because they are boundary coefficients. When all N MODWT wavelet coefficients are used, we obtain a biased MODWT estimator of the wavelet variance which is given by

$$\hat{\nu}_X^2(\tau_j) \equiv \frac{1}{N} \sum_{t=0}^{N-1} \widetilde{W}_{j,t}^2 .$$

Though the DWT can be used to formulate estimators of the wavelet variance, the MODWT is preferred because their estimators are known to have superior sampling properties (Percival and Walden, 2000).

3.3.3 Distribution of the wavelet variance estimator

An approximation to the distribution of the unbiased MODWT wavelet variance estimator $\hat{\nu}_X^2(\tau_j)$ has been worked out and can be used to assess its sampling variability and to obtain confidence intervals for the true wavelet variance $\nu_X^2(\tau_j)$ (see Percival and Walden, 2000, for details). This approximation is based on the assumption that the statistic $\hat{\nu}_X^2(\tau_j)$ has a distribution that is equal to a random variable given by the product of a chi-square random variable χ_η^2 with η degrees of freedom and the constant $\hat{\nu}_X^2(\tau_j)/\eta$. The starting point for this approximation is to note that, if we have M independent and identically distribution Gaussian random variables with mean zero, then the sum of their squares forms a random variable whose distribution is given by

the product of a chi-square random variable χ^2_M with M degrees of freedom and a constant. By assumption, the MODWT wavelet coefficients $\overline{W}_{j,t}$ that we use to form $\hat{\nu}^2_X(\tau_j)$ are Gaussian random variables with mean zero and variance $\nu^2_X(\tau_j)$; however, because these coefficients are in general correlated with each other, their sum of squares is not a chi-square random variable with M_j degrees of freedom.

We can adjust for this correlation by setting η equal to a value such that the random variable $\nu^2_X(\tau_j)\chi^2_\eta/\eta$ has the same theoretical variance as $\hat{\nu}^2_X(\tau_j)$. By appealing to a large sample approximation, we can obtain a good approximation to this theoretical variance. In this approach, η is known as the *equivalent degrees of freedom* (EDOF) and in effect becomes a parameter that we need to determine somehow. The Splus wavelets module which is used in this research supports three different modes for setting the EDOF, η.

1. EDOF, $\hat{\eta}_1$ (based upon large sample theory):

$$\hat{\eta}_1 = \frac{M_j \hat{\nu}^4_X(\tau_j)}{\hat{A}_j}, \tag{3.1}$$

where

$$\hat{A}_j \equiv \frac{\hat{\nu}^4_X(\tau_j)}{2} + \sum_{\tau=1}^{M_j-1} \hat{s}^2_{j,\tau}$$

and $\hat{s}_{j,\tau}$ is a sample lag τ autocovariance defined by

$$\hat{s}_{j,\tau} \equiv \frac{1}{M_j} \sum_{t=L_j-1}^{N-1-|\tau|} \widetilde{W}_{j,t}\widetilde{W}_{j,t+|\tau|}, \qquad 0 \le |\tau| \le M_j - 1.$$

2. EDOF, $\hat{\eta}_2$ (based on the assumption that the shape of the spectral density function (SDF) for $\{X_t\}$ is known *a priori*):

$$\hat{\eta}_2 = \frac{2\left(\sum_{k=1}^{(M_j-1)/2} C_j(f_k)\right)^2}{\sum_{k=1}^{(M_j-1)/2} C_j^2(f_k)}, \tag{3.2}$$

where $f_k \equiv k/M_j$ and $C_j(f) \propto \widetilde{H}_j^{(D)}(f) S_X(f)$. That is, the product of the squared gain functions for the Daubechies MODWT equivalent wavelet filter $\{\widetilde{h}_{j,l}\}$ for level j and the SDF for $\{X_t\}$ (assumed to be known up to a constant of proportionality).

3. EDOF, $\hat{\eta}_3$ (large sample approximation based on a band-pass approximation):

$$\hat{\eta}_3 = \max\{M_j / 2^j, 1\}. \tag{3.3}$$

Once η has been set to $\hat{\eta}_1$, $\hat{\eta}_2$ or $\hat{\eta}_3$, we can calculate an approximate 100(1-2p)% confidence interval for $\nu_X^2(\tau_j)$ via

$$\left[\frac{\eta \hat{\nu}_X^2(\tau_j)}{Q_\eta(1-p)}, \frac{\eta \hat{\nu}_X^2(\tau_j)}{Q_\eta(p)} \right],$$

where $Q_\eta(p)$ is the $p \times 100\%$ percent point for the chi-square distribution with η degrees of freedom (setting $p = 0.025$ yields an approximate 95% confidence interval).

We computed the wavelet variance for the DEM and NDVI data sets, plotted them against corresponding resolutions and used the graphs to investigate whether these data sets exhibit simple scaling or multiple-scale structure. We also computed 95% confidence intervals for the wavelet variance at each scale using Equations (3.1) to (3.3). A discussion of the results of the analysis is presented in Section 4.2.

3.3.4 The choice of suitable wavelet filter

It is always important to select the wavelet that will best suit a particular analysis. There are many different wavelet functions with varying characteristics and functionality. However, there are no hard and fast rules for a choice for any particular analysis (Bruce and Gao, 1996). In selecting a wavelet for an analysis, it is reasonable to examine its properties against the data set to be analyzed and the overall aims of the study. For many applications, the wavelet function must be sufficiently smooth to efficiently represent the characteristics of the underlying data set. Generally, smoothness is inversely related to the support width; very compact wavelets are less

smooth. It is also known that very compact wavelets such as the Haar are very well localized in time and space, but have poor frequency resolution (Bruce and Gao, 1996). Another important attribute of wavelets is their ability to conserve of energy. During a wavelet transformation process, the total energy of the data set is divided up between the approximation and detail coefficients; thus no energy is lost or gained. The energy of a data set is the amount of information it contains. It is proportional to the sum of squares of the pixel (or intensity) values. Thus, the energy in the wavelet transform of a data set is the sum of the squares of the wavelet coefficients.

The Daubechies wavelets are known to be good in terms of their compact representation of signal details; however, they are not efficient in the representation of signal approximation at a given resolution (Reza, 1999). Furthermore, a number of top researchers in wavelets and scaling issues (e.g. Kumar & Foufoula-Georgiou, 1993a, b; Hu *et al*., 1998; Brunsell and Gillies, 2002) preferred to use the Daubechies wavelet for the fact that they are continuous, compact and orthogonal. For these reasons and also based on observations from preliminary analysis, the Daubechies "d6" (i.e. the Daubechies wavelet with a width of 6) was selected as the most suitable for this aspect of the research. However, the Haar wavelet (the first known wavelet) would also be employed to allow for comparison. Figure 3.6 shows the "d6" mother wavelet (or wavelet function) and its corresponding father wavelet (or scaling function). The graph of the Haar wavelet function is shown in Figure 2.3.

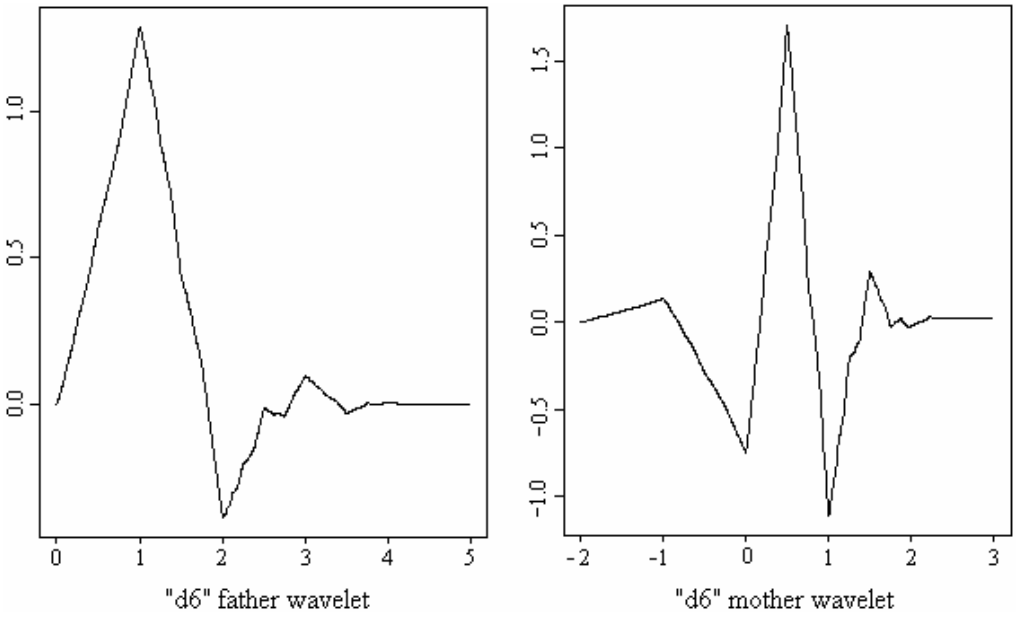

Figure 3.6 Graphs of the "d6" father and mother wavelets

3.4 Determination of scaling behavior of data sets with wavelets

A characteristic feature of remote sensing data sets is that they are extremely variable over temporal and spatial and scales. Therefore, a major challenge to ecologists, hydrologists, meteorologists and climatologists is to measure, model and predict the nature of these variability over different scales. To achieve these, it is necessary to determine the changes in spatial patterns as the resolution of a data set is changed; hence the need for determining the *scaling behavior* of a data set. Scaling behavior refers to the statistical variation (e.g. statistical self-similarity, multiscaling, etc) of a data set across different spatial scales; while scaling characteristics are the parameters necessary to describe such scaling behavior. In other words, the scaling characteristics provide appropriate formulation for the assimilation of remotely sensed data sets into large-scale models. Statistical self-similarity (or simple scaling) is observed when a data set follows a power law spectrum; otherwise we have multiscaling.

Wavelet transforms are preferred because of their key advantage over other forms of analysis: that is, their ability to allow for the breakdown of a data set into a scale frequency space. This permits easy determination of the relative contribution of different spatial scales present within a data set. An additional benefit of the wavelet transform is that, if a process exhibits self-similar scaling behavior, the wavelet coefficients obtained through a wavelet transform preserve that self-similarity (Kumar and Foufoula-Georgiou 1993(a) & 1993(b)). Due to the preservation of this behavior, wavelet coefficients allow for a convenient method of analyzing the fluctuations between spatial resolutions within a data set. If a process does not show self-similar behavior, this methodology still permits analysis of the actual scaling behavior through a multiscaling framework.

3.4.1 Definition of statistical self-similarity

Let $\{Y(\mathbf{x})\}$ be an arbitrary stochastic field indexed by the vector $x \in \Re^d$, where $\Re^d$ is a *d*-dimensional real space. Then $\{Y(\mathbf{x})\}$ is statistically self-similar if for any arbitrary set of points $\mathbf{x}_1, \mathbf{x}_2, \mathbf{x}_3, \ldots, \mathbf{x}_n$, the following equality holds in the joint probability distribution of $\{Y(\mathbf{x})\}$:

$$P\left[Y(\lambda \mathbf{x}_1) < y_1, \ldots, Y(\lambda \mathbf{x}_n) < y_n\right] = P\left[\lambda^{H\theta} Y(\mathbf{x}_1) < y_1, \ldots, \lambda^{H\theta} Y(\mathbf{x}_n) < y_n\right], \quad (3.4)$$

where λ is a positive real scaling factor and H_θ is a real scaling exponent. Self-similar processes that are scaling in the sense of Equation (3.4) are usually termed strict-sense simple scaling. Simple scaling indicates that there is only one scaling exponent H_θ for the process. Strict means that the content of scaling is in the sense of the probability distribution function, that is for all the moments. On the other hand, wide-sense simple scaling means only up to the second order moments. See Gupta and Waymire (1989, 1990) and references therein for detailed discussion of statistical self-similarity.

If the moments of a stochastic process exist, then from Equation (3.4) one consequence of simple scaling is:

$$E\left[Y^p(\lambda)\right] = \lambda^{pH_\theta} E\left[Y^p(1)\right]. \tag{3.5}$$

Gupta and Waymire (1990) demonstrated another important consequence of simple scaling: log–log linearity between moments and the scaling factor λ. Thus, taking the logarithmic transform of Equation (3.5), we obtain:

$$\log m_p(\lambda) = s(p)\log\lambda + \log m_p(1), \tag{3.6}$$

where p is the order of the moments, $m_p(\lambda) = E\left[Y^p(\lambda)\right]$ and $s(p) = pH_\theta$. Thus for a simple scaling process, the following two conditions must be satisfied simultaneously:

1. log– log linearity in log $\log m_p(\lambda)$ versus $\log\lambda$ for each moment of order p;
2. linearity of the slope change $s(p) = pH_\theta$ with order of moment.

This means that to ascertain statistical self-similarity of a data set, we need to show that higher order moments follow power law spectrum as a function of increasing scales; and that the scaling exponents show a linear relationship with the order of moment. If the wavelet coefficients in the three directions exhibit simple scaling, the scaling exponents need not be the same. In the event that a data set is isotropically self-similar, the scaling exponents are the same (Kumar and Foufoula-Georgiou, 1993b). The difference in the values of scaling exponents helps to characterize differences in the dependence structure of a data set in the three directions. Departures from simple

scaling are termed multiscaling, which is indicated if $s(p)$ is a non-linear function of the order of moment (Hu *et al*., 1998).

3.4.2 Determination of statistical self-similarity of wavelet coefficients

Orthogonal wavelets were employed to decompose each data set into approximation and detail coefficients to allow for multiresolution analysis of the self-similarity nature, or otherwise, of the wavelet coefficients. Multiresolution analysis was conducted for seven levels of decomposition using the Daubechies "d6" wavelet. The decomposition resulted in one approximation or residual image ($J = 7$) and detailed coefficients in each of the horizontal, vertical and diagonal directions at each level of decomposition. To examine the self-similar nature of the data sets, the first four statistical moments (mean, variance, skewness and kurtosis) were calculated from the wavelet coefficients produced by the multiresolution at each level of decomposition and in each direction of the detail coefficients. The slope $s(p)$ in Equation (3.6) was estimated using linear regression from a plot of logarithm of moments versus logarithm of resolution. The estimated slope terms from the regression models were then used to examine the scaling behavior in each of the three directions that wavelet coefficients were produced. Linear regression was again used to examine the relationship between the estimated slope terms and order of moment. The results are presented and discussed in Sec. 4.3.

3.5 Indirect multiscale analysis of pattern metrics

Landscape pattern is spatially correlated and scale-dependent. Therefore, to understand the structure and functioning of landscape requires multiscale information. Scaling functions are the most precise and concise way of quantifying multiscale characteristics explicitly. The indirect approach to multiscale analysis employs methods that are designed for single-scale analysis such as landscape metrics. The scale multiplicity in the indirect approach is realized by resampling the data set at different scales, according to grain or extent, and then repeatedly computing the landscape metrics using the resampled data set at different scales. In this section, the existence of scaling relations for 18 landscape metrics (see Section 2.3) of the LULC data sets when measured over a wide range of scales are explored. An outline of the steps in the aggregation procedure

is given, as well as explanation of how landscape metrics will be estimated from maps with changing grain size and extent.

3.5.1 Description of aggregation procedure

Several different methods have been used over time for resampling data sets, common among them being the aggregation methods – the *mean*, *median*, *majority*, *maximum*, *minimum* and *sum* aggregation methods (Jansen and Kelker, 1998). The aggregation methods are more simple and easy to employ than the fractal and geostatistics methods which are more intricate and robust. During an aggregation process, an input $m \times n$ grid data set is systematically resampled to produce a hierarchically nested and a coarser resolution data set based on a method of choice. Given a grid data set, the mean method involves finding the mean value over a $n \times n$ pixel window and replacing the pixel values in the window with the single mean to form a data set of coarse resolution. The process is said to smooth the variance and increase spatial autocorrelation of the data set.

The median method is similar to that of the mean; it uses the median of the values in the pixel window instead of the mean. The majority rule assigns the modal pixel value in the $n \times n$ window. If the window has two or more modes, the assignment is random. The majority rule systematically reduces the representation of less abundant land use and land cover type. The maximum (minimum) method involves replacing the values in an $n \times n$ pixel window with the maximum (minimum) of all the values to form a coarser data. According to Bian (1997), the process may alter the spatial pattern including spatial autocorrelation at coarser resolutions. The maximum (minimum) aggregation method is likely to create bias since smaller (larger) values are not factored into the representation. The sum aggregation method involves finding the arithmetic total of all the values that fall in a $n \times n$ pixel window.

The processes involved in any aggregation can be summarized in the following 4 steps:

Step 1: Multiply the cell resolution of the input grid by the cell factor to obtain the cell resolution of the output grid.

Step 2: Map the spatial extent of the output cells onto the input grid

Step 3: Identify the cells on which to perform the aggregation calculations – cell locations from the input grid that fall within the extent of an output cell must be included in the calculations for determining that cell's output value.

Step 4: Calculate the output value by using the specified method and the values in the cells from the input grid that fall within the output cell's spatial extent.

3.5.2 Estimation of landscape metrics from maps with changing grain size

To estimate the landscape metrics of LULC84 and LULC99 for different grain sizes, the grain size of the original maps was systematically changed through 18 separate aggregation levels; from the finest 1×1 (or 1 original pixel forming an aggregate) through to the coarsest 50×50 (or 2500 original pixels forming an aggregate) while the extent was kept constant. The grain size of each of the two landscape data sets was changed using the "majority" (or mode) aggregation method. Each new map was created by directly aggregating the original data set instead of using the cumulative procedure in which the aggregation at the next grain size is based on the preceding aggregated data set. In other words, we preferred the "independent" to the "iterative" aggregation scheme. When the grain size could not wholly divide the number of rows or columns of the data set during an aggregation, the remainder of rows or columns at the edge was excluded from the new map. This omission of edge rows and/or columns did not seem to be a problem as long as the extent/grain ratio was sufficiently large. In all, 36 maps (2 land use and land cover maps × 18 grain size levels) were used to investigate the effect of changing grain size on landscape metric. Table 3.5 summarizes the features of the set of maps created from each original map. The landscape pattern analysis software, FRAGSTATS 3.3 (McGarigal and Marks, 2002), was used to compute all 18 landscape metrics for each of the 36 maps. The four-neighbor rule was applied in each case.

Table 3.5 Features of maps used to investigate the effects of changing grain size on landscape metrics

Grain size	Resolution (m)	Number of rows	Number of columns
1×1	30	3114	2010
2×2	60	1557	1005
3×3	90	1038	670
4×4	120	779	503
5×5	150	623	402
6×6	180	519	335
7×7	210	445	287
8×8	240	389	251
9×9	270	346	223
10×10	300	311	201
15×15	450	208	134
20×20	600	156	101
25×25	750	125	80
30×30	900	104	67
35×35	1050	89	57
40×40	1200	78	50
45×45	1350	69	45
50×50	1500	62	40

The majority rule is the most commonly used in ecological and remote sensing applications. This is evident in the fact that several recent studies in these areas (Turner *et al*., 1989; Wu *et al*., 2002; Shen *et al*., 2004; Wu, 2004) only used the majority rule, although there are other rules for aggregating spatial data. We wish to employ two more aggregation rules (mean and median) and then compare how the different aggregation rules affect landscape metrics. In this regard, the procedure for changing the grain size was repeated using the mean and median aggregation rules respectively. In total, 108 landscape maps (2 land use and land cover maps × 3 aggregation methods ×18 grain size levels) were analyzed for the purpose of investigating the effect of changing aggregation method on landscape metrics. The effects of changing grain size on landscape metrics are presented and discussed in Section 4.4; while those on changing the method of aggregation are presented and discussed in Section 4.5.

3.5.3 Estimation of landscape metrics from maps with changing extent

To estimate the landscape metrics of LULC84 and LULC99 with different extents, we systematically increased the extent of the maps while keeping the grain size constant.

Nine maps with different extents ranging from $56\,km^2$ to $5{,}633\,km^2$ were clipped from each of LULC84 and LULC99. Starting from the south-western corner and traversing the diagonal to the north-eastern corner, maps with increasing extents were clipped from each original landscape map. The increment in the extents was in the ratio of 1:10 to the extent of the original maps. In all, 18 maps (2 land use and land cover maps × 9 extent levels) were used in this aspect of the study. Table 3.6 summarizes the features of the set of maps created from each original map.

Table 3.6 Features of maps used to investigate the effects of changing extent on landscape metrics

Map	No. of cells in row	No. of cells in column	Area of extent (sq. km)	Ratio to original extent
1	311	201	56	1:10
2	23	402	225	2:10
3	934	603	507	3:10
4	1246	804	902	4:10
5	1557	1005	1408	5:10
6	1868	1206	2028	6:10
7	2180	1407	2761	7:10
8	2491	1608	3606	8:10
9	3114	2010	5633	1: 1

Based on the initial findings from the wavelet multiscale analysis, the effects of the direction in which the extents were clipped from the original maps were further investigated. To do this, landscape maps with different extents were clipped using each of the four corners of the original landscape map as a starting point and proceeding in the direction of the diagonal.

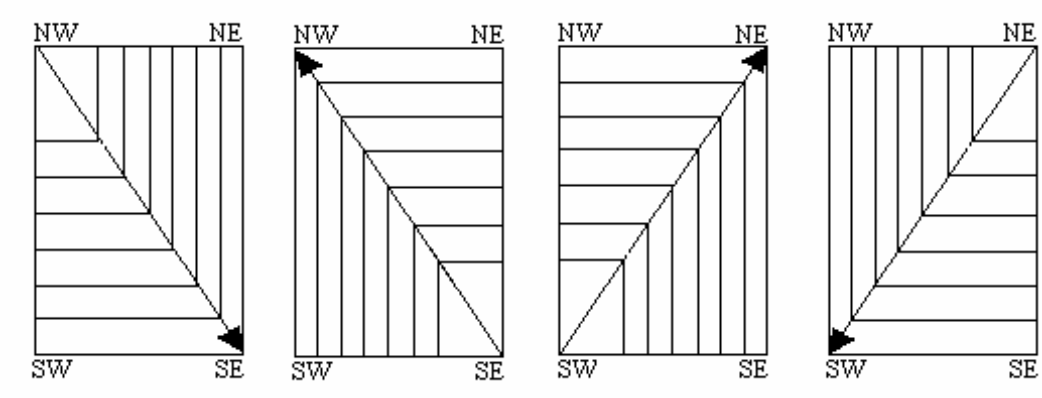

Figure 3.7 Schematic representation of changing the direction of analysis with increasing extent

Figure 3.7 shows (from left to right) the clipping starting from the north-western, south-eastern, south-western and north-eastern corner respectively, and traversing diagonally. Because the maps were clipped in the shape of the original maps, the values of the indices for the four directions converged as the same largest extent was reached. In total, 72 landscape maps (2 land use and land cover maps × 4 directions of analysis × 9 extent levels) were analyzed for the purpose of investigating the effect of changing the direction of analysis on landscape metrics. The effects of changing extent on landscape metrics are presented and discussed in Section 4.6; while those on changing the direction of pattern analysis are presented and discussed in Section 4.7.

4 RESULTS AND DISCUSSION

4.1 Heteroscedasticity and proportional effect in NDVI and DEM data sets

The mean and standard deviation of the pixel values in each of the 228 local windows of NDVI84 and NDVI99 were computed (see Table 7.1, Appendix I) to provide a measure of the average value and a measure of the variability, respectively.

It was observed that the mean and the standard deviation values changed locally across the study area, with the mean values changing slightly more than the standard deviation values for both NDVI data sets. The mean values for NDVI84 had a range of 0.032, while the standard deviation values had a range of 0.016. For NDVI99, the range for the mean and standard deviation values were 0.263 and 0.204 respectively. These statistics also indicated that the mean values in NDVI99 varied more than those in NDVI84, just as the standard deviation values in NDVI99 varied more than those in NDVI84. Estimates of moving window coefficient of variations indicated that, generally, NDVI99 was more variable than NDVI84.

Figure 4.1 shows plots of local means and local standard deviations for NDVI84 and NDVI99. In (a), the trend of change in the mean values from locality to locality within NDVI84 is shown; while (b) shows the trend in the corresponding standard deviation values. The trends in mean and standard deviation values for NDVI99 are shown in (c) and (d) respectively. For NDVI84, it was observed that the mean values within the moving windows to the north and those to the south of the study area remained relatively constant; whereas those in the middle sector showed more variability (Figure 4.1(a)). However, there was a general decrease in the mean values for NDVI99 from the north to the south (Figure 4.1(c)), although the data points in the southern sector appear to be more variable. The standard deviation values for NDVI84 and NDVI99 showed similar patterns across the study area; apart from a few large values scattered across the study area, the variability of the standard deviation values remained fairly constant.

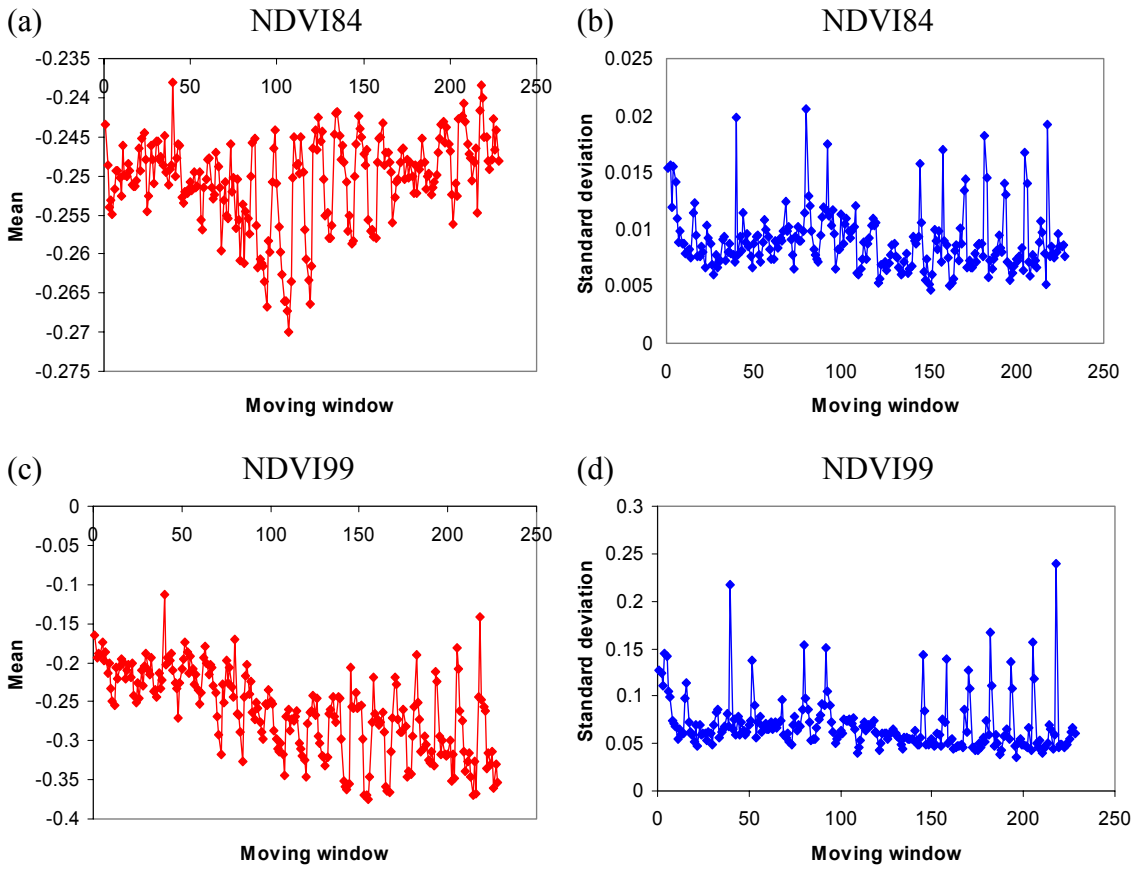

Figure 4.1 Plots of local means and local standard deviations of NDVI84 and NDVI99

Contour maps are very informative visual displays, as they reveal overall trends in data values. For each NDVI data set, two contour maps were produced; one showing moving window means and the other showing corresponding standard deviations. Ordinary kriging, which is a form of statistical modeling that interpolates data from a known set of sample points to a continuous surface, was employed to construct the contour maps. The means and standard deviations within the 228 $5\text{ km} \times 5\text{ km}$ moving windows for NDVI84 are contoured in Figure 4.2(a) and (b), respectively. It is observed from Figure 4.2(a) that the highest local means are concentrated in parts of the northern and south-western sectors, while the lowest are concentrated in the eastern parts of the middle belt of the study area. The distribution of the standard deviation showed mostly low values, with a cluster of large values in the south-western corner and another towards the north (Figure 4.2(b)).

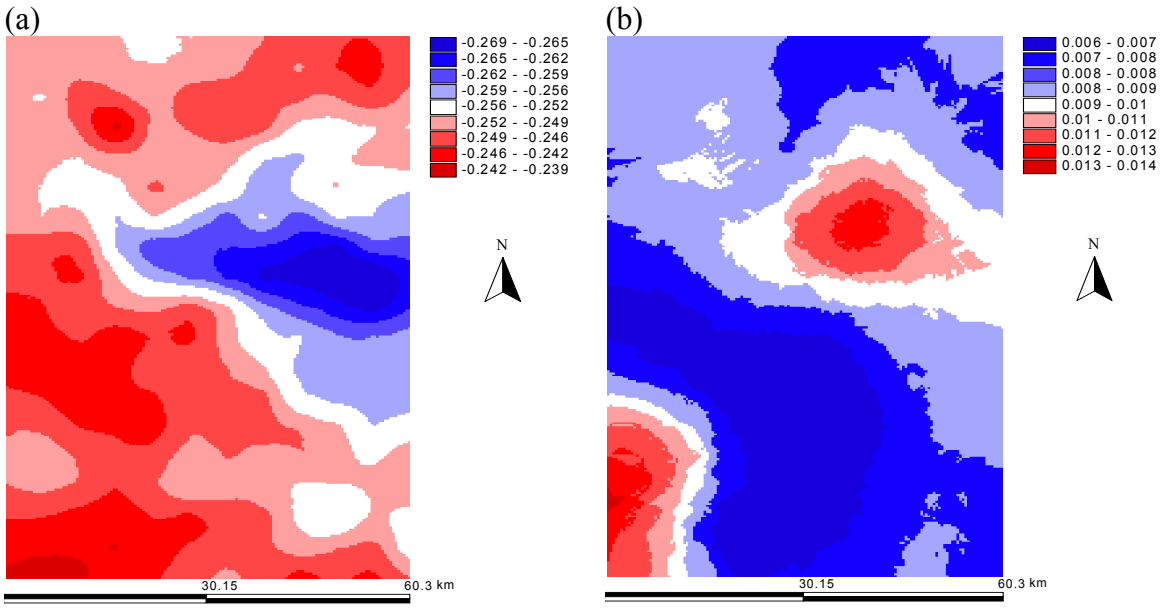

Figure 4.2 Contour maps of local means (a) and local standard deviations (b) of NDVI84

A comparison of the contour maps showed that the moving window means and standard deviations are less correlated, indicating lack of proportional effect. This result is confirmed by the correlation coefficient of the mean-standard deviation pairs, which is -0.23. Figure 4.3(a) is a scatter plot of moving window means against corresponding standard deviations of NDVI84.

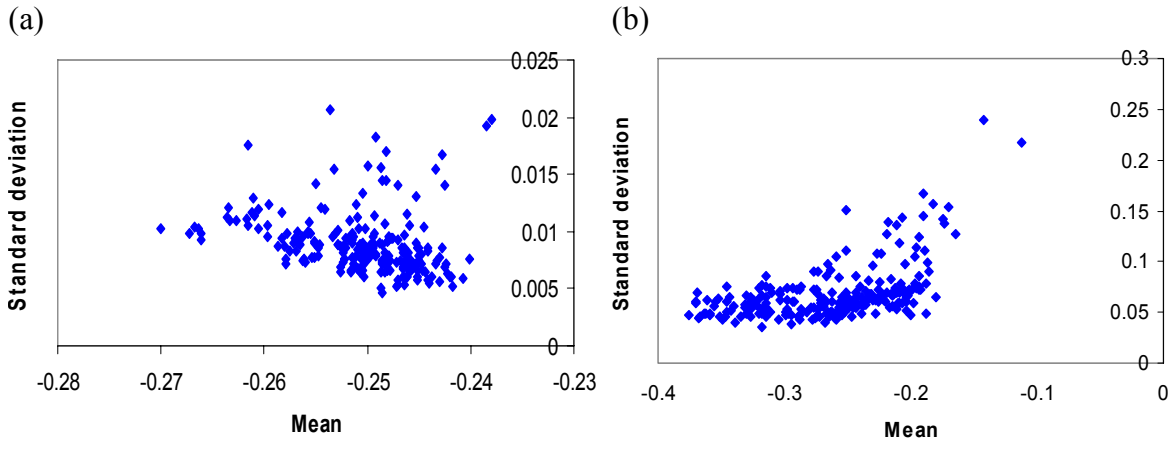

Figure 4.3 Scatter plots of local standard deviations against means of NDVI84 (a) and NDVI99 (b)

The 228 local means for NDVI99 are contoured in Figure 4.4(a); while corresponding standard deviations are contoured in Figure 4.4(b). The contour map of NDVI99 local means showed that lower values were concentrated in the south-eastern part of the study area, while higher values are found mostly in the south. The distribution of the standard deviation values is similar to that shown by the standard deviations of NDVI84 (Figure 4.2(a)).

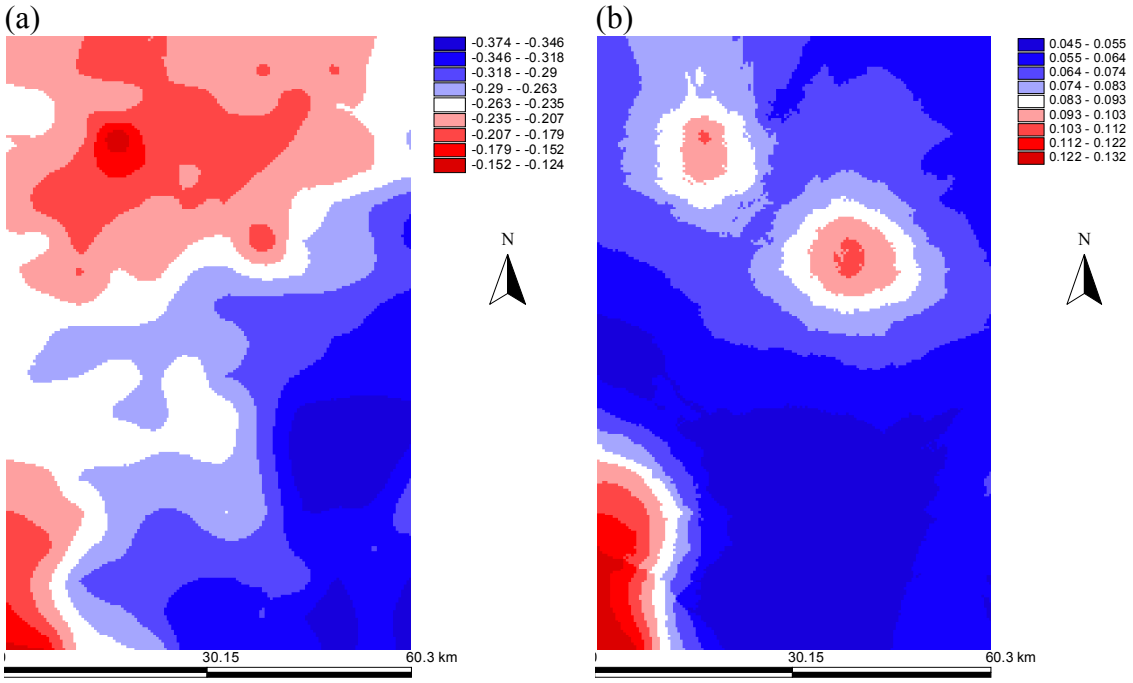

Figure 4.4 Contour maps of local means (a) and local standard deviations (b) of NDVI99

Comparing the maps in Figures 4.4(a) and (b), moderate resemblance was observed between the local means and standard deviations, suggesting that there is just a moderate proportional effect. This result is confirmed by the correlation coefficient of the mean-standard deviation pairs which is 0.53. Figure 4.3(b) is a scatter plot of the moving window means against corresponding standard deviations. Comparing Figures 4.3(a) and 4.3(b), it is observed that the relationship between the local means and corresponding standard deviations is stronger for NDVI99 than for NDVI84.

The DEM was also investigated for heteroscedasticity and proportional effect. There appeared to be a slight general decrease in the moving window mean values from the northern sector through to the southern sector of the study area (Figure 4.5a). The standard deviation values do not show any significant variability over the entire study area. Apart from two large values (36 and 37) in the southern sector, the rest of the values ranged from 5 to 22.

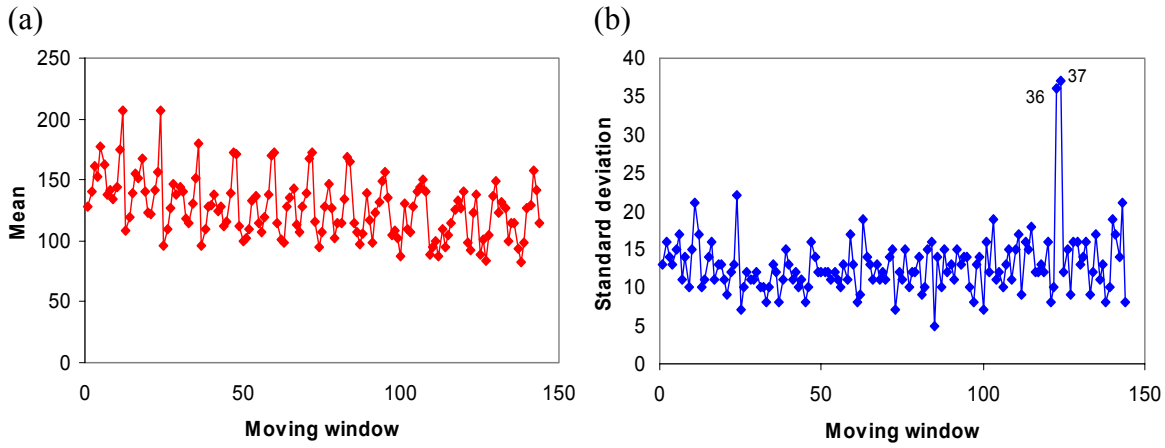

Figure 4.5 Plots of local means (a) and local standard deviation (b) of DEM

The means and standard deviations within the 144 $9\,\text{km} \times 9\,\text{km}$ moving windows for DEM are contoured in Figure 4.6. It was observed that the higher local means are concentrated in the eastern sector as well as forming a cluster in the central part of the northern sector. The lower local means are concentrated in the south-western sector of the study area. The distribution of the standard deviations showed mostly low values over the study area with a cluster of large values in the south-western corner.

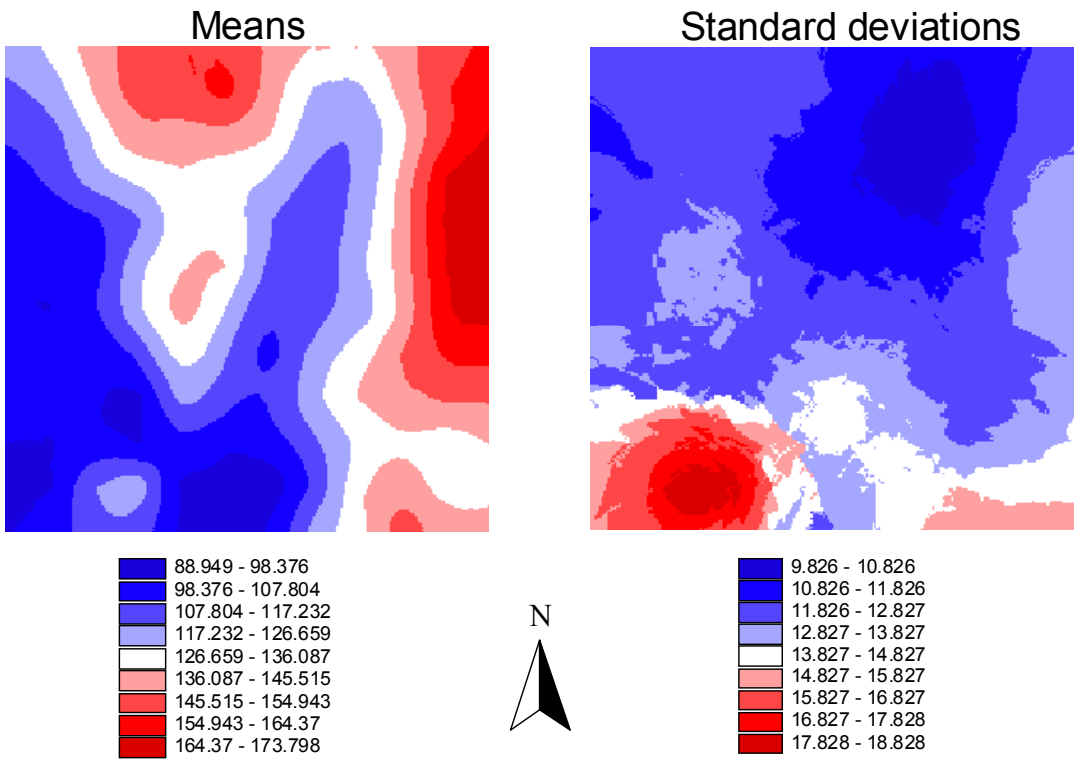

Figure 4.6 Contour maps of moving window means and standard deviations for DEM

A comparison of the contour maps revealed that the moving window means and standard deviations are linearly uncorrelated. The correlation coefficient for the 144 mean–standard deviation pairs is only 0.31, indicating lack of strong proportional effect. Figure 4.7 is a scatter plot of the moving window means and corresponding standard deviation.

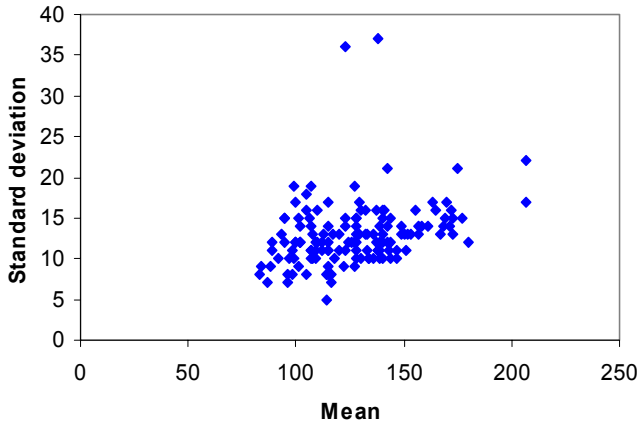

Figure 4.7 A scatter plots of local standard deviations against local means of DEM

4.2 Results of wavelet variance analysis of NDVI and DEM data sets

The "d6" and Haar wavelet filters were employed through seven levels of decomposition to estimate the unbiased MODWT wavelet variance of the DEM and NDVI data sets. Table 4.1 and Figure 4.8 show the results of the analysis of the NDVI data sets. There is no simple and clear relationship between wavelet variance and the resolution for any of the data sets. This implies that the trend of the change in the variability of each data set is not a simple a function of its resolution.

Table 4.1 Wavelet variance at various resolutions of the NDVI data sets with "d6" and Haar wavelet filters

Resolution (m)	Wavelet variance			
	NDVI84		NDVI99	
	"d6"	Haar	"d6"	Haar
30	1.33×10^{-5}	1.82×10^{-5}	5.67×10^{-4}	8.12×10^{-4}
60	2.39×10^{-5}	2.53×10^{-5}	9.13×10^{-4}	1.22×10^{-3}
120	2.67×10^{-5}	2.85×10^{-5}	1.59×10^{-3}	1.99×10^{-3}
240	3.81×10^{-5}	3.25×10^{-5}	3.11×10^{-3}	3.14×10^{-3}
480	1.85×10^{-5}	2.48×10^{-5}	1.98×10^{-3}	3.73×10^{-3}
960	9.67×10^{-6}	2.67×10^{-5}	2.29×10^{-3}	4.81×10^{-3}
920	1.21×10^{-5}	0.21×10^{-5}	7.07×10^{-4}	2.30×10^{-3}

It is observed from Table 4.1 that for lower resolutions (30 to 240 meters), the wavelet variance of both NDVI84 and NDVI99 data sets increased monotonically irrespective of the wavelet filter used. For higher resolutions (greater than 240 meters), the wavelet variance fluctuated for both data sets and both wavelet filters. Also at lower resolutions, the unbiased MODWT wavelet variance estimates using the "d6" and the Haar wavelet filters were almost the same. However, for 480 m and higher resolutions, the estimates from the Haar wavelet filter were higher for both data sets. It is also noteworthy that wavelet variance estimates for NDVI 99 were generally larger than those for NDVI84.

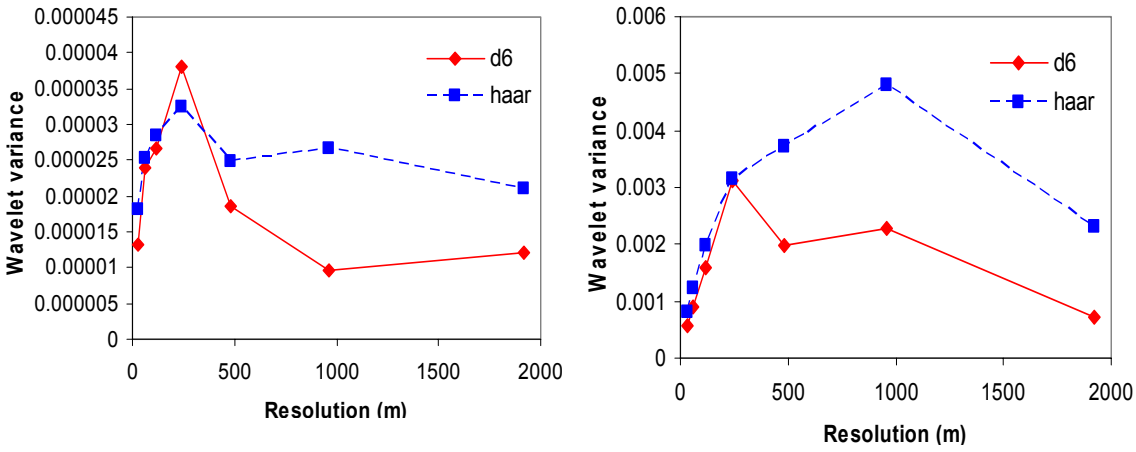

Figure 4.8 Plots of wavelet variance against corresponding resolutions of NDVI84 (left) and NDVI99 (right)

With the Haar wavelet filter, the NDVI84 data set revealed a major peak at the 240 meter scale (or 128×128 pixels data) and a minor peak at the 960 meter scale (or 32×32 pixels data); while with the "d6" it revealed a major peak at the 240 meter scale. The NDVI99 data set revealed two peaks, one at the 240 m scale and another at the 960 m scale with the "d6" wavelet filter; while it revealed a peak at the 960 m scale with the Haar wavelet filter. The presence of peaks in wavelet variance-resolution graph is indicative of hierarchical and hence a multiple-scale structure (Wu *et al*, 2000). For NDVI84 data set, the dominant scale was 240 meters irrespective of the filter used. However, for the NDVI99 data set it varied with the wavelet filter: it was 240 meters with "d6" and 960 meters with the Haar wavelet filter.

Table 4.2 contains the EDOFs $\hat{\eta}_1$ and $\hat{\eta}_3$ (rounded to the nearest integer) as determined by Equations (3.1) and (3.3) respectively, which are associated with the "d6" wavelet variance estimates $\nu_X^2(\tau_j)$, at scales $j = 1, 2, \ldots, 7$. In the bottom row for each data set is the number M_j of wavelet coefficients at each scale.

Table 4.2 Equivalent degrees of freedom η_1 and η_3 associated with the "d6" wavelet variance estimates for the NDVI data sets

		Level (j)						
		1	2	3	4	5	6	7
NDVI84	$\hat{\eta}_1$	820	361	220	101	63	32	64
	$\hat{\eta}_3$	510	252	124	9	27	11	8
	M_j	1019	1009	989	949	869	709	389
NDVI99	$\hat{\eta}_1$	810	345	222	86	71	21	10
	$\hat{\eta}_3$	510	252	124	59	27	11	3
	M_j	1019	1009	989	949	869	709	389

Figure 4.9 shows the "d6" wavelet variance estimates plotted against scale, along with two 95% confidence intervals for the true wavelet variance at each scale for the NDVI99 data set. The confidence intervals are based on the unbiased MODWT estimator and χ^2 approximations to its distribution with EDOFs $\hat{\eta}_1$ and $\hat{\eta}_3$ as listed in Table 4.2. Figure 4.9 shows that the variance in NDVI99 is mainly due to fluctuations at scales 8 and higher. For the four smallest scales, the confidence interval given by the two methods are close. However, the agreement breaks down at the three largest (16, 32 and 64) scales. The fact that the wavelet variance for the four smallest scales (1 to 8) lie roughly on a straight line indicates that the wavelet variance varied approximately as a power law over the 30 to 240 meter scales.

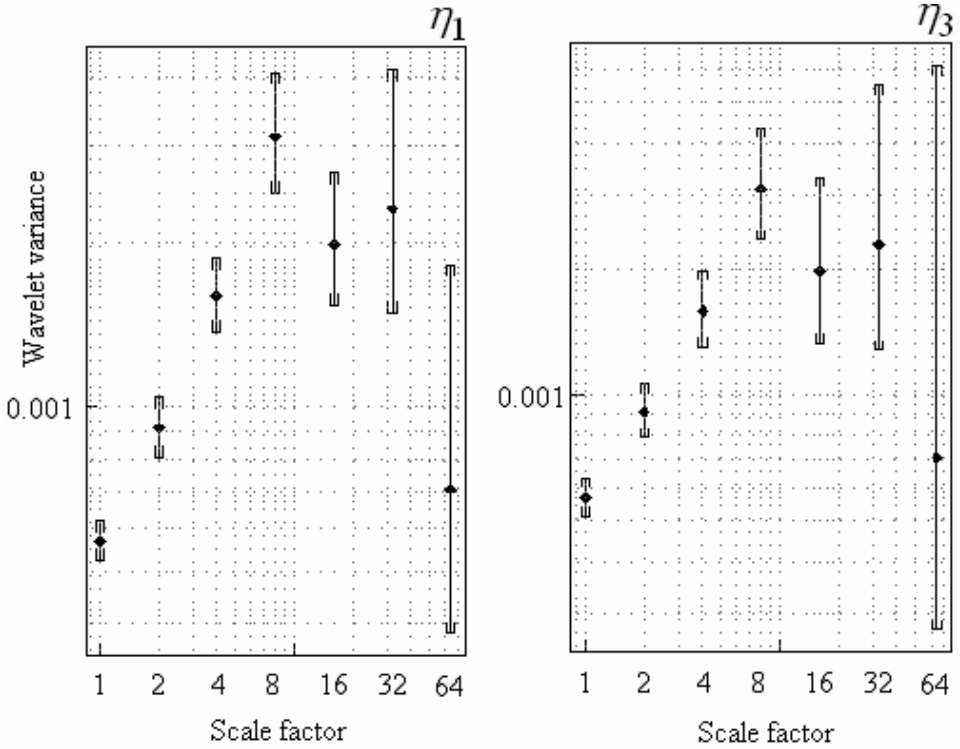

Figure 4.9 Ninety-five percent confidence intervals for "d6" wavelet variance estimates of NDVI99

Results of wavelet variance analysis of DEM are presented in Table 4.3 and Figures 4.10 and 4.11. There was no clear identifiable peak for the DEM with respect to either wavelet filter (see Figure 4.10). The relationship between wavelet variance and resolution appeared to be linear for both wavelet filters. The regression equations with respect to "d6" and Haar wavelets are $y = 0.014x - 3.740$ and $y = 0.010x + 1.271$ respectively, where y is the wavelet variance and x is the resolution in meters. The coefficient of determination is 0.991 with respect to "d6" and 0.976 with respect to the Haar.

Table 4.3 Wavelet variance at various resolutions of the DEM with "d6" and Haar wavelet filters

Resolution (m)	90	180	360	720	1440	2880	5760
Wavelet variance (d6)	0.848	0.839	1.220	4.500	11.500	34.800	77.100
Wavelet variance (Haar)	1.090	1.480	2.930	7.570	17.100	34.400	52.600

It was also observed that at lower resolutions (90 to 2550 meters), the estimates from the Haar wavelet filter were consistently larger than those by “d6”. However from 2880 meters and higher resolutions, the estimates by “d6” exceeded those by Haar.

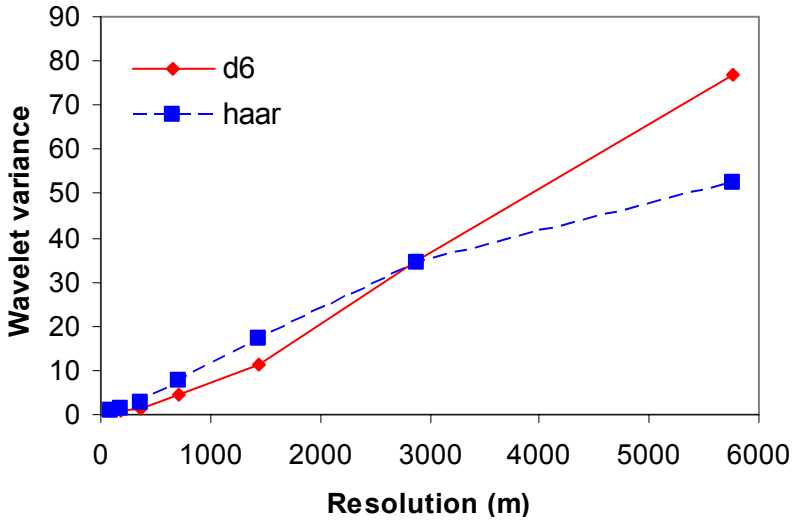

Figure 4.10 Plot of wavelet variance against corresponding resolutions of DEM

Figure 4.11 shows the “d6” wavelet variance estimates plotted against scale, along with two 95% confidence intervals for the true wavelet variance at each scale for the DEM. The figure indicates that the variance in the data set is mainly due to fluctuations at scales 360 meters and lower. For the six smallest scales, the confidence intervals given by the two methods are close; however, the agreement breaks down at the 64 m scale. Again, the fact that the values of wavelet variance for higher scales (4 to 64) lie roughly on a straight line suggests that the wavelet variance varies approximately as a power law over 360 meters to 5.76 kilometers scales.

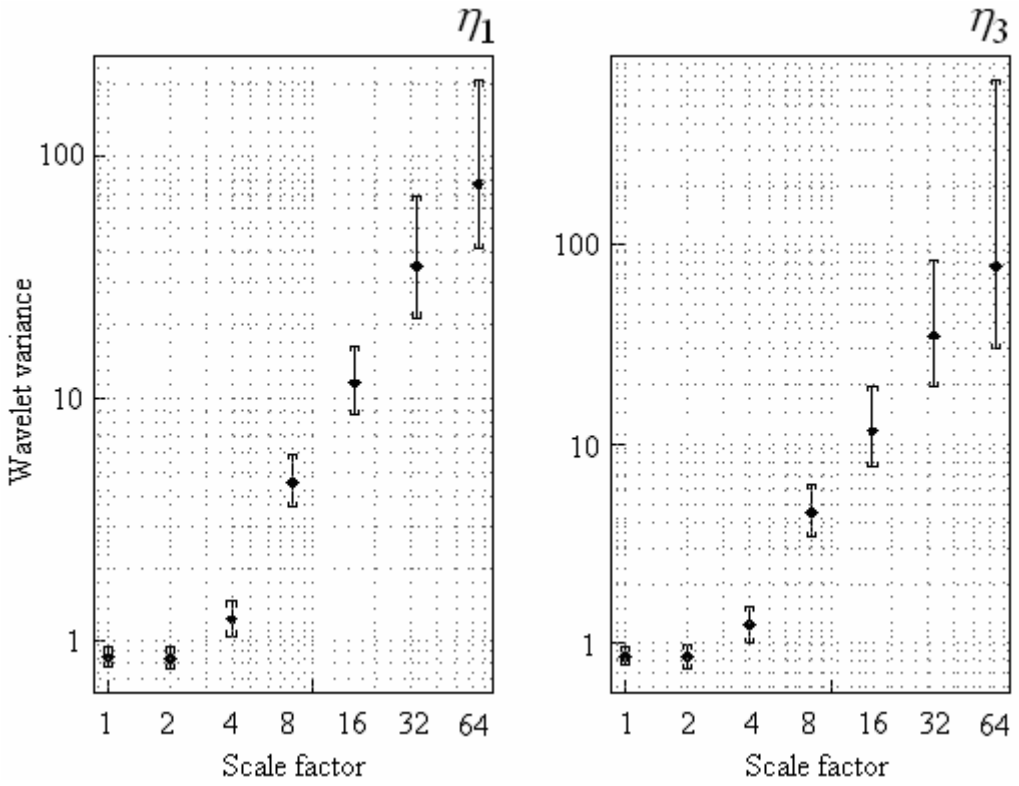

Figure 4.11 Ninety-five percent confidence intervals for "d6" wavelet variance estimates of DEM

In summary, these results suggest that the NDVI data sets exhibit hierarchical and multiple-scale structure; while the DEM data set does not seem to. Based on the "d6" wavelet filter (which is the most widely used for wavelet variance analysis), the dominant scale for the NDVI84 and NDVI99 data sets is the same (i.e. 240 meters).

4.3 Scaling characteristics of NDVI and DEM data sets

Wavelet coefficients were used to investigate whether or not the NDVI and DEM data sets exhibit self-similar scaling behavior. The first four moments of the wavelet coefficients from seven levels of decomposition in the horizontal, vertical and diagonal directions were used (see Appendix II). Using Equation (3.6) and computations of the first four moments at the seven levels and in the three directions, $\log m_p(\lambda)$ was plotted against $\log(\lambda)$. The slope $s(p)$ and intercept $\log m_p(1)$ for each p were estimated via regression. The coefficient of determination r^2 for each fit was also determined. Table 4.4 shows the results of the regression for the NDVI and DEM data

sets. A "-" in the table indicates that the value is not defined. This occurs when the estimate of a moment is ≤ 0, in which case its logarithm is not defined. It is observed from Table 4.4 that, generally, the coefficient of determination r^2 fluctuates with the order of moment; it increases from the first to the second moment, drops from the second to the third and rises again to the fourth. The slope term $s(p)$ also fluctuates with the order of moment; it increases with the first two moments, drops from the second to the third moment and drops further. The regressions fit the data sets reasonably well, fitting almost perfectly at the first and second order moments. The linearity of the regressions indicates the presence of statistical self-similarity.

Slope terms obtained from the regression models involving the logarithm of moment and logarithm of resolution were then used to examine the scaling behavior in each of the three directions that wavelet coefficients were produced. The slope terms were regressed on the order of moment to determine whether or not they are linear. The results of this regression analysis are summarized in Table 4.5. It was observed from Table 4.5 that there is a linear relationship between the estimated slope terms and the order of moment. We are, therefore, able to infer that the detail wavelet coefficients in the three directions of decomposition of the NDVI data sets exhibit statistical self-similarity over the 120 m to 3.84 km scales.

Table 4.4 Regression results for log of moment versus log of resolution in the horizontal, vertical and diagonal wavelet coefficients of NDVI and DEM data sets

Data set	Order of moment	Horizontal details			Vertical details			Diagonal details		
		$s(p)$	a	r^2	$s(p)$	a	r^2	$s(p)$	a	r^2
DEM	1	2.101	- 6.419	0.982	-	-	-	2.324	- 8.182	0.913
	2	3.118	- 6.733	0.991	3.117	- 6.599	0.989	3.024	-7.089	0.984
	3	-1.112	3.440	0.607	-0.685	2.237	0.999	0.570	- 2.902	0.140
	4	-1.702	6.105	0.835	-1.399	5.630	0.886	-0.640	2.449	0.590
NDVI84	1	0.878	0.591	1.000	-	-	-	1.451	- 7.422	0.985
	2	1.881	-7.869	0.998	1.848	-7.777	0.994	1.732	-7.760	0.996
	3	0.261	-0.679	0.340	0.210	-1.050	0.483	0.513	1.800	0.163
	4	-0.811	3.359	0.953	-0.735	2.978	0.614	-1.218	4.162	0.852
NDVI99	1	1.430	- 6.350	0.862	-	-	-	0.779	1.364	1.000
	2	2.163	-6.756	0.998	1.997	- 6.319	0.990	2.063	- 6.864	0.993
	3	0.528	- 1.466	0.588	0.213	- 1.072	0.032	0.254	- 1.200	0.021
	4	0.021	1.139	0.009	-0.642	2.613	0.542	-0.576	2.248	0.340

The wavelet coefficients in the three directions of decomposition of the DEM also exhibits statistical self-similarity, but over the 3.6 km to 11.52 km scales. For all three data sets, the magnitude of the slopes varied according to the direction of the wavelet coefficients; the highest occurring in the vertical direction for all data sets. As an example, the NDVI84 data set has its lowest slope magnitude in the horizontal direction with a value of -0.67 and the highest in the vertical direction with a value of -1.29. Similar inferences can be deduced for the NDVI99 and DEM data sets.

Table 4.5 Regression results for slope versus order of moment in the horizontal, vertical and diagonal wavelet coefficients of NDVI and DEM data sets

Data set	wavelet coefficients	$s(p)$	a	r^2
DEM	horizontal	-1.564	4.511	0.727
	vertical	-2.258	7.118	0.865
	diagonal	-1.135	4.156	0.774
NDVI84	horizontal	-0.669	2.224	0.586
	vertical	-1.292	4.316	0.977
	diagonal	-0.923	2.926	0.801
NDVI99	horizontal	-0.586	2.501	0.633
	vertical	-1.320	4.481	0.960
	diagonal	-0.587	2.099	0.470

4.4 Effects of changing grain size on landscape pattern metrics

Two land use and land cover maps (LULC84 and LULC99) were used to investigate the effects of changing grain size on the 18 selected landscape metrics. The grain size of the original maps was systematically changed through 18 separate aggregation levels; from the finest 1×1 through to the coarsest 50×50 while the extent was kept constant (see Table 3.5). In all, 36 maps (2 land use and land cover maps × 18 grain size levels) were used in this aspect of the study. Figure 4.12 shows samples of the maps used for this analysis. The values of the 18 selected landscape metrics were estimated from each of these maps and the results for LULC84 are summarized in Table 4.6. The corresponding results for LULC99 are presented in Table 7.5 in Appendix III.

In general, changing the grain size had significant effects on the values of the landscape metrics. The magnitude and pattern of responses varied among metrics and across the two landscapes. The effects can be grouped into three main types: Type I – predictable responses with simple scaling relationships; Type II – unpredictable or fluctuating responses with no clear simple scaling relations; and Type III – fixed responses irrespective of changes in grain size. Thirteen of the eighteen landscape metrics studied belonged to Type I. These included number of patches, patch density, landscape shape index, total edge, edge density, mean patch area, patch area standard deviation, patch area coefficient of variation, area-weighted mean shape index, area-weighted mean fractal dimension index, mean shape index, mean fractal dimension index and contagion. These metrics changed predictably with increasing grain size, exhibiting simple scaling relationships that were consistent across the two landscapes (Figure 4.13). The fit of the linear regressions were all very high, with coefficient of determination (r^2) ranging from 0.769 to 0.992. Eleven of the Type I metrics decreased in value with increasing grain size via a power law relationship.

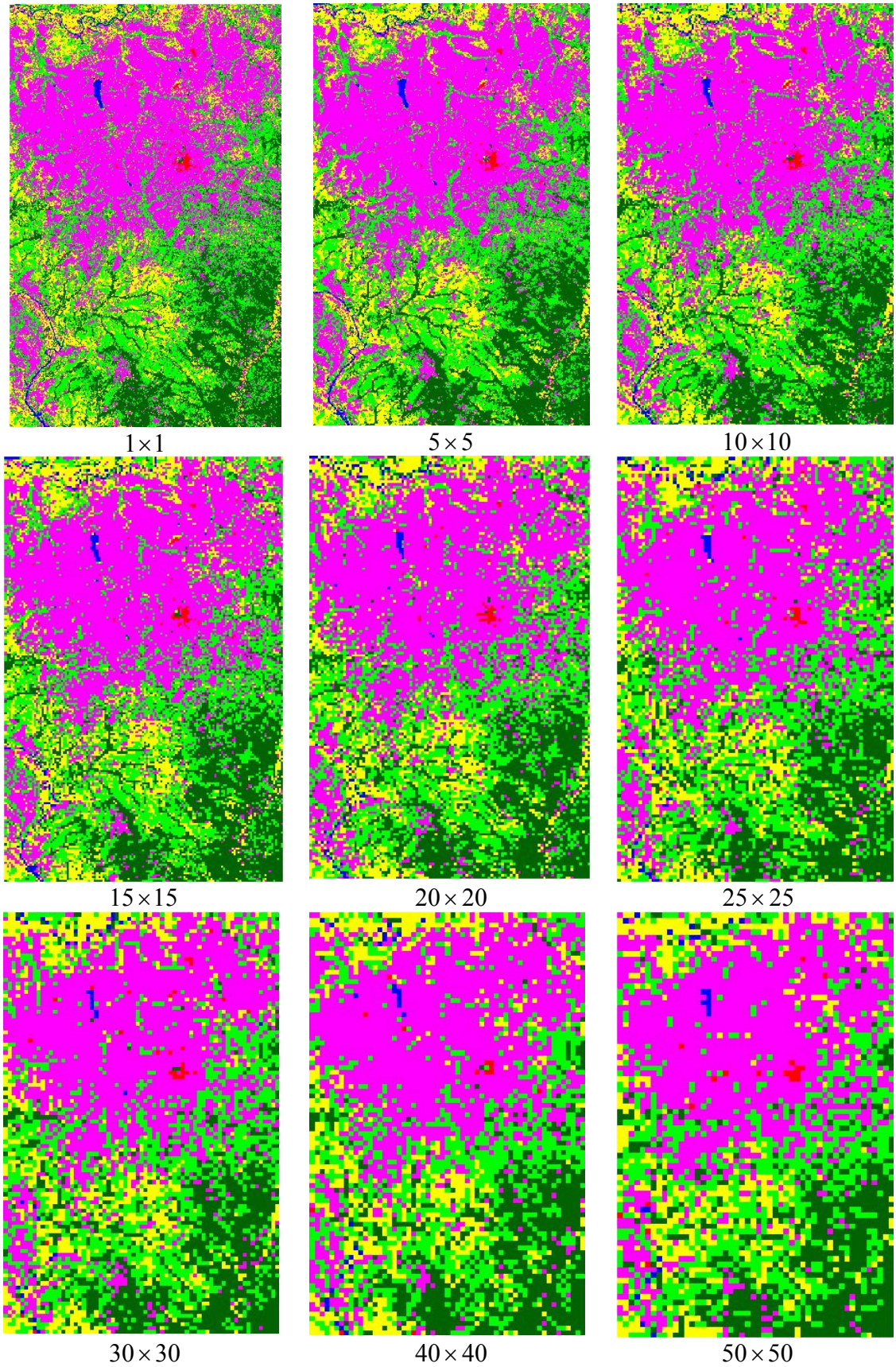

Figure 4.12 Sampled maps of LULC99 with different grain sizes

Table 4.6 Estimates of 18 landscape metrics of LULC84 maps with different grain sizes

Grain size (pixels on a side)	Estimates of landscape metrics								
	No. of patches (*NP*)	Patch density (*PD*)	Largest patch index (*LPI*)	Landscape shape ind. (*LSI*)	Total edge (*TE*)	Edge density (*ED*)	Mean patch area (*MPA*)	Patch area std dev. (*PASD*)	Patch area coeff. of var. (*PACV*)
1	319837	56.78	13.0517	257.26	76930860	136.57	2	200	11337
2	24247	4.30	15.1153	161.91	28184640	39.38	23	819	3526
3	23783	4.22	15.1123	90.09	24937590	38.94	24	827	3490
4	23631	4.19	14.7883	73.52	21783000	38.61	24	823	3447
5	17028	3.02	15.1482	64.15	18957750	33.64	33	990	2992
6	13474	2.39	15.3004	57.76	17034840	30.24	42	1121	2682
7	11177	1.99	14.8902	53.25	15682170	27.84	50	1205	2391
8	9702	1.73	14.5823	49.67	14594400	25.95	58	1288	2222
9	8319	1.48	15.1715	46.27	13583970	24.15	68	1407	2081
10	6934	1.23	15.7012	42.46	12456000	22.14	81	1532	1888
15	3968	0.70	14.0141	32.61	9495000	16.82	142	1949	1370
20	2550	0.45	15.0609	26.33	7653600	13.49	222	2366	1064
25	1763	0.31	15.6800	22.29	6378000	11.34	319	3029	949
30	1351	0.24	15.7865	19.53	5562900	9.86	418	3371	807
35	1025	0.18	16.4203	16.99	4796400	8.58	546	4019	737
40	854	0.15	15.7179	15.56	4360800	7.77	658	4147	631
45	623	0.11	16.8900	14.89	3819635	6.46	785	4571	527
50	471	0.08	15.1167	12.11	3472432	5.92	914	5523	426

Table 4.6 (Continued)

Grain size (pixels on a side)	Estimates of landscape metrics								
	A-w mean shape ind (*AWMSI*)	A-w mean frac dim ind (*AWMFDI*)	Mean shape ind (*MSI*)	Total area (*TA*)	Mean fractal dim index (*MFDI*)	Contagion (*CONTAG*)	Patch richness (*PR*)	Patch rich density (*PRD*)	Shannon's diversity ind (*SHDI*)
1	33.49	1.3024	1.1091	563323	1.0221	40.36	6.0000	0.0011	1.4369
2	12.89	1.2219	1.1368	563323	1.0179	46.81	6.0000	0.0011	1.4260
3	12.67	1.2203	1.1293	563323	1.0212	42.41	6.0000	0.0011	1.4261
4	12.37	1.2179	1.1185	564245	1.0168	38.71	6.0000	0.0011	1.4258
5	11.35	1.2062	1.1195	563504	1.0167	37.43	6.0000	0.0011	1.4264
6	10.46	1.1976	1.1133	563323	1.0159	36.26	6.0000	0.0011	1.4256
7	9.35	1.1870	1.1142	563223	1.0156	35.15	6.0000	0.0011	1.4260
8	8.72	1.1797	1.1088	562401	1.0145	34.17	6.0000	0.0011	1.4260
9	8.19	1.1733	1.1079	562482	1.0142	33.44	6.0000	0.0011	1.4257
10	7.59	1.1678	1.1059	562599	1.0139	33.16	6.0000	0.0011	1.4253
15	5.71	1.1427	1.0972	564408	1.0124	30.85	6.0000	0.0011	1.4290
20	4.55	1.1256	1.0944	567216	1.0117	29.65	6.0000	0.0011	1.4283
25	4.32	1.1177	1.0915	562500	1.0113	28.86	6.0000	0.0011	1.4262
30	3.81	1.1109	1.0850	564408	1.0101	28.18	6.0000	0.0011	1.4258
35	3.51	1.1027	1.0856	559298	1.0102	27.91	6.0000	0.0011	1.4269
40	3.11	1.0931	1.0795	561600	1.0096	27.04	6.0000	0.0011	1.4302
45	2.72	1.0916	1.0827	565886	1.0093	29.28	6.0000	0.0011	1.4261
50	2.34	1.0936	1.0909	558000	1.0085	30.25	6.0000	0.0011	1.4313

Although exponential decay function could also be fitted to the changes in these eleven metrics, r^2 was lower in each case. The remaining two Type I metrics (patch area standard deviation and mean patch area) increased in value via a linear and a power law relationship respectively (Figure 4.13 and Table 4.7). Considering the fact that they are separated by a time difference of 15 years, the consistency of the scaling relations among the two landscape maps is quite remarkable. However, the values of the parameters in the scaling relations changed considerably among the two landscapes, indicating their structural differences at various grain sizes.

Table 4.7 Scaling relations showing the effects of changing grain size on Type I metrics

Type I landscape metric	Scaling relation and characteristics
Number of patches Patch density Landscape shape index Total edge Edge density Patch area coefficient of variation Mean shape index Area-weighted mean shape index Mean fractal dimension index Area-weighted mean fractal dimension index Contagion	A decreasing power law function: $y = ax^b, \quad a > 0, \quad b < 0$ and $x > 0$, where y is the value of the metric, a and b are constants and x is the grain size expressed as the number of pixels on a side
Patch area standard deviation	An increasing linear function: $y = ax + b, \quad a > 0, \; b > 0$ and $x > 0$, where y is the value of the metric, a and b are constants and x is the grain size expressed as the number of pixels on a side
Mean patch area	An increasing power law function: $y = ax^b, \quad a > 0, \; b > 0$ and $x > 0$, where y is the value of the metric, a and b are constants and x is the grain size expressed as the number of pixels on a side

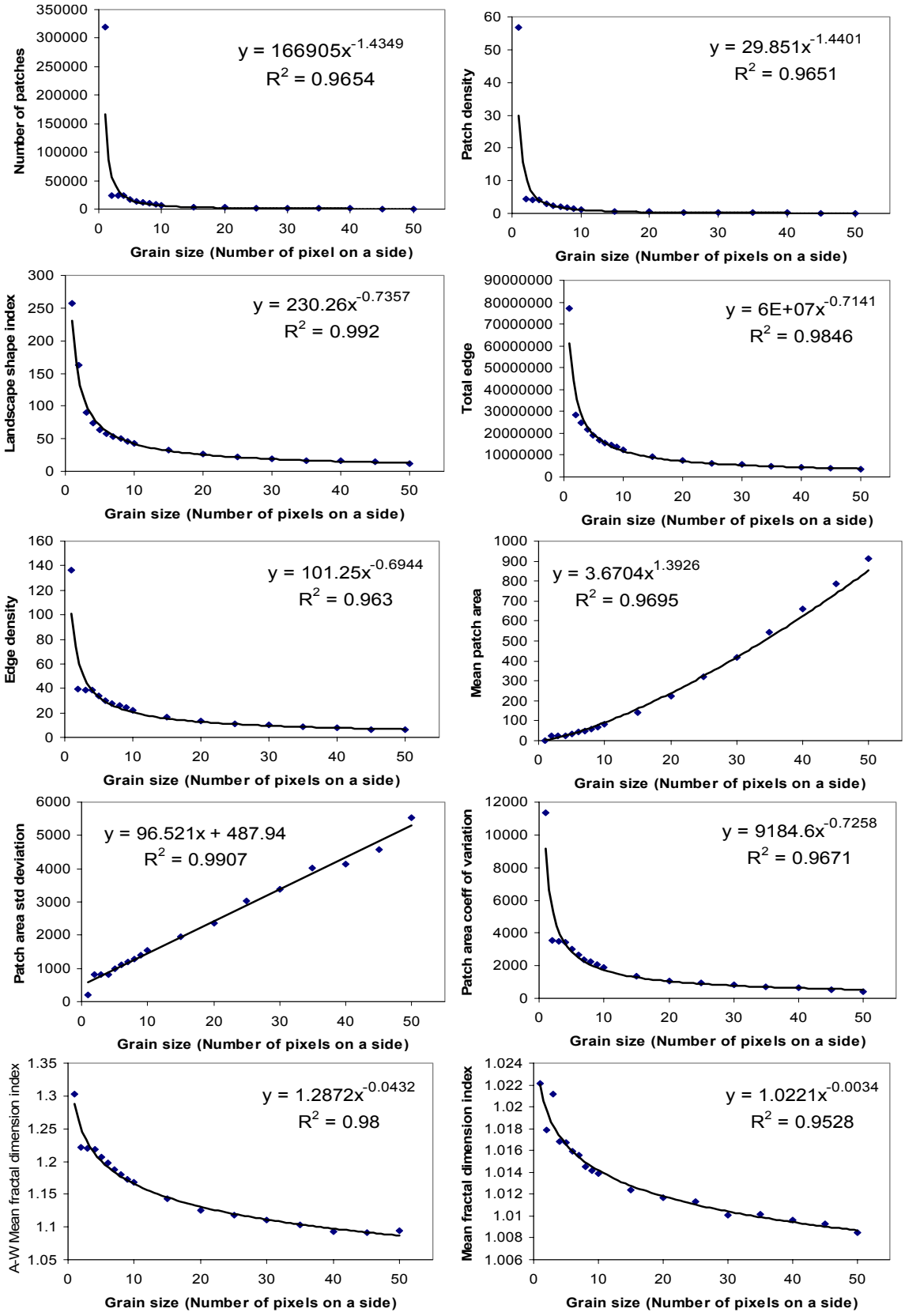

Figure 4.13 Scalograms showing the effects of changing grain size on Type I metrics of LULC84

In contrast to Type I, the values of Type II metrics exhibited unpredictable or fluctuating wave-like responses with increasing grain size. The fluctuations suggest that these metrics are highly sensitive to the specific patterns of the landscape under study, and thus general scaling relations were not possible to derive (Figure 4.14). *LPI* and *SHDI* fluctuated with no clear pattern and lack of consistency, while TA showed consistency across the 2 landscapes.

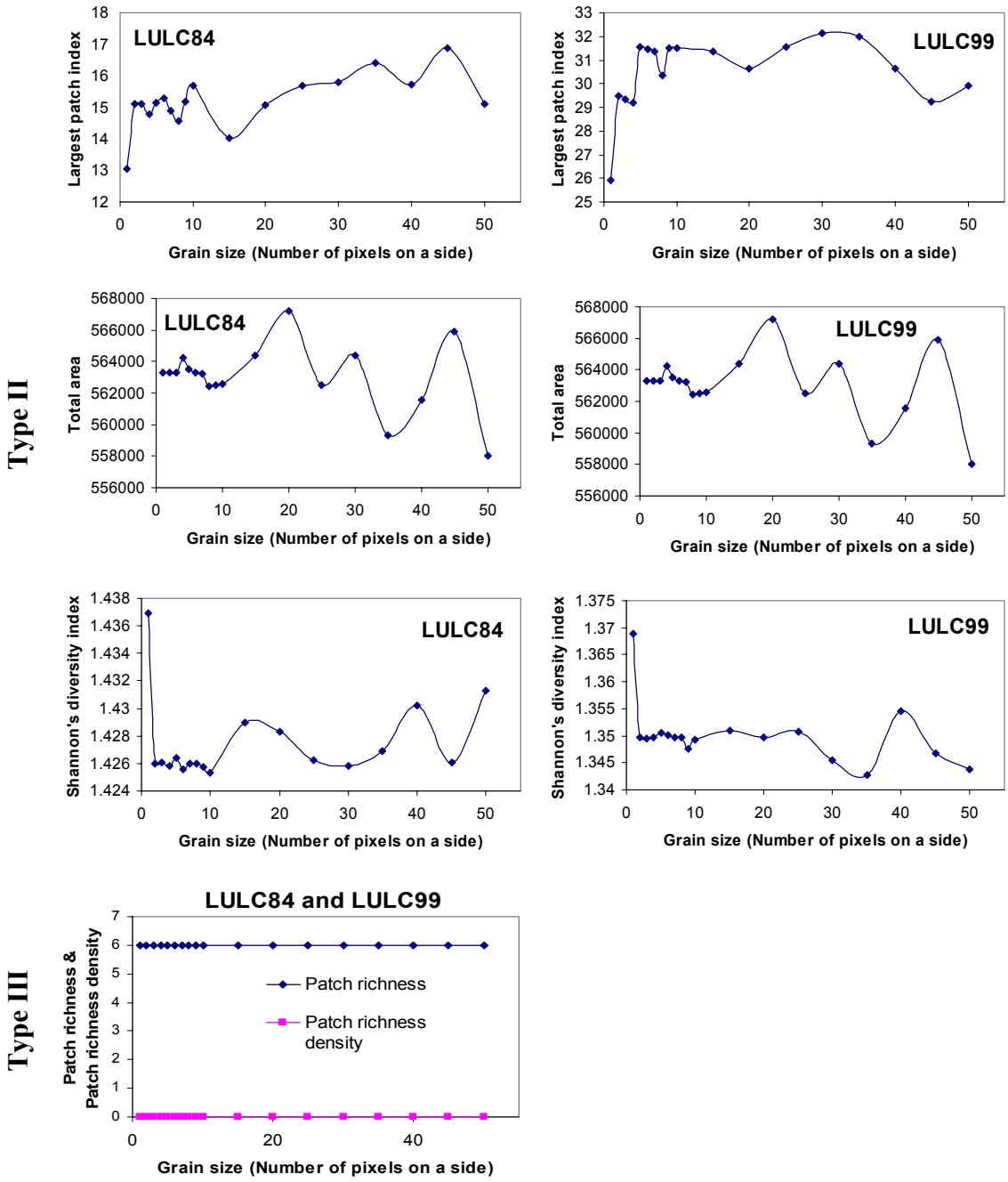

Figure 4.14 Scalograms showing the effects of changing extent on Types II and III metrics of LULC84 and LULC99

Type III included 2 metrics: patch richness and patch richness density. These metrics had fixed values (6 for patch richness and 0.0011 for patch richness density) irrespective of the grain size, indicating that they are not affected by changes in the grain size (see graph at the bottom in Figure 4.14).

4.5 Effects of changing the method of aggregation on pattern analysis

A number of studies have shown that different aggregation methods may have significant effects on spatial model evaluation, land cover classification, and landscape pattern analysis (Costanza, 1989; Justice *et al*., 1989; Bian and Butler, 1999; Turner *et al*., 2001). We have cause to believe, therefore, that aggregation methods may also affect scaling relations of landscape metrics. To investigate these effects on the 18 metrics, we employed the mean, median and mode aggregation methods to systematically change the grain size of our landscape maps from 1×1 to 50×50 pixels while the extent was kept constant. In all, 108 landscape maps (2 land use and land cover maps $\times$ 3 aggregation methods $\times$18 grain size levels) were analyzed for the purpose of investigating the effect of aggregation method on landscape metrics. The results for NDVI84 and NDVI99 are summarized in Tables 7.4 and 7.5, respectively, in Appendix III.

The results (Figure 4.15) showed that, generally, the method of aggregation significantly affected the values of landscapes metrics as did changing grain size. Sixteen out of the 18 metrics showed significant differences among the three methods of aggregation; while patch richness and patch richness density were not affected. Type I metrics were most robust as they maintained their scaling relationships to a large extent, in spite of the fact that the parameter values in the scaling equations among the methods changed slightly. For most Type I metrics (number of patches, patch density, landscape shape index, total edge, edge density, patch area coefficient of variation, area-weighted mean shape index and area-weighted mean fractal dimension index), the values produced by the median and mode aggregation methods were closely related; while those produced by the mean method differed significantly from them. These appear to be the metrics whose responses with change in grain size follow a decaying power law. For the others (mean patch area and patch area standard deviation), values produced by the mean and mode aggregation methods were closely related; while those

produced by the median method differed significantly from them. Mean shape index, mean fractal dimension index and contagion (Type I) together with Shannon's diversity index, largest patch index and total area (Type II) showed the most pronounced differences as a result of changing the method of aggregation. It is noteworthy, however, that the mean and median aggregation methods produced the same values for total area; while the values produced by mode method differed significantly. The Type III metrics (patch richness and patch richness density) were unaffected by changing the method of aggregation.

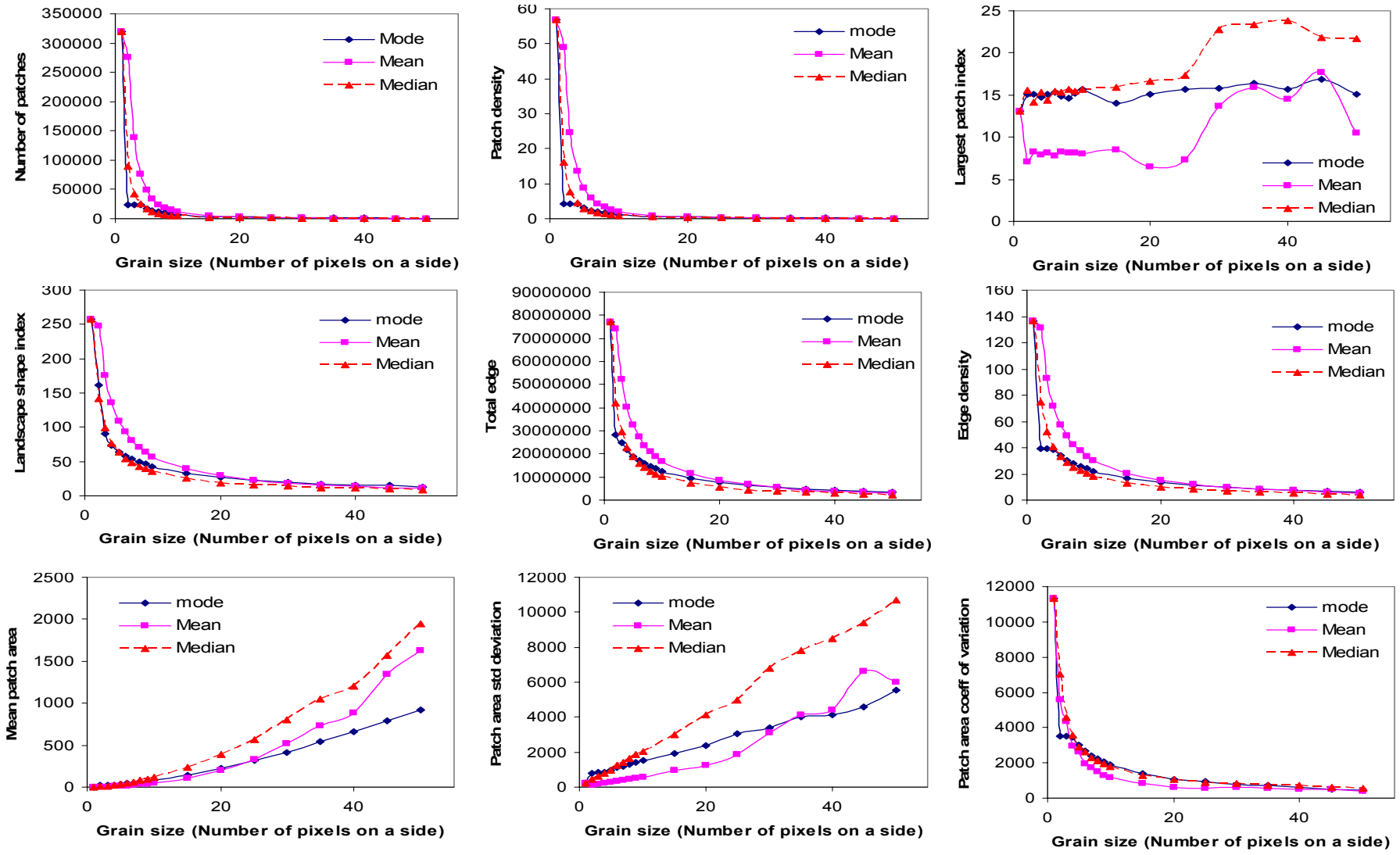

Figure 4.15 Scalograms showing the effects of changing the method of aggregation on landscape metrics of LULC84

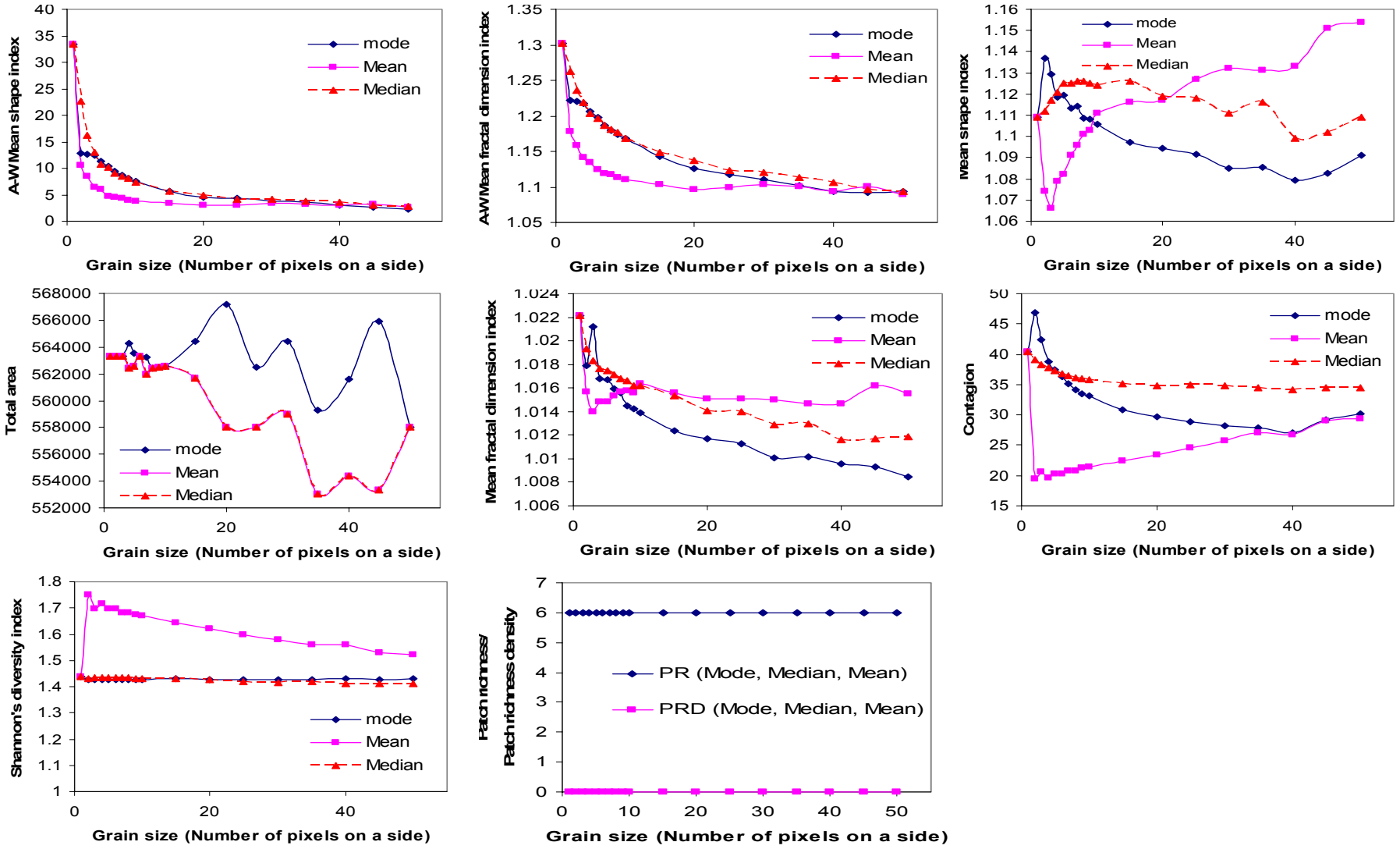

Figure 4.15 (Continued)

4.6 Effects of changing the extent on landscape pattern metrics

LULC84 and LULC99 were used to investigate the effects of changing extent on landscape metrics. From each, nine maps with different extents ranging from 56 km^2 to 5,633 km^2 were clipped (Figure 4.16). Clipping was started from the south-western corner to the north-eastern corner along the diagonal. In all, 18 maps were used in this aspect of the study. The values of all 18 metrics were estimated from each map of LULC84 and summarized in Table 4.8; while corresponding values for LULC99 are presented in Table 7.7, Appendix III.

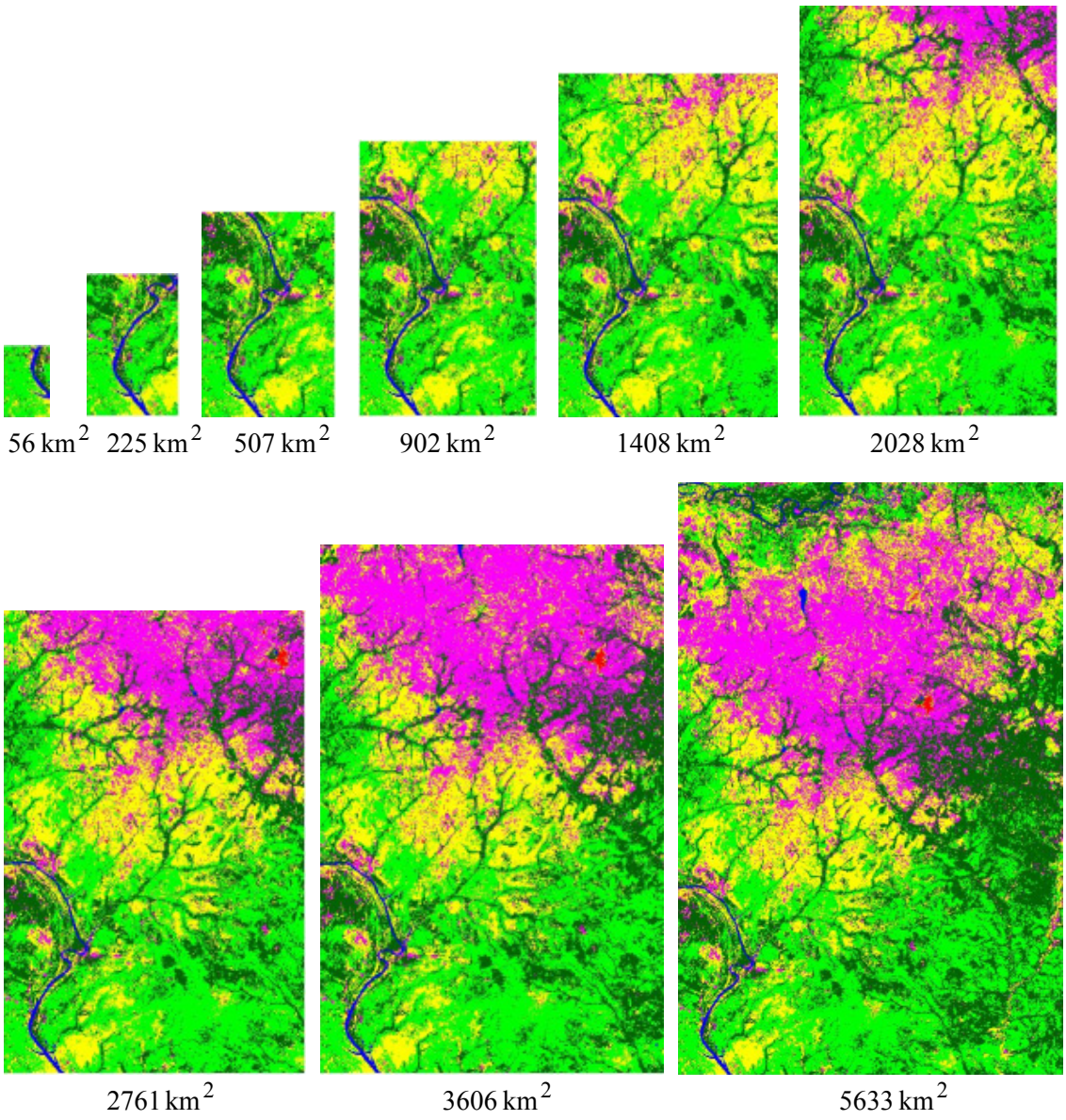

Figure 4.16 LULC84 maps with different extents used to investigate the effects of changing extent on landscape metrics

Table 4.8 Estimates of landscape metrics of LULC84 with different extents

Area of Extent (km^2)	Landscape metrics								
	No. of patches (*NP*)	Patch density (*PD*)	Largest patch ind (*LPI*)	Landscape shape ind. (*LSI*)	Total edge (*TE*)	Edge density (*ED*)	Mean patch area (*MPA*)	Patch area std dev. (*PASD*)	Patch area coeff of var (*PACV*)
56	3424	61	52	25	720930	128	1.6412	51	3115
225	13411	60	16	52	3028650	134	1.6807	47	2767
507	31478	62	9	80	7110450	140	1.6103	49	3012
902	54148	60	19	105	12483390	139	1.6651	84	5038
1408	82294	58	18	129	19143540	136	1.7113	104	6100
2028	121077	60	15	157	28068180	138	1.6746	107	6358
2761	159972	58	17	181	37774020	137	1.7256	150	8678
3606	197525	55	17	198	47341680	131	1.8251	196	10742
5633	319837	57	13	257	76930860	137	1.7613	200	11337

Table 4.8 (Continued)

Area of extent (km^2)	Estimates of landscape metrics								
	Total Area (*TA*)	A-w mean shape ind (*AWMSI*)	A-w mean frac dim (AWMFD)	Mean shape ind (*MSI*)	Mean frac dim ind (*MFDI*)	Contagion (*CONTAG*)	Patch richness (*PR*)	Patch rich density (*PRD*)	Shannon's div. ind. (*SHDI*)
56	5626	11	1.2520	1.1015	1.0212	50	6.0000	0.1066	1.1744
225	22540	10	1.2489	1.1094	1.0215	44	6.0000	0.0266	1.3182
507	50688	11	1.2597	1.1055	1.0208	45	6.0000	0.0118	1.2861
902	90161	17	1.2754	1.1057	1.0211	45	6.0000	0.0067	1.2728
1408	140831	20	1.2848	1.1046	1.0210	45	6.0000	0.0043	1.2810
2028	202753	20	1.2848	1.1043	1.0210	43	6.0000	0.0030	1.3572
2761	276053	28	1.3011	1.1035	1.0212	41	6.0000	0.0022	1.4197
3606	360497	34	1.3105	1.1041	1.0215	41	6.0000	0.0017	1.4331
5633	563323	34	1.3024	1.1091	1.0221	40	6.0000	0.0011	1.4369

In general, changing the extent of landscape maps had significant effects on the values of its metrics. Similar to changing grain size, the responses of metrics to changing extent can be grouped into three main types: Type I, Type II and Type III. The response curves of Type I metrics showed consistent and simple scaling relationships across the two landscapes. However, the values of the parameters in the scaling relation changed considerably among different landscapes, indicating their structural differences for distinctive extents. Equations derived from these response curves could be used to predict the values of such metrics when the extent of a landscape with similar characteristics is known. In contrast, the response curves of the Type II metrics did not show simple trends or consistent patterns across the two landscapes. For these reasons, scaling relations could not be formulated for prediction purposes. Type III metrics remained constant irrespective of size of extent.

Table 4.9 Scaling relations showing the effects of changing extent on Type I metrics

Type I landscape metric	Scaling relation and characteristics
Number of patches Total edge Total area Patch area standard deviation Patch area coefficient of variation Area-weighted mean shape index Area-weighted mean fractal dimension index	An increasing linear function: $y = ax + b, \quad a > 0, \ b > 0$ and $x > 0$, where y is the value of the metric, a and b are constants and x is the value of the extent
Landscape shape index	An increasing power law function: $y = ax^b, \ a > 0, \ b > 0$ and $x > 0$, where y is the value of the metric, a and b are constants and x is the value of the extent
Patch richness density	A decreasing power law function: $y = ax^b, \ a > 0, \ b < 0$ and $x > 0$, where y is the value of the metric, a and b are constants and x is the value of the extent

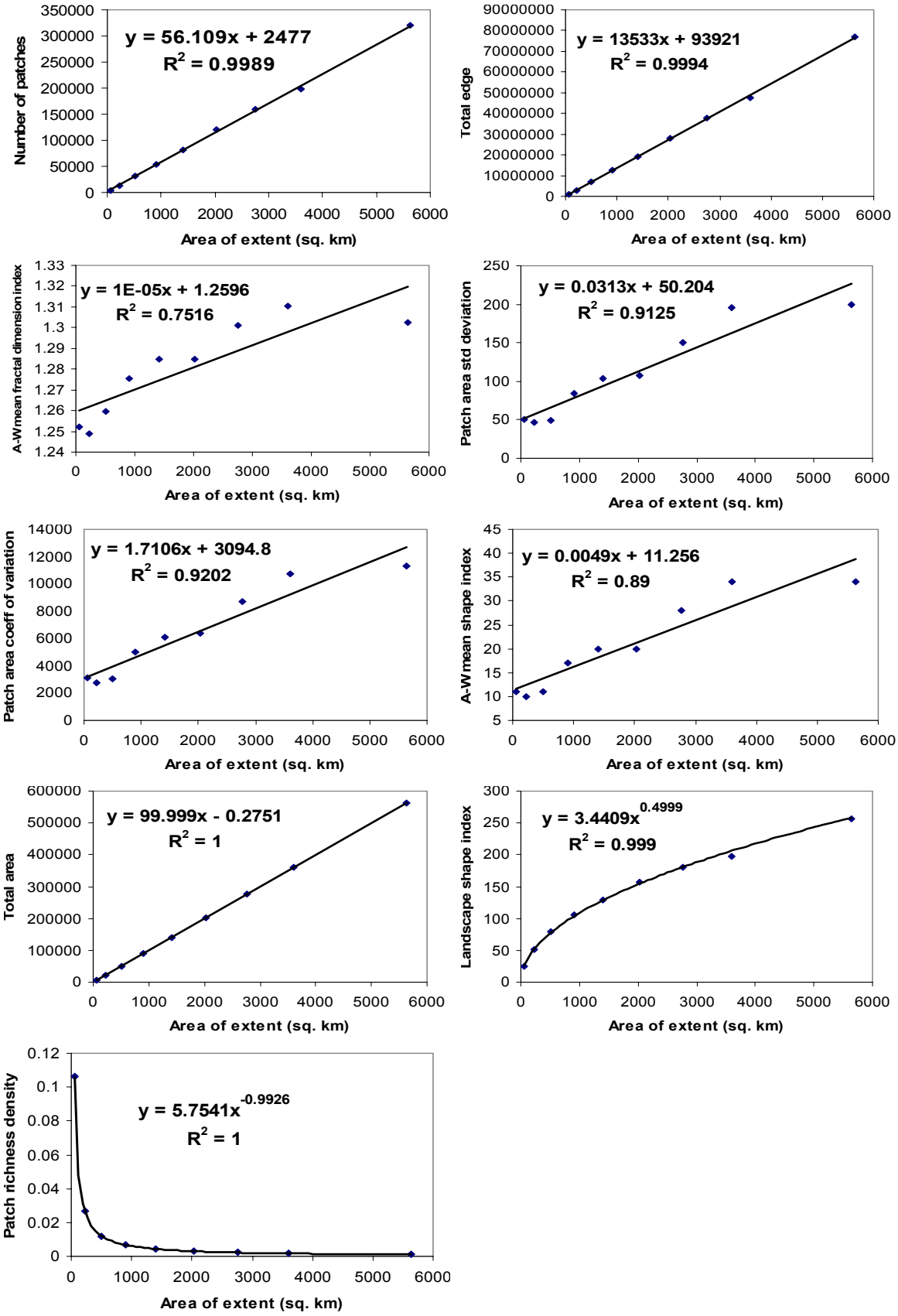

Figure 4.17 Scalograms showing the effects of changing extent on Type I metrics of NDVI84

Half of the 18 landscape metrics belonged to Type I. They included number of patches, total edge, patch area standard deviation, total area, patch area coefficient of variation, area-weighted mean shape index, landscape shape index, area-weighted mean fractal dimension index and patch richness density. Each of these metrics could be described by simple scaling relations such as linear or power law function (Table 4.9 and Figure 4.17). The scaling relations fitted the metrics of both landscape maps very well; with r^2 ranging between 0.752 and 1.000. Seven of the Type I metrics increased in value with increasing extent via a linear relationship. A third-order polynomial function fitted three of these metrics (*PASD*, *PACV* and *AWMSI*) better. Using *PASD* as example, r^2 values for fitting a third-order polynomial function and a linear function were 0.977 and 0.913 respectively. However, for easier interpretation and applicability, we preferred the linear fits. Landscape shape index and patch richness density, the other two Type I metrics, followed a power law relation as the extent was increased.

There were eight Type II metrics for LULC84; these did not exhibit any clear trends with changing extent and did not show consistency in their trends across the two landscapes (Figure 4.18). These included largest patch index, edge density, mean patch area, mean shape index, mean fractal dimension index, contagion, patch density and Shannon's diversity index. For LULC99, there were five Type II metrics. This is because linear models fitted *PD*, *ED* and *MPA* reasonably well, unlike the case of LULC84. This is one of several inconsistencies in Type II metrics across the two landscapes. It was observed that, in general, contagion decreased (LULC84) or increased (LULC99) with increasing extent (the two graphs at the top in Figure 4.18). As the extent of landscape increased, mean fractal dimension index and Shannon's diversity index increased (LULC84) or decreased (LULC99). For both landscapes, largest patch index decreased monotonically as extent increased from $56\,\mathrm{km}^2$ to $507\,\mathrm{km}^2$.

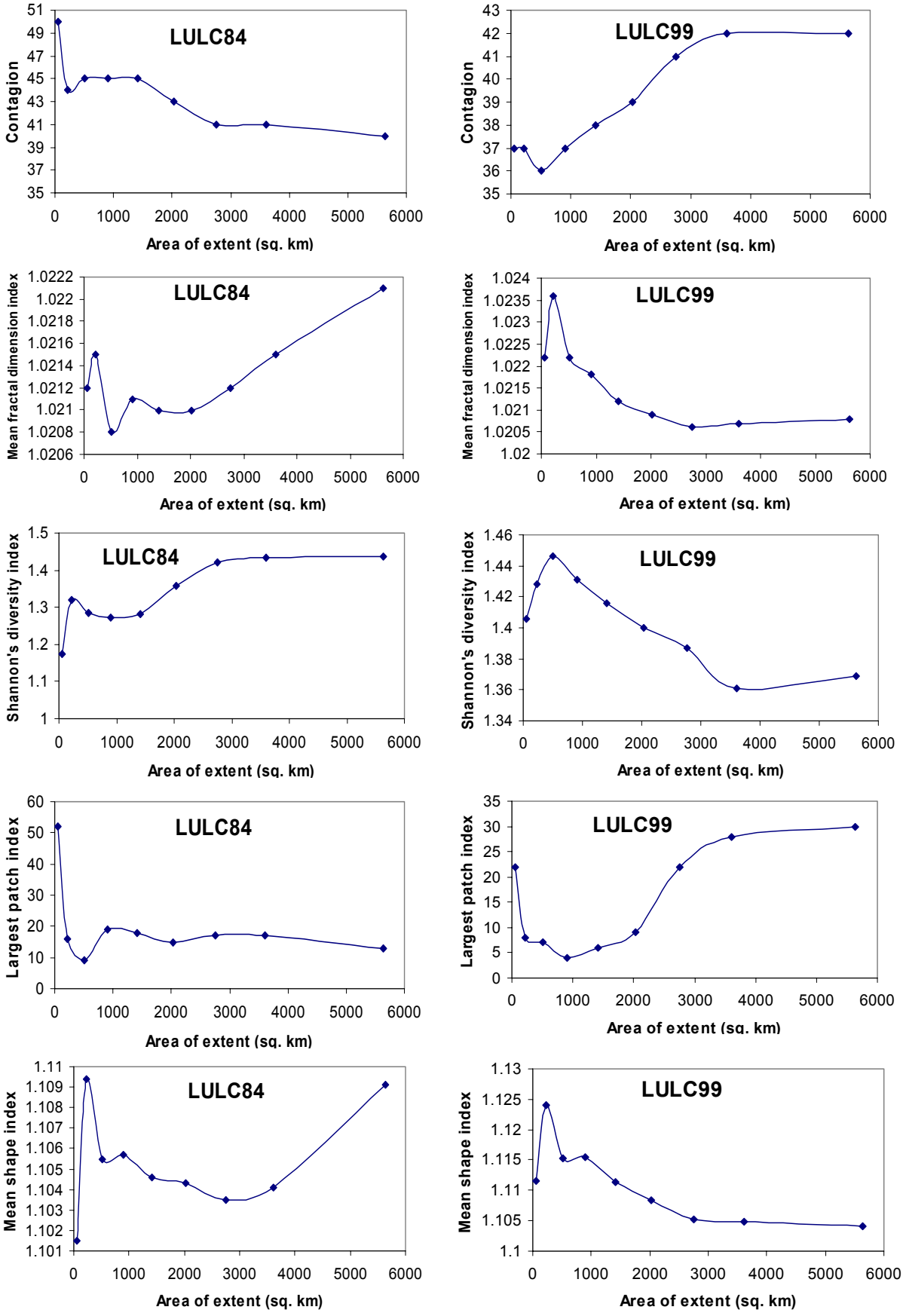

Figure 4.18 Scalograms showing the effects of changing extent on Type II metrics of LULC84 and LULC99

However for larger extents ($1000\,km^2$ or more), largest patch index increased in the case of LULC99, but remained fairly constant for LULC84. Between $56\,km^2$ and $2028\,km^2$, the pattern exhibited by mean shape index for both landscapes is similar. However, from $2761\,km^2$ upwards, it increased in the case of LULC84 and decreased for LULC99. Type III consisted of only one metric (patch richness) which had a constant value of 6 across all extents of the two landscapes. This indicated that even the smallest extent ($56\,km^2$) included all the six land use land cover types in the two landscapes.

4.7 Effects of changing the direction on pattern analysis

The effects of changing the direction (or starting position) of analysis on pattern analysis have long been recognized, particularly, in vegetation analysis (Greig-Smith, 1983; Dale, 1983). In a recent study of landscapes from North America, Wu *et al*. (2002) established that the direction of analysis significantly affected the values of landscapes metrics. Because the distribution of land use and land cover types in our landscapes is not uniform, we suspect that the direction in which maps with different extents were clipped from the original maps is likely to affect landscape pattern analysis. To investigate these effects on the 18 metrics, maps of different extents were clipped starting from each of the four corners and moving along the diagonal of the landscapes (see Figure 3.7). Thus, four directions were investigated in all: SW-NE, SE-NW, NW-SE and NE-SW.

The results (Tables 7.6 and 7.7 and Figure 4.19) showed that the direction of analysis significantly affect the values of landscapes metrics as did changing extent. Apart from three metrics (total edge, patch richness and patch richness density) which were not affected, all other metrics showed significant changes among the four directions of analysis. Type I metrics were most robust as they maintained their scaling relationships to a large extent, in spite of the fact that the parameter values in the scaling equations among the four directions varied considerably. Type II metrics showed the most pronounced directionality. Most of these metrics exhibited large differences at smaller extents among the four directions. However, the differences

became smaller as we approached the full landscape. Eventually, all four response curves converge at the full extent of the landscape.

It was interesting to note that the four response curves for each metric (Figure 4.19) could be grouped into two: NW-SE and NE-SW formed one group, while SW-NE and SE-NW formed another. The two curves in each group resembled each other in terms of the closeness of their values. The divergence of the response curves along different directions was a result of the anisotropy of landscape patterns. The characteristics of the curves and their relationships together carry useful information on landscape structure. For example, if the landscape pattern is completely isotropic, then the response curves of all metrics should be identical. However, isotropy in all directions is at best an idealized situation for real landscapes. In general, the differences among response curves in different directions ought to increase with increasing anisotropy.

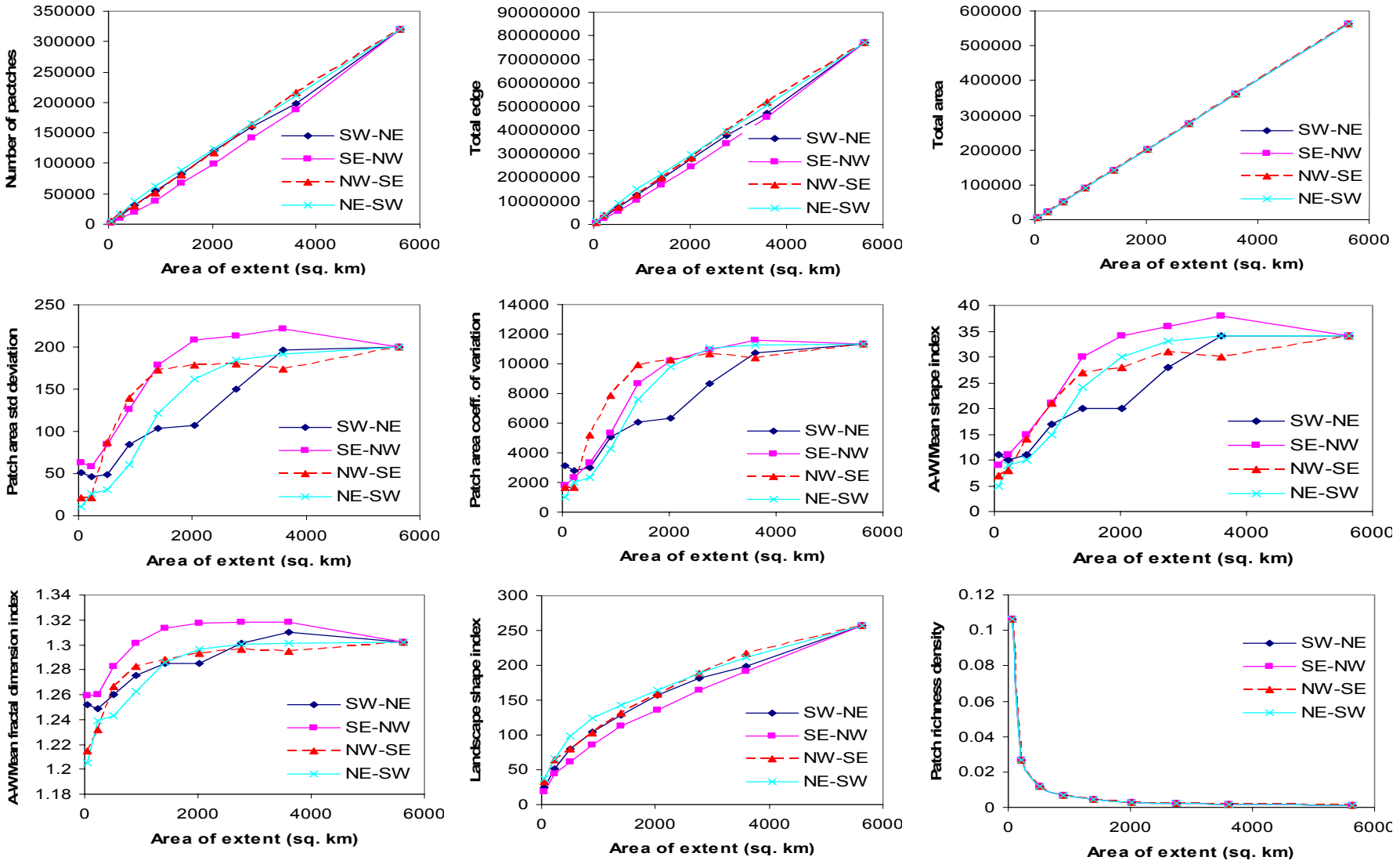

Figure 4.19 Scalograms showing the effects of changing the direction on pattern analysis

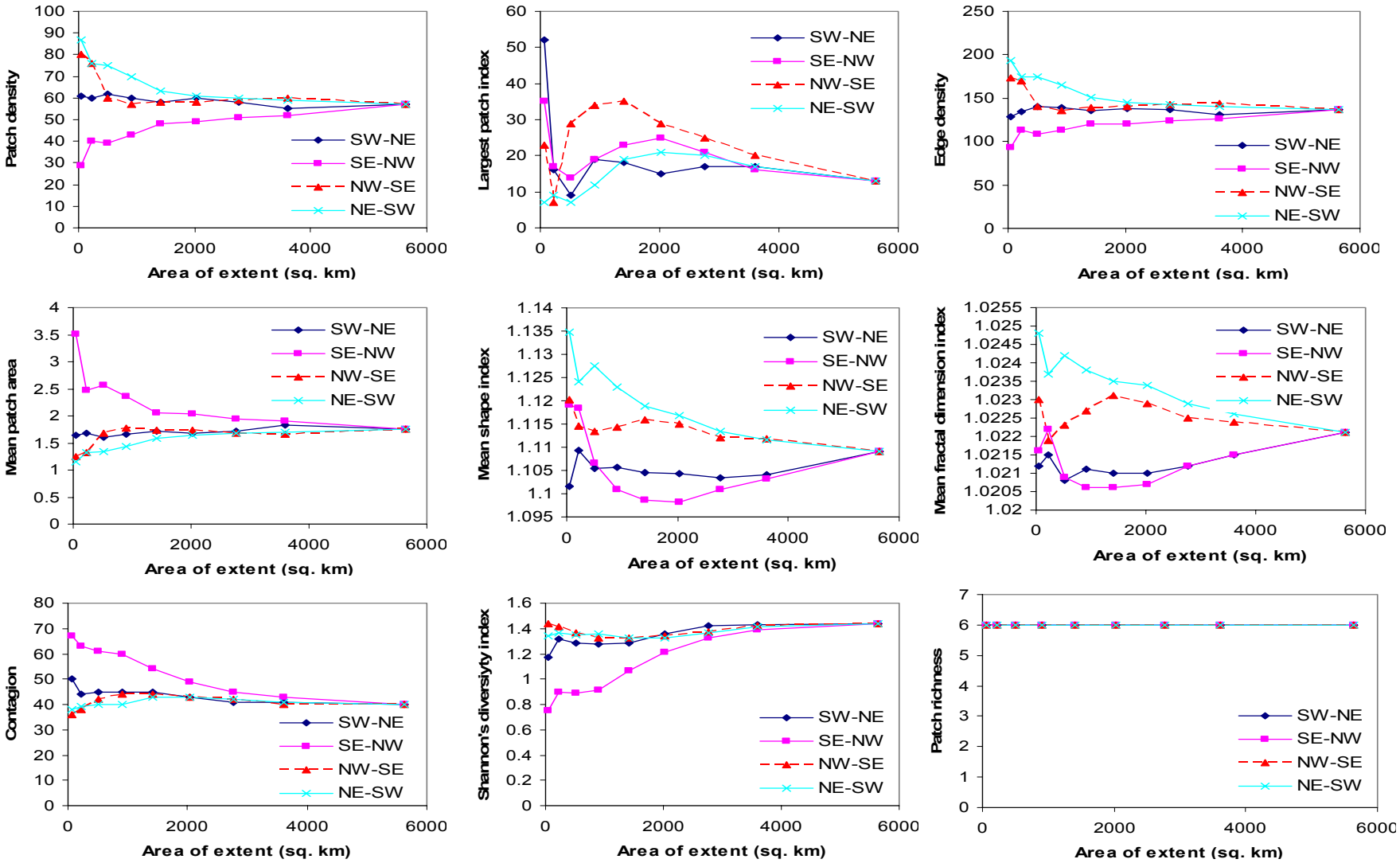

Figure 4.19 (Continued)

4.8 Comparing the effects of changing grain size and extent on landscape pattern metrics

A number of differences and similarities exist between the effects of changing grain size and extent on landscape metrics. In this section, we shall highlight these differences and similarities in the context of the numerical relationships that exist among certain landscape metrics. Overall, the effects of changing grain size on landscape metrics were more predictable than those of changing extent. This is evident in the fact that out of 18, there were 13 (or 72%) Type I metrics associated with changing grain size as compared with 9 (or 50%) for changing extent. Eighty-five percent of the Type I metrics, in relation to changing grain size, followed a power law relationship; while 78%, in relation to changing extent, followed a simple linear function.

Some of the landscape metrics are statistically correlated, and so we would expect these relationships to be reflected in their response curves. For example, $LSI = 0.25\ TE/\sqrt{TA}$, where TA is the total area of the landscape. Thus LSI and TE must have identical response curves for changing grain size, because TA remains constant over changing grain size. This is the case in our study: both LSI and TE exhibited decreasing power law relationships (Figure 4.20 (a) and (b)). However, in the case of changing extent, if TE increases as a power law function ($y = ax^b$) with extent, then LSI must follow a scaling function of the form $y \propto x^{b-1}$ because TA follows a linear trend. Thus, if b is close to 2 we would expect LSI to show a linear trend. Again, this was achieved in our study: LSI exhibited an increasing power law scaling, while TE followed a linear relationship (Figure 4.20 (c) and (d)).

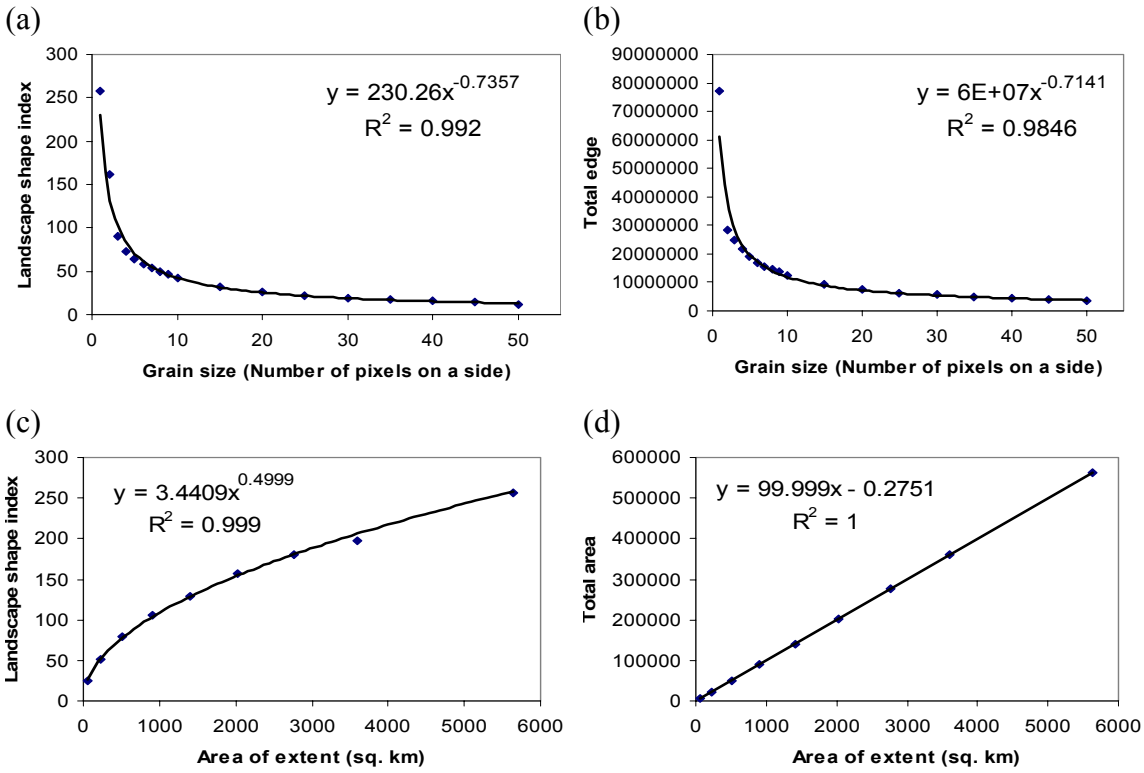

Figure 4.20 Scalograms showing the effects of changing grain size and extent on selected metrics

Similarly, because $PD \propto NP/TA$ and $ED \propto TE/TA$, we would expect a set of identical response curves to changing grain size for *PD* and *NP* and another set for *ED* and *TE*. These expectations are fulfilled in this study as both pair exhibited identical response curves (decreasing power law functions) to changing grain size. Yet, in the case of changing extent, *NP* and *PD* exhibited non identical response curves. The number of patches exhibited an increasing linear trend; while *PD* exhibited inconsistent trends across different landscapes (fluctuated for LULC84 and showed decreasing linear trend for LULC99). Similarly, *TE* and *ED* exhibited non identical responses – *TE* exhibited an increasing linear relation; while *ED* fluctuated for LULC84 and followed a decreasing linear trend for LULC99.

Patch richness (*PR*) and *PRD* are related by $PRD = PR/TA$, so for changing grain size they should have identical scaling patterns. The last graph in Figure 4.15 shows that both *PR* and *PRD* are constant functions over changing grain size. However, in the case of changing extent *TA* increased linearly while *PR* remained constant. Thus,

PRD obeyed a decreasing power law function. These patterns were consistent over the 2 landscape maps.

Since *PACV*, *PASD* and *MPA* are related by $PACV = (PASD/MPA)100$, the trends of any two of the three curves should help determine the trend of the third. For changing grain size, *PASD* increased linearly, while *PACV* decreased and *MPA* increased both as power law functions. However, for changing extent, the response curve for *MPA* is not predictable. This was most obvious for LULC84 landscape.

The comparison also revealed some similarities. *MSI* and *MFDI* exhibited similar patterns in response to changing grain size and changing extent. This is because they share strong mathematical similarity:

$$\frac{MSI}{MFDI} = \frac{\sum_{i=1}^{m}\sum_{j=1}^{n}\left(\frac{\left(0.25 p_{ij}\right)}{\sqrt{a_{ij}}}\right)}{\sum_{i=1}^{m}\sum_{j=1}^{n}\left(\frac{2\ln\left(0.25 p_{ij}\right)}{\ln a_{ij}}\right)},$$

where p_{ij} is the perimeter of patch ij, a_{ij} is the area of patch ij, $i = 1,\ldots,m$ is the number of patch types, $j = 1,\ldots,n$ is the number of patches. This equation shows that, while *MSI* is simply a perimeter-area ratio normalized based on the square shape and averaged over all patches, *MFDI* requires that both the numerator and the denominator are log-transformed before the summation for the entire class and across the landscape. Both *MSI* and *MFDI* exhibited a decreasing power law function for increasing grain size (Figure 4.21 (a) and (b)). *MSI* and *MFDI* also exhibited similar response curves for increasing extent, although these curves could not be described by simple scaling equations (Figure 4.21 (c) and (d)).

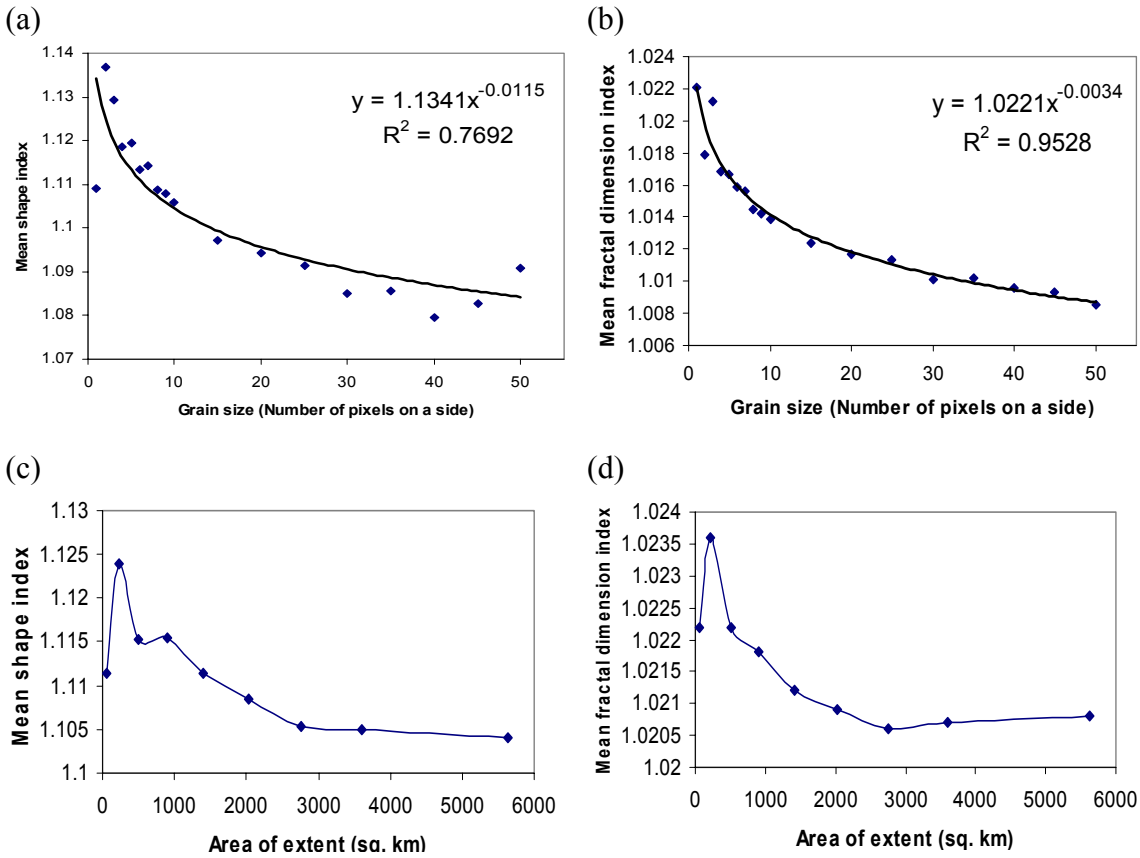

Figure 4.21 Scalograms showing similar effects of MSI and MFDI to both changing grain size and extent

Similar to *MSI* and *MFDI*, the response curves of *AWMSI* and *AWMFDI* to changing grain size and extent resembled each other. This is so because they also share similarities in their mathematical representations:

$$\frac{AWMSI}{AWMFDI} = \frac{\sum_{i=1}^{m}\sum_{j=1}^{n}\left[\left(\frac{2\ln(0.25\,p_{ij})}{\ln a_{ij}}\right)\left(\frac{a_{ij}}{A}\right)\right]}{\sum_{i=1}^{m}\sum_{j=1}^{n}\left[\left(\frac{0.25\,p_{ij}}{\sqrt{a_{ij}}}\right)\left(\frac{a_{ij}}{A}\right)\right]},$$

where the notations have their usual meanings. It was observed that both *AWMSI* and *AWMFDI* exhibited decreasing power law functions with respect to increasing grain size (Figure 4.22 (a) and (b)); while they exhibited increasing linear functions with respect to increasing extent (Figure 4.22 (c) and (d)).

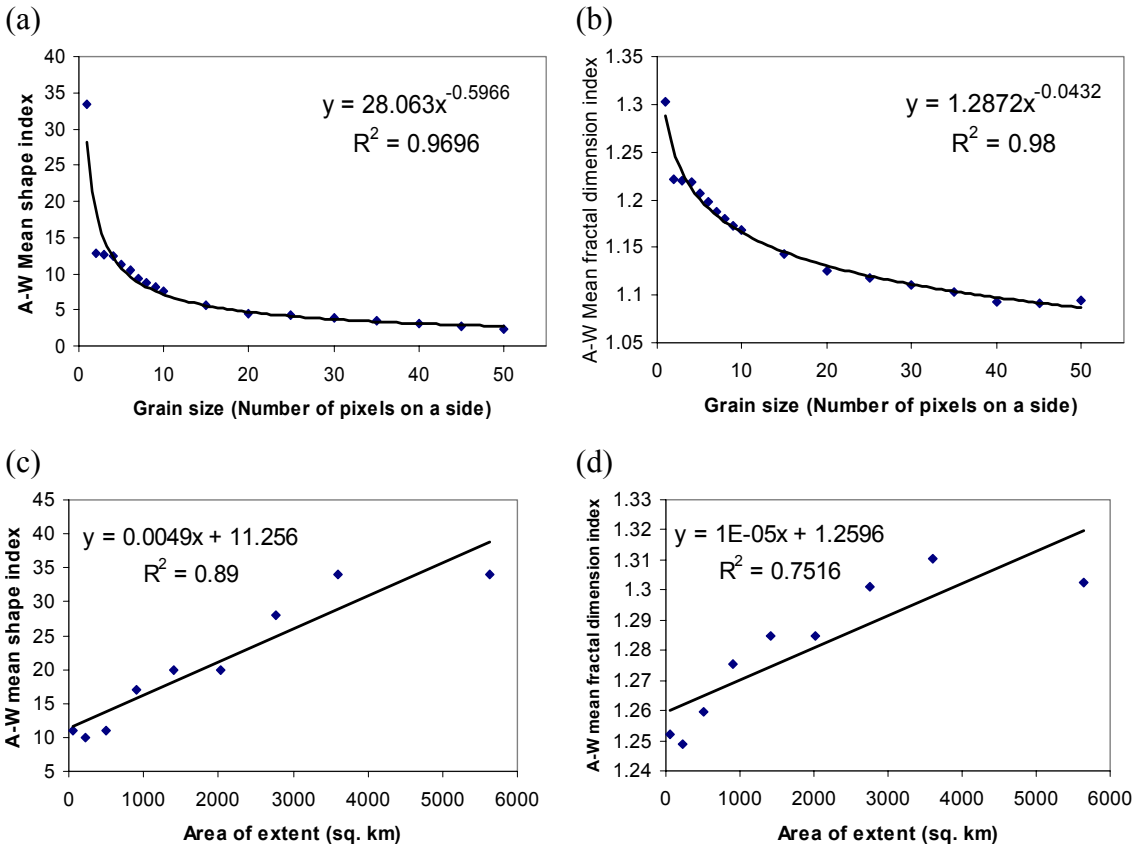

Figure 4.22 Scalograms showing similar effects of AWMSI and AMFDI to both changing grain size and extent

Table 4.10 is a complete summary of the comparison of scaling relations of landscape metrics with respect to changing grain size and extent. In related studies, Wu *et al*. (2002), Shen *et al*. (2004) and Wu (2004) found that the response patterns of commonly used landscape metrics to changing grain size and extent could be grouped into three main types: (1) Type I metrics exhibit consistent and robust scaling relations in the forms of linear, power, or logarithmic functions over a range of scales; (2) Type II metrics show staircase-like responses with changing scale; and (3) Type III metrics behaving erratically in response to changing scale and with no consistent scaling relations among different landscapes. In general, the results of this study corroborate these findings. However, there are apparent differences which are noteworthy. None of the 18 commonly used landscape metrics exhibited clear staircase-like response curves with respect to changing grain size or extent as reported by other studies.

Table 4.10 Comparison of scaling relations of landscape metrics with respect to changing grain size and extent

Landscape metric	Type of scaling relation	
	Grain size	Extent
Total area	unpredictable	linear
Number of patches	power law	linear
Patch density	power law	unpredictable
Largest patch index	unpredictable	unpredictable
Landscape shape index	power law	power law
Total edge	power law	linear
Edge density	power law	unpredictable
Mean patch area	power law	unpredictable
Patch area standard deviation	linear	linear
Patch area coefficient of variation	power law	linear
Mean fractal dimension index	power law	unpredictable
Area-weighted mean fractal dimension index	power law	linear
Mean shape index	power law	unpredictable
Area-weighted mean shape index	power law	linear
Contagion	power law	unpredictable
Patch richness	constant	constant
Patch richness density	constant	power law
Shannon's diversity index	unpredictable	unpredictable

If there were any such trends, they would have been classified into Type II which we described as inconsistent and unpredictable. In the case of changing grain size, Wu (2004) characterized contagion, mean shape index and mean fractal dimension index as having no scaling relations (unpredictable). However, all three exhibited consistent decreasing power law functions with r^2 ranging between 0.77 and 0.95. Patch richness and patch richness density were found to be constants with respect to changing grain size, but Wu (2004) found them to exhibit staircase-like responses. With respect to changing grain size, Wu (2004) found *AWMSI*, *AWMFDI*, *PACV*, *PASD* and *PR* to exhibit staircase-like responses. However, our study found *AWMSI*, *AWMFDI*, *PACV* and *PASD* to follow linear relationships; while *PR* remained constant with increasing extent. We also noticed that specific forms of the scaling functions for Type I metrics changed in the case of changing extent.

So why were there these differences? Two major factors might account for the discrepancies between our results and those of previous studies: (1) the composition and configuration of the landscapes and (2) the form of extents used in relation to the original extent. The landscapes used by Wu *et al*. (2002), Shen *et al*. (2004) and Wu

(2004) differ markedly from ours. Their landscapes were all from North America, so we believe compositional (e.g. diversity of patch types) and configurational (e.g. spatial arrangement of different patch types) differences might have influenced the results. We also thought it wise to clip the different extents in the shape of and in specified ratios to the original extent so as to facilitate easy interpretation of the results. However, other studies clipped the different extents in the shape of squares irrespective of the shape of the original data. These differences might have also contributed to the slight differences registered.

5 SUMMARY AND CONCLUSION

5.1 Summary

In this study, the researcher adapted statistical applications of a modern tool (wavelets) to help provide answers to the two fundamental questions of multiscale analysis in a landscape ecological study. In particular, the Daubechies and Haar wavelet filters were employed to investigate what scales are important contributors to the overall variability of the NDVI and DEM data sets. Furthermore, wavelet multiresolution decomposition facilitated the separate study of small- and large-scale wavelet coefficients for statistical self-similarity. Statistical scalograms were also constructed to characterize the multiscale structure of landscapes from northern Ghana.

A summary of the research findings, following the outline of the objectives, are presented in the ensuing paragraphs. Moving window statistics of the NDVI and DEM data sets were computed to investigate for heteroscedasticity and proportional effect. The local means of the NDVI fields appeared to be heteroscedastic, while their corresponding standard deviations remained fairly constant over the entire study area. For the DEM, both local means and local standard deviations remained fairly constant over the study area. No proportional effect was observed between local means and corresponding standard deviations for all three data sets. These results are good for the purpose of estimation, because estimates from any particular sector will be as good as estimates elsewhere in the study area.

Wavelet variance analysis was conducted using the Daubechies “d6” and the Haar wavelet filters to determine the dominant scales for the NDVI and DEM data sets. The trend of change in the wavelet variance of the NDVI data is not a simple function of its resolution. However for DEM, the trend of wavelet variance was a linear function of its resolution. With the “d6” wavelet filter, the NDVI84 revealed one major peak at the 240 meter scale; while the NDVI99 revealed two peaks: a major one at the 240 meter scale and a minor at the 960 meter scale. Thus, for both NDVI84 and NDVI99, the dominant scale is the 240 meter scale. DEM did not exhibit a dominant scale as there was no clear identifiable peak. The presence of peaks in the wavelet variance-resolution graph is indicative of hierarchical and hence a multiple-scale structure in the

landscape (Wu *et al*., 2000). Thus, the results of the wavelet variance analysis suggest that the NDVI fields exhibit hierarchical and multiple-scale structure.

The knowledge of multiple-scale structure led to a statistical self-similarity analysis of the wavelet coefficients of the NDVI and DEM data sets. A wavelet multi-resolution analysis was conducted using NDVI84, NDVI99 and DEM. The small-scale wavelet coefficients were used to investigate whether these data sets exhibit statistical self-similar scaling behavior. The first four moments of the coefficients were used through seven levels of dyadic decompositions. The NDVI data sets were shown to be statistically self-similar over the 120 meter to 3.84 km scales in all the three directions of wavelet decomposition, while DEM was shown to be statistically self-similar over the 3.6 km to 11.52 km scales in all the three directions of wavelet decomposition. NDVI84 had slopes of -0.67, -1.29 and -0.92 in the horizontal, vertical and diagonal directions, respectively. NDVI99 had slopes of -0.59, -1.32 and -0.59 in the horizontal, vertical and diagonal directions, respectively; while DEM had slopes of -0.56, -2.26 and -1.14 in the horizontal, vertical and diagonal directions, respectively. The negative slopes are indicative of increasing variability with decreasing scales; while the differences in their magnitudes are indicative of the anisotropic nature of the landscapes. The magnitude of the slopes indicates long range behavior and may imply a methodology for statistically assimilating remotely sensed data into large-scale meso and global climate models.

Two land use and land cover maps (LULC84 and LULC99) were used in the indirect approach to multiscale analysis. Both maps were resampled at different scales, according to grain size and extent, after which the values of 18 commonly used landscape metrics were estimated from each aggregated map. The study then investigated how these landscape metrics responded to changing grain size and extent, by exploring for general scaling relations and idiosyncratic behaviors. The results showed that changing grain size and extent both had significant effects on landscape metrics. In general, the results corroborate findings of related studies. The patterns exhibited by the landscape metrics as a result of changing grain size and extent also reflected the statistical correlations that exit among them. The response curves of the metrics to both changing grain size and extent could be grouped into three main types: Type I – predictable responses with simple scaling relationships (e.g. power law,

linear); Type II – unpredictable or fluctuating responses with no clear simple scaling relations; and Type III – fixed responses irrespective of changes to grain size or extent.

In general, more landscape metrics (72%) showed consistent scaling relations with changing grain size than with changing extent (50%) – indicating that the effects of changing grain size are generally more predictable than those of changing map sizes. The study also established that the direction of analysis, in the case of changing extent, had significant effects on landscape pattern analysis. Type II metrics showed the most pronounced directionality. Most metrics in this category exhibited large differences at smaller extents among the four directions. However, the differences became smaller with increasing extent until eventually all four response curves converge at the full extent of the landscape. The four response curves for each metric (Figure 4.19) could be grouped into two: NW-SE and NE-SW in one group, and SW-NE and SE-NW in another. The two curves in each group resembled each other in terms of the closeness of their values. The divergence of the response curves along different directions was a result of the anisotropy of landscape patterns. The characteristics of the curves and their relationships together carry useful information on landscape structure. For example, if the landscape pattern were completely isotropic, then the response curves of all metrics would be identical. However, isotropy in all directions is at best an idealized situation for real landscapes. In general, the differences among response curves in different directions increases with increasing anisotropy.

It was also observed that the method of aggregation in the case of changing grain size had significant effects on landscape pattern analysis. Sixteen out of 18 metrics showed significant differences among the three methods (mean, median and mode) of aggregation. Type I metrics were most robust as they maintained their scaling relationships, although the parameter values in the scaling equations among the different methods changed slightly. Type III metrics were unaffected by the different methods of aggregation. For most other metrics, the values produced by the median and mode aggregation methods were more closely related, suggesting that they could be used interchangeably.

5.2 Conclusion

An understanding of the nature of scale in landscape data is important when extrapolating to coarser resolutions, or in the assimilation of data into meso-scale and global climate models. The knowledge that the NDVI and DEM fields are statistical self-similarity is useful for the assimilation of these fields into large-scale models as well as for comparison of model output with the observed satellite data. One may have reasonable confidence through the robustness of the scaling exponents, as determined by the r^2 values, in the aggregation procedure for maintaining the statistical properties present within the original data. Moreover, the high magnitude of the slope values may lead to a larger scale view of the dynamics observed by coarser resolution sensors. In other words, the high magnitudes of the slope values indicate the existence of larger scale correlation over the entire range of scales examined in this study.

Knowledge of how biophysical variables vary in space is an important issue in many areas of science. The use of landscape data to ascertain the observed scaling behavior has implications for any large-scale ecological and the climatological modeling, where model output is necessary at scales larger than those at which the data are collected. The results of the direct multiscale analysis (i.e. wavelet analysis of the statistical variability of the NDVI and DEM fields with changes in spatial resolution) contribute to the basis for understanding how to assimilate landscape data into coarser resolution models. As a further example in the ecological field, research in phenology involves examining the spatial distribution of the length of the growing season as a function of environmental forces. Thus understanding the spatial scaling of input parameters will represent more realistically, the underlying physical processes. This will lead to more pragmatic agricultural considerations as to when to plant, length of growing season, etc. Furthermore, the incorporation of representative scaled parameters into such models may lead to further insights into non-linear processes that affect the overall physiological mechanisms that underlie plant atmosphere systems.

The quantification of spatial pattern is necessary to link the effects of landscape heterogeneity with ecological function and to use remotely sensed data to measure change in large spatial units. The study results demonstrate that the spatial scale at which these patterns are quantified influences the results and measurements made at different scales may not be comparable. In other words, there is no *optimal*

scale for characterizing spatial heterogeneity and comparison between landscapes using pattern indices must be based on the same spatial scales. Furthermore, qualitative and quantitative changes in measurements across spatial scales will differ according to how scale is defined. Thus, the definition and directions and methods of changing scale must always be explicitly stated. It is important to define the scale of ecological data in terms of both grain size and extent.

In addition, the results may provide practical guidelines for scaling of spatial pattern. For example, landscape metrics that do not change (Type III) and those that change predictably (Type I) across scales reflect landscape features that can easily be extrapolated or interpolated from fine scales to broad scales. In contrast, unpredictable metrics (Type II) represent landscape features whose extrapolation may be difficult and which may require information on the specifics of the landscape of concern at several different scales. Finally, to quantify spatial heterogeneity using landscape metrics, it is both necessary and desirable to use landscape metric scalograms, instead of single-scale values. Indeed, a comprehensive empirical database containing pattern metric scalograms and other forms of multiple-scale information of diverse landscapes is crucial for achieving a general understanding of landscape patterns and developing spatial scaling rules.

5.3 Suggestions for further research

One issue that needs further study is the effect of the choice of wavelet. This is because the success of both analysis and modeling depends largely on an appropriate choice of wavelet. It will be interesting to compare results of multiscale analysis using different orthogonal and biorthogonal wavelets. The findings of the indirect multiscale analysis can be investigated further by using several landscape maps which are different in composition and configuration. This study covered only landscape-level metrics, which were computed for the entire landscape and thus measured the landscape pattern rendered by all patch types. However, certain ecological applications require information on the abundance and configuration of different habitat or cover types that are provided by class-level metrics. There is the need, therefore, to investigate whether

class-level metrics show similar patterns to those found for landscape-level metrics in terms of their responses to changing grain size and extent. Furthermore, this study considered 2 out of 3 situations in which scale effects on spatial pattern analysis may be observed. The third situation which involves changing the grain size and extent simultaneously could be a candidate for further research.

6 REFERENCES

Abatania, L and Albert, H. 1993. Potentials and constraints of legume production in the farming systems of northern Ghana. In: Proceedings of the Third Workshop on Improving Farming Systems in the Interior Savannah Zone of Ghana. Nyankpala Agricultural Experimental Station, Tamale, Ghana, pp. 170-181.

Allen, R.F.H., O'Neill, R.V. and Hoekstra, T.W. 1984. Interlevel relations in ecological research and management. Some working principles from Hierarchy theory. USDA Forest Service Gen. Tech. Rep. RM-110, Rocky Mountain Forest and Range Experiment Station. Fort Collins, CO, U.S.A.

Allen, T.F.H. and Hoekstra, T.W. 1991. Role of heterogeneity in scaling of ecological systems under analysis. Ecological Studies 86: 47-68.

Allen, T.F.H. and Starr, T. B. 1982. Hierarchy: perspectives for ecological complexity. University of Chicago Press, Chicago, U.S.A.

Anselin, L. 1995. Local indicators of spatial association – LISA. Geographical Analysis 27: 93-115.

Arbia, G. 1989. Spatial Data Configuration in Statistical Analysis of Regional Economic and Related Problems. Dordrecht: Kluwer Academic Publishers, Boston, USA.

Atkinson, P.M. and Curran, P.J. 1995. Defining an optimal size of support for remote sensing investigations. IEEE Transactions on Geoscience and Remote Sensing 33(3): 768-776.

Benson B.J. and Mackenzie M.D. 1995. Effects of sensor spatial resolution on landscape structure parameters. Landscape Ecology 10: 113–120.

Bian L. and Walsh S.J. 1993. Scale dependencies of vegetation and topography in a mountainous environment of Montana. Professional Geographer 45: 1–11.

Bian, L. 1997. Multiscale nature of spatial data in scaling up environmental methods. In: Quattrochi, D.A and Goodchild, M.F. (eds) Scale in Remote Sensing and GIS. CRC Press, Inc., pp. 13-26.

Bian, L. and Butler, R. 1999. Comparing effects of aggregation methods on statistical and spatial properties of simulated spatial data. Photogram. Eng. Rem. Sens. 65: 73-84.

Bradshaw, G.A. and Spies, T.A. 1992. Characterizing canopy gap structure in forests using wavelet analysis. Journal of Ecology 80: 205-215.

Braimoh, A.K. 2004. Modeling land-use change in the Volta Basin of Ghana. Ph.D. Thesis. Cuvillier, Göttingen, Germany.

Bruce, A.G. and Gao, H-Y. 1996. Applied Wavelet Analysis with S-plus. Spinger-Verlag, New York, USA.

Brunsell, N.A. and Gillies, R.R. 2002. Incorporating surface emissive into a thermal atmospheric correction. Photogrammetric Engineering and Remote Sensing 68(12): 1263-1269.

Brunsell, N.A. and Gillies, R.R. 2003. Determination of scaling characteristics of AVHRR data with wavelets: Application to SGP97. International Journal of Remote Sensing 24(14): 2945-2957.

Burrough, P.A. 1995. Spatial aspects of ecological data. In: Jongman, R.H.G. and Ter Braak, C.J.F. (eds) Data Analysis in Community and Landscape Ecology. Cambridge University Press, Cambridge, pp. 213-265.

Burrough, P.A. and McDonnell, R.A. 1998. Principles of Geographical Information Systems. 2nd ed. Oxford University Press, New York, U.S.A.

Cao, C. and Lam, S-N. 1997. Understanding the scale and resolution effects in remote sensing and GIS. In: Quattrochi, D.A. and Goodchild, M.F. (eds) Scale in Remote sensing and GIS. Lewis Publishers, pp. 57-72.

Cliff, A.D. and Ord, J.K 1981. Spatial Process: Models and Applications. Pion, London, U.K.

Constantine, W.L.B. and Percival, D.B. 2002. S+Wavelets 2.0. Insightful Corporation, Seattle, U.S.A.

Costanza, R. 1989. Model goodness of fit - A multiple resolution procedure. Ecological Modeling 47: 199-215.

Cressie, N. 1991. Statistics for Spatial Data. John Wiley & Sons, New York, U.S.A.

Cullinan, V.I.M. and Thomas, J.M. 1992. A comparison of quantitative methods for examining landscape pattern and scale. Landscape Ecology 7(3): 211-227.

Cullinan, V.I.M., Simmons, A. and Thomas, J.M. 1997. A Bayesian test of hierarchy theory: scaling up variability in plant cover from field to remotely sensed data. Landscape Ecology 12: 273-285.

Curran, P.J. 1988. The semi-variogram in remote sensing: an introduction. Remote Sensing of Environment 24: 493-507.

Dale, M.R.T. 1983. Spatial Pattern Analysis in Plant Ecology. Cambridge University Press, Cambridge, UK.

Daubechies, I. 1992. Ten Lectures on Wavelets. SIAM, Philadelphia, U.S.A.

De Cola, L. 1989. Fractal analysis of a classified Landsat scene. Photogrammetric Engineering and Remote Sensing 55(5): 601-610.

De Cola, L. 1994. Simulating and mapping spatial complexity using multiscale techniques. International Journal of Geographic Information Systems 8(5): 411-427.

De Cola, L. 1997. Multiresolution covariation among Landsat and AVHHR vegetation indices. In: Quattrochi, D.A. and Goodchild, M.F. (eds) Scale in Remote Sensing and GIS. CRC Press Inc., pp. 73-92.

Dodds, P.S. and Rothman, D.H. 2000. Scaling, university, and geomorphology. Annual Review of Earth and Planetary Sciences 28: 571-610.

Dubayah, R., Wood, E.F. and Lavallee, D. 1997. Multiscaling analysis in distributed modeling and remote sensing: an application using soil moisture. In: Quattrochi, D. A. and Goodchild, M.F. (eds) Scale in Remote Sensing and GIS. Lewis Publishers, pp. 93-112.

Ehleringer, J.R. and Fields, C.B. (eds) 1993. Scaling Physiological Processes, Leaf to Globe. Academic Press, New York, U.S.A.

Fact file 2003. [Online] Available at http://www.ghana.gov. gh/living/region/northern.php (accessed 23 March, 2004).

Foody, G.M and Curran, P.J. 1994. Estimation of tropical forest extent and regeneration stage using remotely sensed data. Journal of Biogeography 21(1): 223– 244.

Getis, A. and Ord, J.K. 1992. The analysis of spatial association by use of distance statistics. Geographical Analysis 24: 189-206.

Ghana Statistical Service 2002. 2000 Population and housing census. Special Report on 20 Largest Localities. Ghana Statistical Service, Accra, Ghana.

Goodchild, M.F. and Quattrochi, D.A. (1997). Scale, multiscaling, remote sensing and GIS. In: Quattrochi, D.A. and Goodchild, M.F. (eds) Scale in Remote Sensing and GIS. Boca Raton, FL: CRC/Lewis Publishers, Inc., pp. 1-11.

Gordon, C. and Amatekpor, J.K. (eds) 1999. The sustainable Integrated Development of the Volta Basin in Ghana. Volta Basin Research Project, Accra, Ghana.

Greig-Smith, P. 1983. Quantitative Plant Ecology. University of California Press, Berkeley, California, USA.

Grimes, D.I.F., Coppola, E., Verdecchia, M. and Visconti, G. 2003. A neural network approach to real-time rainfall estimation for Africa using satellite data. Journal of Hydrometeorology 4: 1119-1133.

Gupta, V. and Waymire, E. 1990. Multiscaling properties of spatial rainfall and river flow distributions. Journal of Geophysical Research 95: 1999-2009.

Gupta, V.K. and Waymire, E.C. 1989. Statistical self-similarity in river networks parameterized by elevation. Water Resources Research 25(3): 463-476.

Haar, A. 1910. Zur Theorie der orthogonalen Funktionen-Systeme. Mathematische Annalen 69: 331-371.

Harvey, L.D.D. 1997. Upscaling in global change research. In: Hassol, S.J. and Katzenberger, J. (eds) Elements of Change. Aspen, Colorado, U.S.A., pp. 14-33.

Hay, G., Marceau, D.J., Dubé, P. and Bouchard, A. 2001. A multiscale framework for landscape analysis: object-specific analysis and upscaling. Landscape Ecology 16: 471–490.

Hay, G.J., Niemann, K.O. and Goodenough, D.G. 1997. Spatial thresholds, image-objects and upscaling: a multiscale evaluation. Remote Sensing of Environment 62: 1-19.

Helmlinger, K.R., Kumar, P. and Foufoula-Georgiou, E. 1993. On the use of digital elevation model data for Hortonian and fractal analyses of channel networks. Water Resources Research 29(8): 2599–2613.

Henebry, G.M. and Kux, H.J.H. 1995. Lacunarity as a texture measure for SAR imagery. International Journal of Remote Sensing 16: 565-571.

Holben, B.N. 1986. Characteristics of maximum-value composite images from temporal AVHRR data. International Journal of Remote Sensing l7(11): 1417-1434.

Hu, Z., Chen, Y. and Islam, S. 1998. Multiscaling properties of soil moisture images and decomposition of large and small scale features using wavelet transforms. International Journal of Remote Sensing 19: 2451–2467.

Isaaks, E.H. and Srivastava, R.M. 1989. An Introduction to Applied Geostatistics. Oxford University Press Inc., New York, U.S.A.

Jansen, F.E. 1996. Reservoir Description from Production Data. University of Tulsa, Tulsa, Oklahoma, U.S.A.

Jansen, F.E. and Kelkar, M. 1998. Upscaling of reservoir properties using wavelets. Presented at an Oil and Gas Conference and Exhibition by the Society of Petroleum Engineers in New Delhi, India.

Jelinski, D.E. and Wu, J. 1996. The modifiable areal unit problem and implications for landscape ecology. Landscape Ecology 11: 129-140.

Jupp, D.L.B., Strahler, A.H. and Woodcock, C.E. 1988(a). Autocorrelation and regularization in digital images. I. Basic theory. IEEE Transactions on Geosciences and Remote Sensing. 26(4): 463-473.

Jupp, D.L.B., Strahler, A.H. and Woodcock, C.E. 1988(b). Autocorrelation and regularization in digital images. II. Simple image models. IEEE Transactions on Geosciences and Remote Sensing 26(4): 247-258.

Justice, C.O., Markham, B.L., Townshend, J.R.G. and Kennard, R.L. 1989. Spatial degradation of satellite data. International Journal of Remote Sensing 10: 1539-1561.

Kipo, T. 1993. Farmers' perception of the factors of production and agriculture in Northern Region. In: Proceedings of the Third Workshop on Improving Farming Systems in the Interior Savannah Zone of Ghana. Nyankpala Agricultural Experimental station, Tamale, Ghana, pp. 189-197.

Klinkenberg, B. and Goodchild, M.F. 1992. The fractal properties of topography: a comparison of methods. Earth Surface Process 17: 217-234

Kolasa, J. and Pickett, S.T.A. (eds) 1991. Ecological Heterogeneity. Springer-Verlag, New York, U.S.A.

Krummel, J.R., Gardner, R.H., Sugihara, G., O'Neill, R.V. and Coleman, P.R. 1987. Landscape patterns in a disturbed environment. Oikos 48: 321-324.

Kumar, P. and Foufoula-Georgiou, E. 1993(a). A multicomponent decomposition of spatial rainfall fields. 1. Segregation of large- and small-scale features using wavelet transforms. Water Resources Research 29(8): 2515–2532.

Kumar, P. and Foufoula-Georgiou, E. 1993(b). A multicomponent decomposition of spatial rainfall fields. 2. Self-similarity in fluctuations. Water Resources Research 29(8): 2533–2544.

Kumar, P. and Foufoula-Georgiou, E. 1997. Wavelet analysis for Geophysical applications. Reviews of Geophysics 35(4): 385–412.

Lam, N.S-N. and Quattrochi, D.A. 1992. On the issues of scale, resolution, and fractal analysis in the mapping sciences. Professional Geographer 44(1): 88-98.

Levin, S.A. 1992. The problem of pattern and scale in ecology. Ecology 73: 1943-1967.

Mallat, S.G. 1989. A theory for multiresolution signal decomposition: the wavelet representation. IEEE Transactions on Pattern Analysis and Machine Intelligence 11(7): 674-693.

Mallat, S.G. 1998. A Wavelet Tour of Signal Processing. Academic Press, San Diego, U.S.A.

McGarigal, K. and Marks, B. 2002. Spatial Pattern Analysis Program for Categorical Maps: Computer Software. University of Massachusetts, Amherst, U.S.A.

Meentmeyer, V. and Box, E. 1987. Scale effects in landscape studies. In: Turner, M. (ed) Landscape Heterogeneity and Disturbance. New York, Springer Verlag, pp. 15-34.

Meyer, Y. 1993. Wavelets: Algorithms and Applications. SIAM, Philadelphia, U.S.A.

Miller, D.H. 1978. The factor of scale: ecosystem, landscape mosaic, and region. In: Hammond, K.A., Macinio, G. and Fairchild, W.B. (eds) Environment: A Guide to the Literature. University of Chicago Press, Chicago, U.S.A., pp. 63-88.

Milne, B.T. 1991. Lessons from applying fractal models to landscape patterns. In: Turner, G.R.H.G. (ed) Quantitative Methods in Landscape Ecology. Springer-Verlag, New York, U.S.A., pp. 199-235.

Misiti, M., Misiti, Y., Oppenheim, G. and Poggi, J-M. 2001. Wavelet Toolbox Users' Guide. Version 2.1. The Mathworks, Inc., Massachusetts, U.S.A.

Moellering, H. and Tobler, W.R. 1972. Geographical variances. Geographical Analysis 4: 34-42.

Monteith, J.L. 1965. Evaporation and environment. In: Proceedings of the 19th Symposium of the Society for Experimental Biology. Cambridge, New York, U.S.A., pp. 205-233.

Moody A. and Woodcock C.E. 1994. Scale-dependent errors in the estimation of land-cover proportions: implications for global land-cover datasets. Photogrammatic Engineering and Remote Sensing 60: 585–594.

Moreno, J.F. and Melia, J. 1994. An optimal interpolation method applied to the resampling of NOAA AVHRR data. IEEE Transaction on Geoscience and Remote Sensing 32(1): 131-151.

Morettin, P.A. 1997. Wavelets in statistics. Resenhas 3(2): 211-272.

Nikora, V.I., Pearson, C.P. and Shankar, U. 1999. Scaling properties in landscape patterns: New Zealand experience. Landscape Ecology 14: 17-33.

O'Neill, R.V., Hunsaker, C.T., Timmins, S.P., Timmins, B.L., Jackson, K.B., Jones, K.B., Riitters, K.H. and Wickham, J.D. 1996. Scale problems in reporting landscape pattern at the regional scale. Landscape Ecology 11: 169–180.

Ogden, R.T. 1997. Essential Wavelets for Statistical Applications and Data Analysis. Birkhäuser, Boston, U.S.A.

Ogden, R.T. 1997. On preconditioning the data for the wavelet transform when the sample size is not a power of two. Communications in Statistics 26: 467-485.

O'Neill, R.V., DeAngelis, D.L., Waide, J.B. and Allen, T.F.H. 1986. A Hierarchical Concept of Ecosystems. Princeton University Press, Princeton, U.S.A.

Overseas Development Institute 1999. Rethinking natural resource degradation in semi-arid sub-Saharan Africa: The case of Semi-Arid Ghana. ODI Rural Policy and Environment Group, UK.

Pecknold, S., Lovejoy, S., Schertzer, D. and Hooge, C. 1997. Multifractals and resolution dependence of remotely sensed data: GSI to GIS. In: Quattrochi, D.A. and Goodchild, M.F. (eds) Scale in Remote Sensing and GIS. Lewis Publishers, pp. 361-394.

Percival, D.B. and Walden, A. 2000. Wavelets Methods for Time Series Analysis. Cambridge University Press, Cambridge, U.K.

Platt, T. and Denman, K.L. 1975. Spectral analysis in ecology. Annual Review of Ecological Systems 6: 189-210.

Plotnick, R.E., Gardner, R.H. and O'Neill, R.V. 1993. Lacunarity indices as measures of landscape texture. Landscape Ecology 8: 201-211.

Qi, Y. and Wu, J. 1996. Effects of changing spatial resolution on the results of landscape pattern analysis using spatial autocorrelation indices. Landscape Ecology 11: 39–49.

Quattrochi, D.A., Lam, N.S-N., Qiu, H-L. and Zhao, W. 1997. A geographic information system for the characterization and modeling of multiscale remote sensing data. In: Quattrochi, D.A. and Goodchild, M.F. (eds) Scale in Remote Sensing and GIS. Lewis Publishers, pp. 295-308.

Rees, W.G. 1992. Measurement of the fractal dimension of ice-sheet surfaces using Landsat data. International Journal of Remote Sensing 13: 663-676.

Reza, A.M. 1999. Wavelet Characteristics: What Wavelet Should I Use? [Online] Available at http://www.xilinx-china.com/products/logicore/dsp/wavlet_char.pdf (accessed 19 October, 2003).

Ripley, B.D. 1978. Spectral analysis and the analysis of pattern in plant communities. Journal of Ecology 66: 965-981.

Robertson, G.P. and Gross, K.L. 1994. Assessing the heterogeneity of belowground resources: quantifying pattern and scale. In: Caldwell, M.M. and Pearcy, R.W. (eds) Exploitation of Environmental Heterogeneity by Plants: Ecophysiological Processes Above- and Belowground. Academic Press, San Diego, U.S.A., pp. 237-253.

Saunders, S.C., Chen, J., Crow, T.R. and Brosofske, K.D. 1998. Hierarchical relationships between landscape structure and temperature in a managed forest landscape. Landscape Ecology 13: 381-395.

Schneider, D.C. 1994. Quantitative Ecology: Spatial and Temporal Scaling. Academic Press, San Diego, U.S.A.

Shen, W., Jenerette, G.D., Wu, J. and Gardner, R.H. 2004. Evaluating empirical scaling relations of pattern metrics with simulated landscapes. Ecography 27: 459-469.

Soil Research Institute 2001. Soil Map of Ghana. Soil Research Institute, Accra, Ghana.

Strahler, A.H., Woodcock, C.E. and Smith, J.A. 1986. On the nature of models in remote sensing. Remote Sensing Environment 20: 121-139.

Thornthwaite, C.W. and Mather, J.R. 1955. The water balance. Climatological Laboratory Publication #8. Drexel Institute of Technology, Philadelphia, U.S.A.

Townshend, J.R.G. and Justice, C.O. 1988. Selecting the spatial resolution of satellite sensors required for global monitoring of land transformations. International Journal of Remote Sensing 9: 187-236.

Townshend, J.R.G. and Justice, C.O. 1990. The spatial variation of vegetation changes at very coarse scales. International Journal of Remote Sensing. 11: 149-157.

Turner M.G., Gardner R.H. and O'Neill R.V. 2001. Landscape Ecology in Theory and Practice: Pattern and Process. Springer-Verlag, New York, New York, USA.

Turner, M.G., O'Neill R.V., Gardner R.H. and Milne B.T. 1989. Effects of changing spatial scale on the analysis of landscape pattern. Landscape Ecology 3: 153–162.

Turner, S.J., O'Neill, R.V., Conley, W., Conley, M.R. and Humphries, H.C. 1991. Pattern and scale: statistics for landscape ecology. In: Turner, M.G. and Gardner, R.H. (eds) Quantitative Methods in Landscape Ecology: the Analysis and Interpretation of Landscape Heterogeneity. Springer-Verlag, New York, U.S.A, pp. 17-49.

Urban, D.L., O'Neill, R.V. and Shugart, H.H. 1987. Landscape ecology. BioScience 37: 119-127

van Gardingen, P.R., Foody, G.M. and Curran, P.J. (eds) 1997. Scaling-Up: From Cell to Landscape. Cambridge University Press, Cambridge, U.S.A.

Vidakovic, B. 1999. Statistical Modeling by Wavelets. John Wiley & Sons, New York, U.S.A.

Vidakovic, B. and Mueller, P. 1994. "Wavelets for kids, a tutorial introduction." Discussion Paper (Institute of Statistics and Decision Sciences, Duke University, Durham, U.S.A.). No. 95–21.

Werner, B.T. 1999. Complexity in natural landform patterns. *Science 28*4: 102-104.

Wessman, C.A. 1992. Spatial scales and global change: Bridging the gap from plots to GCM grid cells. Annual Review of Ecology and Systematics 23: 175-200.

Wickham, J.D. and Riitters, K.H. 1995. Sensitivity of landscape metrics to pixel size. International Journal of Remote Sensing 16: 3585–3595.

Wieczorek, U. 1992. Scale reduction and maximum information loss of different information categories. Photogrammetric Engineering and Remote Sensing 58(12): 1679-1684.

Wood, E.F. and Lakshmi, V. 1993. Scaling water and energy fluxes in climate systems: three land-atmospheric modeling experiments. Journal of Climate 6(5): 839-857.

Woodcock, C.E. and Strahler, A.H. 1987. The factor of scale in remote sensing. Remote Sensing of Environment 21: 311-332.

Wu, J. 1999. Hierarchy and scaling: extrapolating information along a scaling ladder. Canadian Journal of Remote Sensing 25: 367-380.

Wu, J. 2004. Effects of changing scales on landscape pattern analysis: scaling relations. Landscape Ecology 19: 125-138

Wu, J. and Loucks, O.L. (1995). From balance-of-nature to hierarchical patch dynamics: A paradigm shift in ecology. Quarter Review of Biology 70: 439-466.

Wu, J., Jelinski, D.E., Luck, M. and Tueller, P.T. 2000. Multiscale analysis of landscape heterogeneity: scale variance and pattern metrics. Geographic Information Sciences 6(1): 6-19.

Wu, J., Shen, W., Sun, W. and Tueller, P.T. 2002. Empirical patterns of the effects of changing scale on landscape metrics. Landscape Ecology 17: 761–782.

Xia, Z-G. and Clarke, K.C. 1997. Approaches to scaling of geo-spatial data. In: Quattrochi, D.A. and Goodchild, M.F. (eds) Scale in Remote Sensing and GIS. Lewis Publishers, pp. 309-360.

7 APPENDICES

Appendix I: On heteroscedasticity and proportional effect

Table 7.1 contains the mean and standard deviation of the pixel values in each of the 228 local windows of NDVI84 and NDVI99, as well as those of the 144 local windows of DEM used in the analysis of heteroscedasticity and proportional effect. Also contained in the table are the *x* and *y* coordinates of each statistic.

Table 7.1 Moving window statistics of NDVI84, NDVI99 and DEM together with their *x*- and *y*-coordinates

x	*y*	Moving window statistics					
		NDVI84		NDVI99		DEM	
		Mean	Standard deviation	Mean	Standard deviation	Mean	Standard deviation
1	1	-0.2434	0.0154	-0.1645	0.1274	128	13
1	2	-0.2487	0.0156	-0.1929	0.1238	141	16
1	3	-0.2541	0.0120	-0.1889	0.1112	161	14
1	4	-0.2532	0.0155	-0.1897	0.1446	153	13
1	5	-0.2550	0.0142	-0.1748	0.1418	177	15
1	6	-0.2517	0.0109	-0.1967	0.1046	163	17
1	7	-0.2493	0.0089	-0.1866	0.0997	138	11
1	8	-0.2493	0.0099	-0.2127	0.0745	142	14
1	9	-0.2503	0.0087	-0.2016	0.0703	134	10
1	10	-0.2526	0.0087	-0.2323	0.0681	144	15
1	11	-0.2462	0.0079	-0.2488	0.0552	175	21
1	12	-0.2499	0.0081	-0.2548	0.0656	207	17
2	1	-0.2500	0.0082	-0.2069	0.0587	108	10
2	2	-0.2485	0.0075	-0.2204	0.0608	120	11
2	3	-0.2493	0.0114	-0.2045	0.0972	139	14
2	4	-0.2511	0.0123	-0.1955	0.1143	155	16
2	5	-0.2513	0.0095	-0.1994	0.0718	151	11
2	6	-0.2514	0.0076	-0.2211	0.0626	167	13
2	7	-0.2506	0.0076	-0.2104	0.0585	140	13
2	8	-0.2464	0.0085	-0.2034	0.0516	123	11
2	9	-0.2493	0.0080	-0.2184	0.0694	122	9
2	10	-0.2452	0.0066	-0.2004	0.0468	142	12
2	11	-0.2445	0.0104	-0.2428	0.0689	157	13
2	12	-0.2479	0.0092	-0.2511	0.0596	207	22
3	1	-0.2546	0.0088	-0.2254	0.0610	96	7
3	2	-0.2526	0.0069	-0.2452	0.0609	109	10
3	3	-0.2461	0.0060	-0.2107	0.0535	127	12
3	4	-0.2480	0.0078	-0.2302	0.0624	147	11
3	5	-0.2510	0.0067	-0.2036	0.0605	138	11

Table 7.1 (Continued)

x	*y*	NDVI84		NDVI99		DEM	
		Mean	Standard deviation	Mean	Standard deviation	Mean	Standard deviation
3	6	-0.2456	0.0071	-0.1882	0.0490	144	12
3	7	-0.2456	0.0073	-0.2107	0.0698	140	10
3	8	-0.2480	0.0091	-0.2161	0.0824	118	10
3	9	-0.2476	0.0094	-0.1936	0.0858	114	8
3	10	-0.2486	0.0073	-0.2376	0.0567	130	10
3	11	-0.2448	0.0080	-0.2357	0.0622	152	13
3	12	-0.2495	0.0088	-0.2432	0.0647	180	12
4	1	-0.2511	0.0079	-0.2130	0.0684	96	8
4	2	-0.2492	0.0078	-0.2332	0.0808	109	11
4	3	-0.2486	0.0072	-0.2223	0.0678	128	15
4	4	-0.2380	0.0198	-0.1122	0.2168	129	13
4	5	-0.2500	0.0077	-0.2033	0.0650	138	11
4	6	-0.2477	0.0094	-0.1935	0.0760	124	12
4	7	-0.2460	0.0081	-0.1974	0.0585	128	10
4	8	-0.2461	0.0115	-0.1875	0.0776	112	11
4	9	-0.2528	0.0089	-0.2094	0.0584	116	8
4	10	-0.2534	0.0096	-0.2255	0.0723	139	10
4	11	-0.2521	0.0085	-0.2328	0.0636	172	16
4	12	-0.2522	0.0076	-0.2716	0.0590	171	14
5	1	-0.2516	0.0066	-0.2254	0.0614	112	12
5	2	-0.2507	0.0088	-0.2085	0.0699	100	12
5	3	-0.2518	0.0094	-0.1955	0.0738	102	12
5	4	-0.2495	0.0095	-0.1736	0.1376	110	12
5	5	-0.2515	0.0077	-0.1858	0.0908	133	11
5	6	-0.2514	0.0072	-0.2142	0.0566	137	12
5	7	-0.2496	0.0089	-0.1920	0.0728	115	11
5	8	-0.2556	0.0108	-0.2076	0.0781	107	10
5	9	-0.2568	0.0100	-0.2281	0.0620	120	13
5	10	-0.2515	0.0093	-0.2161	0.0682	138	11
5	11	-0.2504	0.0082	-0.2356	0.0707	170	17
5	12	-0.2479	0.0074	-0.2530	0.0647	173	13
6	1	-0.2478	0.0074	-0.2387	0.0654	115	8
6	2	-0.2515	0.0090	-0.1937	0.0730	101	9
6	3	-0.2529	0.0089	-0.1795	0.0645	99	19
6	4	-0.2524	0.0084	-0.2008	0.0731	128	14
6	5	-0.2470	0.0092	-0.2150	0.0662	136	13
6	6	-0.2488	0.0090	-0.2022	0.0713	143	11
6	7	-0.2515	0.0099	-0.2068	0.0741	113	13
6	8	-0.2596	0.0124	-0.2299	0.0962	107	11
6	9	-0.2531	0.0098	-0.2381	0.0595	128	12
6	10	-0.2508	0.0102	-0.2696	0.0560	139	11
6	11	-0.2551	0.0091	-0.2921	0.0599	168	14
6	12	-0.2554	0.0077	-0.3167	0.0520	173	15

Table 7.1 (Continued)

x	*y*	NDVI84		NDVI99		DEM	
		Mean	Standard deviation	Mean	Standard deviation	Mean	Standard deviation
7	1	-0.2459	0.0065	-0.2278	0.0493	116	7
7	2	-0.2521	0.0094	-0.2516	0.0693	95	12
7	3	-0.2502	0.0102	-0.1971	0.0783	107	11
7	4	-0.2567	0.0090	-0.2267	0.0633	128	15
7	5	-0.2505	0.0090	-0.2061	0.0689	147	10
7	6	-0.2557	0.0099	-0.2311	0.0686	127	12
7	7	-0.2609	0.0114	-0.2434	0.0857	102	12
7	8	-0.2536	0.0206	-0.1705	0.1542	115	14
7	9	-0.2611	0.0129	-0.2652	0.0974	115	9
7	10	-0.2545	0.0121	-0.2664	0.0862	134	10
7	11	-0.2555	0.0099	-0.2881	0.0722	169	15
7	12	-0.2575	0.0083	-0.3271	0.0528	165	16
8	1	-0.2500	0.0078	-0.2434	0.0542	114	5
8	2	-0.2458	0.0074	-0.2170	0.0540	107	14
8	3	-0.2452	0.0072	-0.2018	0.0667	97	10
8	4	-0.2563	0.0095	-0.2397	0.0754	106	15
8	5	-0.2617	0.0111	-0.2246	0.0796	139	12
8	6	-0.2606	0.0119	-0.2633	0.0920	117	13
8	7	-0.2612	0.0117	-0.2731	0.0900	98	11
8	8	-0.2616	0.0175	-0.2509	0.1512	123	15
8	9	-0.2636	0.0112	-0.2585	0.1045	132	13
8	10	-0.2667	0.0104	-0.2771	0.0898	149	14
8	11	-0.2583	0.0117	-0.2896	0.0723	157	14
8	12	-0.2597	0.0096	-0.2979	0.0628	136	10
9	1	-0.2507	0.0065	-0.2523	0.0496	105	8
9	2	-0.2465	0.0082	-0.2539	0.0552	108	13
9	3	-0.2441	0.0083	-0.2356	0.0573	102	14
9	4	-0.2510	0.0113	-0.2488	0.0642	87	7
9	5	-0.2565	0.0088	-0.2526	0.0608	130	16
9	6	-0.2597	0.0105	-0.2866	0.0751	109	12
9	7	-0.2627	0.0109	-0.2982	0.0742	107	19
9	8	-0.2661	0.0099	-0.3111	0.0740	128	11
9	9	-0.2661	0.0092	-0.3139	0.0750	140	12
9	10	-0.2673	0.0099	-0.3034	0.0702	144	10
9	11	-0.2700	0.0102	-0.3175	0.0765	150	13
9	12	-0.2635	0.0121	-0.3436	0.0653	140	15
10	1	-0.2503	0.0061	-0.2683	0.0406	89	11
10	2	-0.2451	0.0060	-0.2599	0.0460	95	15
10	3	-0.2487	0.0065	-0.2864	0.0526	100	17
10	4	-0.2485	0.0074	-0.2728	0.0674	88	9
10	5	-0.2497	0.0089	-0.2741	0.0725	110	16
10	6	-0.2450	0.0074	-0.2686	0.0642	95	15
10	7	-0.2496	0.0088	-0.2623	0.0693	105	18

Table 7.1 (Continued)

x	*y*	NDVI84		NDVI99		DEM	
		Mean	Standard deviation	Mean	Standard deviation	Mean	Standard deviation
10	8	-0.2568	0.0092	-0.3028	0.0683	115	12
10	9	-0.2606	0.0103	-0.3099	0.0693	126	12
10	10	-0.2633	0.0109	-0.3197	0.0736	133	13
10	11	-0.2664	0.0103	-0.3249	0.0616	127	12
10	12	-0.2616	0.0106	-0.3454	0.0600	140	16
11	1	-0.2464	0.0053	-0.2779	0.0434	98	8
11	2	-0.2441	0.0057	-0.2638	0.0508	92	10
11	3	-0.2466	0.0069	-0.2618	0.0605	123	36
11	4	-0.425	0.0069	-0.2430	0.0603	138	37
11	5	-0.2455	0.0071	-0.2665	0.0602	89	12
11	6	-0.2444	0.0064	-0.2455	0.0547	101	15
11	7	-0.2504	0.0070	-0.2938	0.0601	84	9
11	8	-0.2551	0.0077	-0.3031	0.0617	105	16
11	9	-0.2548	0.0086	-0.3192	0.0651	137	16
11	10	-0.2580	0.0087	-0.3219	0.0608	149	13
11	11	-0.2579	0.0076	-0.3315	0.0572	123	14
11	12	-0.2563	0.0075	-0.3214	0.0558	132	16
12	1	-0.2446	0.0066	-0.2662	0.0483	127	9
12	2	-0.2420	0.0060	-0.2599	0.0436	100	12
12	3	-0.2419	0.0061	-0.2436	0.0568	115	17
12	4	-0.2448	0.0071	-0.2684	0.0568	115	11
12	5	-0.2479	0.0079	-0.2763	0.0542	93	13
12	6	-0.2462	0.0061	-0.2434	0.0541	83	8
12	7	-0.2483	0.0065	-0.2454	0.0550	99	10
12	8	-0.2508	0.0068	-0.2980	0.0527	127	19
12	9	-0.2570	0.0094	-0.3522	0.0636	129	17
12	10	-0.2551	0.0090	-0.3594	0.0491	158	14
12	11	-0.2587	0.0087	-0.3622	0.0484	142	21
12	12	-0.2583	0.0094	-0.3552	0.0566	114	8
13	1	-0.2500	0.0158	-0.2071	0.1428	-	-
13	2	-0.2459	0.0106	-0.2562	0.0836	-	-
13	3	-0.2423	0.0063	-0.2581	0.0494	-	-
13	4	-0.2440	0.0055	-0.2393	0.0489	-	-
13	5	-0.2450	0.0074	-0.2582	0.0521	-	-
13	6	-0.2472	0.0052	-0.2562	0.0543	-	-
13	7	-0.2486	0.0047	-0.2547	0.0467	-	-
13	8	-0.2466	0.0060	-0.2969	0.0482	-	-
13	9	-0.2557	0.0100	-0.3702	0.0604	-	-
13	10	-0.2571	0.0090	-0.3698	0.0588	-	-
13	11	-0.2569	0.0083	-0.3752	0.0475	-	-
13	12	-0.2578	0.0098	-0.3453	0.0752	-	-
14	1	-0.2579	0.0072	-0.2770	0.0718	-	-
14	2	-0.2482	0.0170	-0.2181	0.1392	-	-

Table 7.1 (Continued)

x	*y*	NDVI84		NDVI99		DEM	
		Mean	Standard deviation	Mean	Standard deviation	Mean	Standard deviation
14	3	-0.2453	0.0090	-0.2659	0.0503	-	-
14	4	-0.2451	0.0086	-0.2728	0.0537	-	-
14	5	-0.2433	0.0075	-0.2794	0.0547	-	-
14	6	-0.2487	0.0051	-0.2761	0.0444	-	-
14	7	-0.2470	0.0053	-0.2639	0.0461	-	-
14	8	-0.2470	0.0057	-0.2882	0.0470	-	-
14	9	-0.2483	0.0081	-0.3587	0.0477	-	-
14	10	-0.2495	0.0086	-0.3635	0.0488	-	-
14	11	-0.2560	0.0073	-0.3664	0.0452	-	-
14	12	-0.2528	0.0101	-0.3140	0.0861	-	-
15	1	-0.2507	0.0088	-0.2711	0.0622	-	-
15	2	-0.2505	0.0134	-0.2186	0.1266	-	-
15	3	-0.2482	0.0144	-0.2271	0.1073	-	-
15	4	-0.2466	0.0067	-0.2724	0.0463	-	-
15	5	-0.2464	0.0073	-0.2893	0.0462	-	-
15	6	-0.2505	0.0066	-0.2881	0.0427	-	-
15	7	-0.2480	0.0066	-0.2593	0.0433	-	-
15	8	-0.2503	0.0079	-0.2817	0.0508	-	-
15	9	-0.2482	0.0072	-0.3463	0.0454	-	-
15	10	-0.2501	0.0086	-0.3395	0.0562	-	-
15	11	-0.2522	0.0088	-0.3420	0.0522	-	-
15	12	-0.2486	0.0088	-0.2934	0.0734	-	-
16	1	-0.2522	0.0076	-0.2563	0.0592	-	-
16	2	-0.2492	0.0182	-0.1905	0.1671	-	-
16	3	-0.2485	0.0145	-0.2506	0.1102	-	-
16	4	-0.2452	0.0058	-0.2735	0.0474	-	-
16	5	-0.2483	0.0073	-0.3143	0.0589	-	-
16	6	-0.2516	0.0065	-0.3111	0.0500	-	-
16	7	-0.2501	0.0074	-0.2949	0.0378	-	-
16	8	-0.2497	0.0078	-0.3049	0.0424	-	-
16	9	-0.2524	0.0081	-0.3238	0.0576	-	-
16	10	-0.2515	0.0095	-0.3278	0.0589	-	-
16	11	-0.2508	0.0084	-0.3142	0.0655	-	-
16	12	-0.2499	0.0080	-0.3310	0.0543	-	-
17	1	-0.2470	0.0140	-0.2112	0.1353	-	-
17	2	-0.2453	0.0131	-0.2237	0.1083	-	-
17	3	-0.2434	0.0071	-0.2943	0.0477	-	-
17	4	-0.2430	0.0056	-0.3173	0.0358	-	-
17	5	-0.2457	0.0068	-0.2988	0.0497	-	-
17	6	-0.2437	0.0061	-0.3166	0.0546	-	-
17	7	-0.2459	0.0068	-0.3199	0.0486	-	-
17	8	-0.2468	0.0074	-0.3173	0.0495	-	-
17	9	-0.2524	0.0073	-0.2994	0.0478	-	-

Table 7.1 (Continued)

x	*y*	NDVI84		NDVI99		DEM	
		Mean	Standard deviation	Mean	Standard deviation	Mean	Standard deviation
17	10	-0.2561	0.0076	-0.3514	0.0465	-	-
17	11	-0.2510	0.0084	-0.3181	0.0662	-	-
17	12	-0.2526	0.0064	-0.3484	0.0427	-	-
18	1	-0.2428	0.0167	-0.1819	0.1563	-	-
18	2	-0.2425	0.0140	-0.2085	0.1179	-	-
18	3	-0.2424	0.0072	-0.2618	0.0499	-	-
18	4	-0.2407	0.0059	-0.2749	0.0451	-	-
18	5	-0.2430	0.0077	-0.3135	0.0535	-	-
18	6	-0.2460	0.0069	-0.3394	0.0397	-	-
18	7	-0.2472	0.0073	-0.3266	0.0460	-	-
18	8	-0.2478	0.0066	-0.3150	0.0451	-	-
18	11	-0.2464	0.0097	-0.3266	0.0647	-	-
18	12	-0.2548	0.0079	-0.3676	0.0439	-	-
19	1	-0.2417	0.0052	-0.2436	0.0590	-	-
19	2	-0.2384	0.0192	-0.1424	0.2398	-	-
19	3	-0.2401	0.0076	-0.2469	0.0458	-	-
19	4	-0.2450	0.0085	-0.2568	0.0487	-	-
19	5	-0.2450	0.0079	-0.2612	0.0493	-	-
19	6	-0.2481	0.0075	-0.3349	0.0452	-	-
19	7	-0.2492	0.0080	-0.3155	0.0494	-	-
19	8	-0.2479	0.0096	-0.3302	0.0484	-	-
19	9	-0.2428	0.0085	-0.3147	0.0545	-	-
19	10	-0.2467	0.0085	-0.3610	0.0617	-	-
19	11	-0.2441	0.0086	-0.3298	0.0658	-	-
19	12	-0.2481	0.0076	-0.3539	0.0606	-	-

Appendix II: On scaling characteristics of NDVI and DEM data sets

The first four moments of the detail wavelet coefficients from seven levels of decomposition in the horizontal, vertical and diagonal directions which were used to analyze the scaling characteristics of the NDVI data sets and DEM are presented in Table 7.2. The logarithms of these four moments are also presented in Table 7.3. A "-" in the table indicates that the value is non available. This occurred when the estimate of a moment is $\leq 0,$ in which case the logarithm was not defined.

Table 7.2 The first four moments of wavelet coefficients at seven levels of decomposition in the horizontal, vertical and diagonal directions

Data	Resolution (m)	q^{th} order moment											
		Horizontal details				Vertical details				Diagonal details			
		1	2	3	4	1	2	3	4	1	2	3	4
NDVI84	30	-	-	-	-	-	-	-	-	-	-	-	-
	60	0.0000	0.0000	-0.8431	80.4664	0.0000	0.0000	0.0432	29.7705	0.0000	0.0000	-0.0372	92.266
	120	0.0000	0.0001	0.5394	33.5541	0.0000	0.0001	0.8265	44.0771	0.0000	0.0000	0.0796	18.907
	240	0.0001	0.0004	1.3662	35.5691	-0.0004	0.0005	0.6585	31.8551	0.0001	0.0002	1.1922	41.529
	480	0.0012	0.0017	1.0858	15.1061	-0.0004	0.0018	0.6741	16.1544	-0.0001	0.0009	0.2344	11.512
	960	0.0000	0.0063	1.0650	11.5842	-0.0044	0.0046	-0.3753	1.6785	0.0010	0.0027	0.4482	5.105
	1920	-0.0056	0.0174	-1.0602	5.9069	-0.0122	0.0161	0.0474	1.5382	0.0019	0.0082	-0.0664	0.711
	3840	-0.0425	0.0734	-0.8053	1.9594	-0.0415	0.0807	1.3583	6.3947	-0.0437	0.0268	-0.2201	-0.162
NDVI99	30	-	-	-	-	-	-	-	-	-	-	-	-
	60	0.0000	0.0010	-0.0399	9.2045	0.0000	0.0011	-0.0052	12.2797	0.0000	0.0005	0.0362	4.439
	120	0.0000	0.0055	0.2999	18.4721	-0.0001	0.0071	0.2228	26.4820	0.0001	0.0022	-0.0872	9.309
	240	0.0009	0.0295	1.0829	25.4590	-0.0024	0.0405	0.5128	30.8400	-0.0003	0.0144	0.1183	23.080
	480	-0.0026	0.1314	0.8433	13.9811	-0.0062	0.1533	0.8728	17.8816	-0.0034	0.0643	-0.0986	11.249
	960	0.0163	0.5217	1.1039	20.3756	-0.0043	0.4264	0.0257	2.3681	0.0177	0.2479	0.0282	5.782
	1920	0.0140	2.0587	-1.4624	12.9355	-0.0542	1.4433	-0.2372	1.0409	-0.0230	0.7361	0.8111	6.152
	3840	-0.6465	8.8370	-3.1858	14.3730	0.3840	5.9187	1.4200	3.9310	-0.2150	2.5122	-0.1906	0.224
DEM	90	-	-	-	-	-	-	-	-	-	-	-	-
	180	-0.042	4	-7.6908	146.727	0.03	5	5.0155	268.544	-0.0002	1.2	-0.2565	10.011
	360	0.070	8	1.8655	18.665	-0.09	9	-1.7624	41.662	0.0102	3.4	0.1817	4.704
	720	0.534	122	4.5465	48.760	-0.42	181	-1.0587	95.526	0.0121	13.1	0.0043	2.427
	1440	1.744	1551	1.2958	17.878	-1.43	2421	1.1301	43.453	-0.0315	235.5	-0.6217	5.403
	2880	6.079	13581	0.2169	1.857	-4.42	18149	-0.0841	3.811	0.9600	3442.0	0.7655	6.720
	5760	-6.503	93114	-0.0435	0.186	-12.20	130125	0.4712	3.543	-3.6649	25577.1	0.0282	0.395
	11520	-18.646	875407	-0.0043	-0.272	-135.28	1067996	-0.2130	0.477	-28.950	152692.7	0.5913	0.591

Table 7.3 Logarithm of the first four moments of wavelet coefficients at seven levels of decomposition in the horizontal, vertical and diagonal directions

Data	Resolution (m)	Logarithm of the q^{th} order moment											
		Horizontal details				Vertical details				Diagonal details			
		1	2	3	4	1	2	3	4	1	2	3	4
NDVI84	1.4771	-	-	-	-	-	-	-	-	-	-	-	-
	1.7782	-	-	-	1.9056	-	-	-1.3645	1.4738	-	-	-	1.9650
	2.0792	-	-4.0000	-0.2681	1.5258	-	-4.0000	-0.0828	1.6442	-	-	-1.0991	1.2766
	2.3802	-4.0000	-3.3979	0.1355	1.5511	-	-3.3010	-0.1814	1.5032	-4.0000	-3.6990	0.0764	1.6183
	2.6812	-2.9208	-2.7696	0.0358	1.1792	-	-2.7447	-0.1713	1.2083	-	-3.0458	-0.6300	1.0612
	2.9823	-	-2.2007	0.0273	1.0639	-	-2.3372	-	0.2249	-3.0000	-2.5686	-0.3485	0.7080
	3.2833	-	-1.7595	-	0.7714	-	-1.7932	-1.3242	0.1870	-2.7212	-2.0862	-	-0.1484
	3.5843	-	-1.1343	-	0.2921	-	-1.0931	0.1330	0.8058	-	-1.5719	-	-
NDVI99	1.4771	-	-	-	-	-	-	-	-	-	-	-	-
	1.7782	-	-3.0000	-	0.9640	-	-2.9586	-	1.0892	-	-3.3010	-1.4413	0.6473
	2.0792	-	-2.2596	-0.5230	1.2665	-	-2.1487	-0.6521	1.4230	-4.0000	-2.6576	-	0.9689
	2.3802	-3.0458	-1.5302	0.0346	1.4058	-	-1.3925	-0.2901	1.4891	-	-1.8416	0.9270	1.3632
	2.6812	-	-0.8814	-0.0740	1.1455	-	-0.8145	-0.0591	1.2524	-	-1.1918	-	1.0511
	2.9823	-1.7878	-0.2826	0.0429	1.3091	-	-0.3702	-1.5901	0.3744	-1.7502	-0.6057	-1.5498	0.7621
	3.2833	-1.8539	0.3136	-	1.1118	-	0.1594	-	0.0174	-	-0.1331	-0.0909	0.7890
	3.5843	-	0.9463	-	1.1576	-0.4157	0.7722	0.1523	0.5945	-	0.4001	-	-0.6492
DEM	1.9542	-	-	-	-	-	-	-	-	-	-	-	-
	2.2553	-	0.5911	-	2.1665	-1.4802	0.7160	0.7003	2.4290	-	0.0792	-	1.0005
	2.5563	-1.1530	0.8808	0.2708	1.2710	-	0.9494	-	1.6197	-1.9914	0.5315	-0.7407	0.6725
	2.8573	-0.2728	2.0857	0.6577	1.6881	-	2.2574	-	1.9801	-1.9172	1.1173	-2.3665	0.3851
	3.1584	0.2415	3.1906	0.1125	1.2523	-	3.3841	0.0531	1.6380	-	2.3720	-	0.7326
	3.4594	0.7838	4.1329	-0.6637	0.2688	-	4.2588	-	0.5810	-0.0177	3.5368	-0.1161	0.8274
	3.7604	-	4.9690	-	-0.7310	-	5.1144	-0.3268	0.5494	-	4.4079	-1.5498	-0.4037
	4.0615	-	5.9422	-	-	-	6.0286	-	-0.3219	-	5.1838	-0.2282	-0.2282

Appendix III: On indirect multiscale analysis of pattern metrics

During the estimation of landscape metrics from maps with changing grain size, it was realized that the Grid Aggregate request in ArcView does not support the majority (mode) statistic. Therefore, the program below was written to invoke the majority statistic in the Map Calculator:

```
[Mygrid].BlockStats(#GRID_STATYPE_MAJORITY,
NbrHood.MakeRectangle(2,2,false),false)
```

It was also observed that ArcView's implementation of the majority statistic could not resolve ties. Thus, for example, if two classes appeared twice each within an $n \times n$ block, the result was NoData. To overcome this problem, a pyramid of grids was created by replacing the "2,2" in the Map Calculator expression by "3,3", "4,4", and so on. This resulted in a series of aggregated outputs with $n \times n$ neighborhood sizes. The results were then patched together in the Map Calculator with an extended version of the expression

```
[A2].IsNull.Con([A3].IsNull.Con([A4], [A3]), [A2])
```

in order to fix the NoData holes in the output data.

Estimates of the 18 landscape metrics from LULC84 maps with different grain sizes using the mean, median and mode aggregation methods are presented in Table 7.4; while those for LULC99 with the same three methods are summarized in Table 7.5. The estimates of the 18 landscape metrics of LULC84 maps with different extents clipped from each of the four corners are presented in Table 7.6; while those for LULC99 are presented in Table 7.7.

.

Table 7.4 Estimates of 18 landscape metrics of LULC84 maps with different grain sizes using the mean, median and mode aggregation methods

Grain size	Estimates of landscape metrics with different aggregation methods											
	Number of patches (*NP*)			Patch density (*PD*)			Largest patch index (*LPI*)			Landscape shape index (*LSI*)		
	Mean	Median	Mode	Mean	Median	Mode	Mean	Median	Mode	Mean	Median	Mode
1	319837	319837	319837	56.78	56.78	56.78	13.05	13.05	13.05	257	257	257
2	276287	90252	24247	49.05	16.02	4.30	7.07	15.58	15.12	247	141	162
3	138627	42377	23783	24.61	7.52	4.22	8.28	14.20	15.11	175	99	90
4	76499	24952	23631	13.60	4.44	4.19	7.87	15.33	14.79	136	77	74
5	48862	16625	17028	8.69	2.96	3.02	8.17	14.33	15.15	109	64	64
6	33456	12022	13474	5.94	2.13	2.39	7.76	15.41	15.30	93	54	58
7	24331	9245	11177	4.33	1.65	1.99	8.30	15.34	14.89	80	48	53
8	18384	7252	9702	3.29	1.29	1.73	8.19	15.68	14.58	71	43	50
9	14462	5907	8319	2.57	1.05	1.48	8.11	15.48	15.17	63	39	46
10	11297	4906	6934	2.01	0.87	1.23	7.99	15.64	15.70	57	35	44
15	5003	2422	3968	0.89	0.43	0.70	8.45	15.87	14.01	39	25	33
20	2811	1441	2550	0.50	0.26	0.45	6.49	16.61	15.06	30	19	27
25	1671	985	1763	0.30	0.18	0.31	7.27	17.39	15.68	23	16	22
30	1084	701	1351	0.19	0.13	0.24	13.71	22.78	15.79	19	14	20
35	759	524	1025	0.14	0.10	0.18	15.91	23.33	16.42	16	12	17
40	627	462	854	0.11	0.08	0.15	14.52	23.77	15.72	14	11	16
45	410	353	623	0.07	0.06	0.11	17.66	21.87	16.89	12	10	15
50	343	286	471	0.06	0.05	0.08	10.48	21.65	15.12	11	9	12

Table 7.4 (Continued)

Grain size	Estimates of landscape metrics with different aggregation methods											
	Total edge (*TE*)			Edge density (*ED*)			Mean patch area (*MPA*)			Patch area standard deviation (*PASD*)		
	Mean	Median	Mode	Mean	Median	Mode	Mean	Median	Mode	Mean	Median	Mode
1	76930860	76930860	76930860	136.57	136.57	136.57	2	2	2	200	200	200
2	73951260	42053700	28184640	131.28	74.65	39.38	2	6	23	114	438	819
3	52117920	29470860	24937590	92.52	52.32	38.94	4	13	24	176	607	827
4	40327320	22791000	21783000	71.71	40.53	38.61	7	22	24	219	803	823
5	32463150	18789300	18957750	57.70	33.40	33.64	12	34	33	303	980	990
6	27600300	16033140	17034840	49.00	28.46	30.24	17	47	42	326	1238	1121
7	23768010	14074410	15682170	42.30	25.05	27.84	23	61	50	396	1395	1205
8	21018960	12524640	14594400	37.37	22.27	25.95	31	78	58	455	1624	1288
9	18672660	11303010	13583970	33.20	20.10	24.15	39	95	68	508	1855	1407
10	16826400	10305000	12456000	29.91	18.32	22.14	50	115	81	572	2030	1532
15	11363400	7226550	9495000	20.23	12.87	16.82	112	232	142	947	3000	1949
20	8522400	5482800	7653600	15.27	9.83	13.49	199	387	222	1224	4144	2366
25	6661500	4494000	6378000	11.94	8.05	11.34	334	567	319	1866	5009	3029
30	5371200	3753000	5562900	9.61	6.71	9.86	516	797	418	3112	6766	3371
35	4441500	3243450	4796400	8.03	5.87	8.58	729	1055	546	4106	7838	4019
40	4014000	2976000	4360800	7.24	5.37	7.77	884	1200	658	4392	8481	4147
45	3291300	2542050	3819635	5.95	4.59	6.46	1350	1568	785	6638	9419	4571
50	3003000	2299500	3472432	5.38	4.12	5.92	1627	1951	914	6026	10712	5523

Table 7.4 (Continued)

Grain size	Estimates of landscape metrics with different aggregation methods											
	Patch area coefficient of variation (*PACV*)			Area-weighted mean shape index (*AWMSI*)			Area-weighted mean fractal dimension index (*AWMFDI*)			Mean shape index (*MSI*)		
	Mean	Median	Mode	Mean	Median	Mode	Mean	Median	Mode	Mean	Median	Mode
1	11337	11337	11337	33.49	33.49	33.49	1.302	1.302	1.302	1.109	1.109	1.109
2	5596	7013	3526	10.53	22.68	12.89	1.178	1.262	1.222	1.074	1.112	1.137
3	4327	4564	3490	8.48	16.19	12.67	1.158	1.236	1.220	1.066	1.117	1.129
4	2977	3564	3447	6.50	12.99	12.37	1.141	1.219	1.218	1.079	1.121	1.119
5	2631	2895	2992	6.08	10.79	11.35	1.135	1.203	1.206	1.082	1.125	1.120
6	1937	2642	2682	4.81	10.22	10.46	1.124	1.197	1.198	1.091	1.125	1.113
7	1714	2295	2391	4.51	9.02	9.35	1.119	1.187	1.187	1.096	1.126	1.114
8	1486	2094	2222	4.26	8.40	8.72	1.117	1.181	1.180	1.101	1.126	1.109
9	1307	1949	2081	3.89	8.05	8.19	1.113	1.177	1.173	1.103	1.125	1.108
10	1149	1770	1888	3.74	7.30	7.59	1.111	1.168	1.168	1.111	1.124	1.106
15	843	1293	1370	3.41	5.65	5.71	1.104	1.149	1.143	1.116	1.126	1.097
20	617	1070	1064	3.00	4.91	4.55	1.097	1.137	1.126	1.117	1.119	1.094
25	559	884	949	3.06	4.11	4.32	1.099	1.123	1.118	1.127	1.118	1.092
30	604	849	807	3.31	4.19	3.81	1.103	1.121	1.111	1.132	1.111	1.085
35	564	743	737	3.25	3.82	3.51	1.100	1.114	1.103	1.131	1.116	1.086
40	497	707	631	2.93	3.56	3.11	1.093	1.107	1.093	1.133	1.099	1.080
45	492	601	527	3.17	3.02	2.72	1.100	1.096	1.092	1.151	1.102	1.083
50	371	549	426	2.61	2.82	2.34	1.089	1.093	1.094	1.154	1.109	1.091

Table 7.4 (Continued)

Grain size	Estimates of landscape metrics with different aggregation methods											
	Total area (*TA*)			Mean fractal dimension index (*MFDI*)			Contagion (*CONTAG*)			Patch richness (*PR*)		
	Mean	Median	Mode	Mean	Median	Mode	Mean	Median	Mode	Mean	Median	Mode
1	563323	563323	563323	1.0221	1.0221	1.0221	40.36	40.36	40.36	6.000	6.000	6.000
2	563323	563323	563323	1.0157	1.0193	1.0179	19.48	39.13	46.81	6.000	6.000	6.000
3	563323	563323	563323	1.0140	1.0183	1.0212	20.58	38.20	42.41	6.000	6.000	6.000
4	562401	562401	564245	1.0148	1.0176	1.0168	19.56	37.71	38.71	6.000	6.000	6.000
5	562599	562599	563504	1.0148	1.0175	1.0167	20.33	37.24	37.43	6.000	6.000	6.000
6	563323	563323	563323	1.0153	1.0171	1.0159	20.21	36.85	36.26	6.000	6.000	6.000
7	561958	561958	563223	1.0157	1.0168	1.0156	20.74	36.44	35.15	6.000	6.000	6.000
8	562401	562401	562401	1.0158	1.0166	1.0145	20.79	36.21	34.17	6.000	6.000	6.000
9	562482	562482	562482	1.0156	1.0162	1.0142	21.23	36.01	33.44	6.000	6.000	6.000
10	562599	562599	562599	1.0164	1.0162	1.0139	21.38	35.81	33.16	6.000	6.000	6.000
15	561695	561695	564408	1.0156	1.0153	1.0124	22.46	35.09	30.85	6.000	6.000	6.000
20	558000	558000	567216	1.0151	1.0141	1.0117	23.34	34.82	29.65	6.000	6.000	6.000
25	558000	558000	562500	1.0151	1.0140	1.0113	24.64	34.91	28.86	6.000	6.000	6.000
30	558981	558981	564408	1.0150	1.0129	1.0101	25.76	34.83	28.18	6.000	6.000	6.000
35	553014	553014	559298	1.0147	1.0130	1.0102	27.06	34.41	27.91	6.000	6.000	6.000
40	554400	554400	561600	1.0147	1.0116	1.0096	26.69	34.11	27.04	6.000	6.000	6.000
45	553311	553311	565886	1.0162	1.0117	1.0093	29.00	34.49	29.28	6.000	6.000	6.000
50	558000	558000	558000	1.0155	1.0119	1.0085	29.30	34.45	30.25	6.000	6.000	6.000

Table 7.4 (Continued)

Grain size	Estimates of landscape metrics with different aggregation methods					
	Patch richness density (*PRD*)			Shannon's diversity index (*SHDI*)		
	Mean	Median	Mode	Mean	Median	Mode
1	0.0011	0.0011	0.0011	1.4369	1.4369	1.4369
2	0.0011	0.0011	0.0011	1.7494	1.4304	1.4260
3	0.0011	0.0011	0.0011	1.6959	1.4339	1.4261
4	0.0011	0.0011	0.0011	1.7144	1.4325	1.4258
5	0.0011	0.0011	0.0011	1.6965	1.4326	1.4264
6	0.0011	0.0011	0.0011	1.6959	1.4331	1.4256
7	0.0011	0.0011	0.0011	1.6836	1.4326	1.4260
8	0.0011	0.0011	0.0011	1.6817	1.4324	1.4260
9	0.0011	0.0011	0.0011	1.6725	1.4312	1.4257
10	0.0011	0.0011	0.0011	1.6701	1.4321	1.4253
15	0.0011	0.0011	0.0011	1.6424	1.4289	1.4290
20	0.0011	0.0011	0.0011	1.6201	1.4282	1.4283
25	0.0011	0.0011	0.0011	1.5984	1.4177	1.4262
30	0.0011	0.0011	0.0011	1.5780	1.4171	1.4258
35	0.0011	0.0011	0.0011	1.5582	1.4186	1.4269
40	0.0011	0.0011	0.0011	1.5582	1.4109	1.4302
45	0.0011	0.0011	0.0011	1.5295	1.4111	1.4261
50	0.0011	0.0011	0.0011	1.5203	1.4131	1.4313

Table 7.5 Estimates of 18 landscape metrics of LULC99 maps with different grain sizes using the mean, median and mode aggregation methods

Grain size	Estimates of landscape metrics with different aggregation methods											
	Number of patches (*NP*)			Patch density (*PD*)			Largest patch index (*LPI*)			Landscape shape index (*LSI*)		
	Mean	Median	Mode	Mean	Median	Mode	Mean	Median	Mode	Mean	Median	Mode
1	374752	374752	374752	66.53	66.53	66.53	25.91	25.91	25.91	272	272	272
2	222319	98614	26813	39.47	17.51	4.76	14.09	30.75	29.49	219	142	77
3	97427	46681	26271	17.30	8.29	4.66	17.57	29.48	29.36	149	102	76
4	53902	28124	26124	9.58	5.00	4.63	14.22	28.43	29.19	116	79	75
5	33462	19020	18635	5.95	3.38	3.31	14.43	30.34	31.57	92	66	65
6	22726	13979	14691	4.03	2.48	2.61	15.36	31.09	31.47	78	56	59
7	16197	10559	12117	2.88	1.88	2.15	17.03	28.74	31.36	67	49	54
8	12339	8529	10485	2.19	1.52	1.86	13.76	31.80	30.37	59	44	50
9	9336	6962	9030	1.66	1.24	1.61	12.09	29.49	31.53	52	40	47
10	7427	5770	7806	1.32	1.03	1.39	16.53	30.67	31.50	47	37	43
15	3180	2931	4282	0.56	0.52	0.76	17.31	32.20	31.37	32	26	33
20	1715	1737	2796	0.31	0.31	0.49	21.00	33.04	30.62	24	20	27
25	1058	1133	1944	0.19	0.20	0.35	24.38	32.62	31.55	19	16	22
30	698	845	1480	0.13	0.15	0.26	27.97	34.08	32.15	16	14	20
35	474	598	1089	0.09	0.11	0.20	29.55	34.15	31.97	13	12	17
40	357	462	874	0.06	0.08	0.16	28.36	34.39	30.62	11	10	15
45	297	379	682	0.05	0.07	0.11	27.04	34.25	29.24	10	10	14
50	217	310	546	0.04	0.06	0.10	31.90	35.20	29.89	9	9	12

Table 7.5 (Continued)

Grain size	Estimates of landscape metrics with different aggregation methods											
	Total edge (*TE*)			Edge density (*ED*)			Mean patch area (*MPA*)			Patch area standard deviation (*PASD*)		
	Mean	Median	Mode	Mean	Median	Mode	Mean	Median	Mode	Mean	Median	Mode
1	81224070	81224070	81224070	144.19	144.19	144.19	2	2	2	257	257	257
2	65298840	42334980	22784460	115.92	75.15	40.45	3	6	21	213	596	1101
3	44439930	30168900	22561920	78.89	53.56	40.05	6	12	21	360	826	1108
4	34331040	23367960	22341120	61.04	41.55	39.60	10	20	22	424	1040	1109
5	27354000	19393500	19284900	48.62	34.47	34.22	17	30	30	552	1336	1397
6	23181300	16625340	17316360	41.15	29.51	30.74	25	40	38	695	1596	1566
7	19671330	14490000	15854580	35.01	25.79	28.15	35	53	47	883	1723	1722
8	17403840	12994080	14712480	30.95	23.11	26.16	46	66	54	908	2087	1797
9	15335460	11761200	13706010	27.26	20.91	24.37	60	81	62	949	2180	1995
10	13857900	10744800	12727800	24.63	19.10	22.62	76	98	72	1338	2478	2137
15	9263250	7570350	9517500	16.49	13.48	16.86	177	192	132	2404	3617	2824
20	6834000	5711400	7765200	12.25	10.24	13.69	325	321	203	3819	4836	3455
25	5355000	4581000	6392250	9.60	8.21	11.36	527	493	289	5203	5982	4280
30	4401000	3881700	5561100	7.87	6.94	9.85	801	662	381	7090	7167	4976
35	3631950	3255000	4704000	6.57	5.89	8.41	1167	925	514	8784	8334	5648
40	3112800	2817600	4246800	5.62	5.08	7.56	1553	1200	643	10066	9640	6101
45	2781000	2542050	4045280	5.03	4.59	6.44	1863	1460	722	10458	10991	6603
50	2451000	2247000	3769499	4.39	4.03	5.30	2571	1800	798	13839	12273	7228

Table 7.5 (Continued)

Grain size	Estimates of landscape metrics with different aggregation methods											
	Patch area coefficient of variation (*PACV*)			Area-weighted mean shape index (*AWMSI*)			Area-weighted mean fractal dimension index (*AWMFDI*)			Mean shape index (*MSI*)		
	Mean	Median	Mode	Mean	Median	Mode	Mean	Median	Mode	Mean	Median	Mode
1	17119	17119	17119	36.16	36.16	36.16	1.300	1.300	1.300	1.104	1.104	1.1041
2	8386	10430	5243	14.53	23.22	14.29	1.200	1.250	1.223	1.085	1.118	1.1348
3	6222	6841	5169	11.34	17.26	14.02	1.180	1.232	1.221	1.096	1.117	1.1280
4	4065	5202	5134	8.60	12.90	13.80	1.170	1.209	1.219	1.110	1.121	1.1145
5	3285	4516	4619	7.92	11.85	13.04	1.160	1.201	1.209	1.112	1.121	1.1155
6	2806	3961	4085	7.30	10.47	11.80	1.160	1.191	1.199	1.122	1.120	1.1112
7	2544	3238	3706	7.25	8.80	11.04	1.160	1.180	1.191	1.121	1.119	1.1087
8	1992	3165	3350	6.36	8.76	9.74	1.150	1.177	1.182	1.125	1.117	1.1040
9	1575	2699	3203	5.88	7.70	9.55	1.150	1.170	1.178	1.130	1.115	1.0998
10	1767	2541	2965	6.66	7.29	8.79	1.154	1.164	1.170	1.133	1.120	1.0969
15	1361	1887	2142	6.46	5.56	6.42	1.147	1.143	1.144	1.140	1.112	1.0926
20	1174	1506	1703	6.38	4.83	5.52	1.148	1.135	1.132	1.140	1.100	1.0850
25	987	1215	1479	5.72	4.09	4.89	1.141	1.123	1.121	1.139	1.106	1.0802
30	885	1083	1305	5.52	3.64	4.44	1.141	1.113	1.113	1.150	1.099	1.0753
35	753	901	1100	4.99	3.19	3.68	1.135	1.104	1.101	1.162	1.105	1.0765
40	648	803	949	4.29	2.96	3.26	1.126	1.097	1.093	1.166	1.098	1.0789
45	561	753	873	3.70	3.00	2.98	1.115	1.098	1.090	1.161	1.097	1.0702
50	538	682	790	3.77	2.63	2.57	1.118	1.088	1.088	1.186	1.094	1.0675

Table 7.5 (Continued)

Grain size	Estimates of landscape metrics with different aggregation methods											
	Total area (*TA*)			Mean fractal dimension index (*MFDI*)			Contagion (*CONTAG*)			Patch richness (*PR*)		
	Mean	Median	Mode	Mean	Median	Mode	Mean	Median	Mode	Mean	Median	Mode
1	563323	563323	563323	1.0208	1.0208	1.0208	41.63	41.63	41.63	6.000	6.000	6.000
2	563323	563323	563323	1.0175	1.0201	1.0180	33.57	40.87	48.73	6.000	6.000	6.000
3	563323	563323	563323	1.0178	1.0185	1.0212	33.96	39.67	44.32	6.000	6.000	6.000
4	562401	562401	564245	1.0186	1.0180	1.0166	34.04	39.13	40.66	6.000	6.000	6.000
5	562599	562599	563504	1.0180	1.0173	1.0165	34.83	38.55	39.50	6.000	6.000	6.000
6	563323	563323	563323	1.0184	1.0168	1.0160	35.10	38.08	38.38	6.000	6.000	6.000
7	561958	561958	563223	1.0176	1.0165	1.0153	35.91	37.86	37.39	6.000	6.000	6.000
8	562401	562401	562401	1.0175	1.0159	1.0143	36.21	37.52	36.46	6.000	6.000	6.000
9	562482	562482	562482	1.0176	1.0154	1.0137	36.92	37.23	35.78	6.000	6.000	6.000
10	562599	562599	562599	1.0178	1.0157	1.0134	37.22	37.03	35.27	6.000	6.000	6.000
15	561695	561695	564408	1.0173	1.0142	1.0124	38.94	36.43	33.47	6.000	6.000	6.000
20	558000	558000	567216	1.0160	1.0127	1.0111	40.18	36.59	32.25	6.000	6.000	6.000
25	558000	558000	562500	1.0151	1.0125	1.0105	41.47	36.65	31.77	6.000	6.000	6.000
30	558981	558981	564408	1.0148	1.0117	1.0095	42.61	36.63	31.15	6.000	6.000	6.000
35	553014	553014	559298	1.0152	1.0121	1.0099	43.57	37.10	31.38	6.000	6.000	6.000
40	554400	554400	561600	1.0153	1.0113	1.0100	44.27	37.04	30.46	6.000	6.000	6.000
45	553311	553311	565886	1.0146	1.0108	1.0095	38.55	36.99	30.17	5.000	6.000	6.000
50	558000	558000	558000	1.0159	1.0107	1.0089	39.53	37.40	29.30	5.000	6.000	6.000

Table 7.5 (Continued)

Grain size	Estimates of landscape metrics with different aggregation methods					
	Patch richness density (*PRD*)			Shannon's diversity index (*SHDI*)		
	Mean	Median	Mode	Mean	Median	Mode
1	0.0011	0.0011	0.0011	1.3689	1.3689	1.3689
2	0.0011	0.0011	0.0011	1.4241	1.3643	1.3498
3	0.0011	0.0011	0.0011	1.4110	1.3711	1.3495
4	0.0011	0.0011	0.0011	1.4040	1.3696	1.3497
5	0.0011	0.0011	0.0011	1.3847	1.3707	1.3505
6	0.0011	0.0011	0.0011	1.3753	1.3713	1.3502
7	0.0011	0.0011	0.0011	1.3577	1.3707	1.3498
8	0.0011	0.0011	0.0011	1.3484	1.3700	1.3496
9	0.0011	0.0011	0.0011	1.3327	1.3711	1.3476
10	0.0011	0.0011	0.0011	1.3245	1.3707	1.3493
15	0.0011	0.0011	0.0011	1.2807	1.3650	1.3509
20	0.0011	0.0011	0.0011	1.2504	1.3580	1.3498
25	0.0011	0.0011	0.0011	1.2241	1.3549	1.3508
30	0.0011	0.0011	0.0011	1.1990	1.3481	1.3454
35	0.0011	0.0011	0.0011	1.1842	1.3431	1.3428
40	0.0011	0.0011	0.0011	1.1657	1.3423	1.3546
45	0.0009	0.0011	0.0011	1.1575	1.3423	1.3467
50	0.0009	0.0011	0.0011	1.1467	1.3379	1.3438

Table 7.6 Estimates of 18 landscape metrics of LULC84 maps with different extent clipped from each of the four corners

Area	Number of patches (*NP*)				Patch density (*PD*)				Largest patch index (*LPI*)			
(km^2)	SW-NE	SE-NW	NW-SE	NE-SW	SW-NE	SE-NW	NW-SE	NE-SW	SW-NE	SE-NW	NW-SE	NE-SW
56	3424	1603	4486	4913	61	29	80	87	52	35	23	7
225	13411	9096	17041	17067	60	40	76	76	16	17	7	9
507	31478	19771	30175	37769	62	39	60	75	9	14	29	7
902	54148	38356	50922	62971	60	43	57	70	19	19	34	12
1408	82294	68184	81309	88661	58	48	58	63	18	23	35	19
2028	121077	99423	116832	123005	60	49	58	61	15	25	29	21
2761	159972	141842	164041	165050	58	51	59	60	17	21	25	20
3605	197525	188252	216442	211428	55	52	60	59	17	16	20	17
5633	319837	319837	319837	319837	57	57	57	57	13	13	13	13

Table 7.6 (Continued)

Area	Landscape shape index (*LSI*)				Total edge (*TE*)				Edge density (*ED*)			
(km^2)	SW-NE	SE-NW	NW-SE	NE-SW	SW-NE	SE-NW	NW-SE	NE-SW	SW-NE	SE-NW	NW-SE	NE-SW
56	25	18	33	37	720930	521790	974070	1088250	128	93	173	193
225	52	44	65	66	3028650	2552250	3841050	3924120	134	113	170	174
507	80	62	80	99	7110450	5527140	7113390	8853540	140	109	140	175
902	105	86	103	125	12483390	10151520	12290100	14866260	139	113	136	165
1408	129	113	131	143	19143540	16855320	19589880	21310020	136	120	139	151
2028	157	136	159	165	28068180	24248730	28452660	29540700	138	120	140	145
2761	181	164	189	188	37774020	34293360	39479490	39329880	137	124	143	143
3605	198	191	217	212	47341680	45500370	51820950	50545290	131	126	144	140
5633	257	257	257	257	76930860	76930860	76930860	76930860	137	137	137	137

Table 7.6 (Continued)

Area	Mean Patch area (*MPA*)				Patch area standard deviation (*PASD*)				Patch area coeff of variation (*PACV*)			
(km^2)	SW-NE	SE-NW	NW-SE	NE-SW	SW-NE	SE-NW	NW-SE	NE-SW	SW-NE	SE-NW	NW-SE	NE-SW
56	1.6412	3.5097	1.2541	1.1451	51	63	21	11	3115	1781	1680	973
225	1.6807	2.4780	1.3227	1.3207	47	58	22	26	2767	2322	1672	1995
507	1.6103	2.5638	1.6798	1.3421	49	85	87	31	3012	3326	5199	2303
902	1.6651	2.3506	1.7706	1.4318	84	126	139	61	5038	5353	7846	4238
1408	1.7113	2.0655	1.732	1.5884	104	179	173	121	6100	8665	9960	7621
2028	1.6746	2.0393	1.7354	1.6483	107	208	178	162	6358	10188	10238	9826
2761	1.7256	1.9462	1.6828	1.6725	150	213	180	185	8678	10948	10679	11064
3605	1.8251	1.915	1.6656	1.7051	196	222	174	192	10742	11584	10421	11259
5633	1.7613	1.7613	1.7613	1.7613	200	200	200	200	11337	11337	11337	11337

Table 7.6 (Continued)

Area	Mean patch area (*MPA*)				Area-weighted mean shape index (*AWMSI*)				Area-weighted mean fractal dimension index (*AWMFDI*)			
(km^2)	SW-NE	SE-NW	NW-SE	NE-SW	SW-NE	SE-NW	NW-SE	NE-SW	SW-NE	SE-NW	NW-SE	NE-SW
56	5626	5626	5626	5626	11	9	7	5	1.252	1.259	1.2149	1.2047
225	22540	22540	22540	22540	10	11	8	9	1.2489	1.26	1.232	1.2386
507	50688	50688	50688	50688	11	15	14	10	1.2597	1.2828	1.2665	1.2429
902	90161	90161	90161	90161	17	21	21	15	1.2754	1.3009	1.2828	1.2623
1408	140831	140831	140831	140831	20	30	27	24	1.2848	1.3133	1.2886	1.286
2028	202753	202753	202753	202753	20	34	28	30	1.2848	1.3173	1.2931	1.2963
2761	276053	276053	276053	276053	28	36	31	33	1.3011	1.3184	1.2965	1.3002
3605	360497	360498	360498	360498	34	38	30	34	1.3105	1.3179	1.2951	1.3016
5633	563323	563323	563323	563323	34	34	34	34	1.3024	1.3024	1.3024	1.3024

Table 7.6 (Continued)

Area	Mean shape index (*MSI*)				Mean fractal dimension index (*MFDI*)				Contagion (*CONTAG*)			
(km^2)	SW-NE	SE-NW	NW-SE	NE-SW	SW-NE	SE-NW	NW-SE	NE-SW	SW-NE	SE-NW	NW-SE	NE-SW
56	1.1015	1.119	1.1202	1.1348	1.0212	1.0216	1.023	1.0248	50	67	36	38
225	1.1094	1.1184	1.1145	1.1241	1.0215	1.0222	1.0219	1.0237	44	63	38	39
507	1.1055	1.1065	1.1135	1.1276	1.0208	1.0209	1.0223	1.0242	45	61	42	40
902	1.1057	1.1008	1.1144	1.123	1.0211	1.0206	1.0227	1.0238	45	60	44	40
1408	1.1046	1.0987	1.1158	1.1189	1.021	1.0206	1.0231	1.0235	45	54	44	43
2028	1.1043	1.0981	1.1149	1.1168	1.021	1.0207	1.0229	1.0234	43	49	43	43
2761	1.1035	1.1008	1.1121	1.1135	1.0212	1.0212	1.0225	1.0229	41	45	42	42
3605	1.1041	1.1031	1.1118	1.1115	1.0215	1.0215	1.0224	1.0226	41	43	40	41
5633	1.1091	1.1091	1.1091	1.1091	1.0221	1.0221	1.0221	1.0221	40	40	40	40

Table 7.6 (Continued)

Area	Patch richness density (*PRD*)				Shannon's diversity index (*SHDI*)				Patch richness (*PR*)			
(km^2)	SW-NE	SE-NW	NW-SE	NE-SW	SW-NE	SE-NW	NW-SE	NE-SW	SW-NE	SE-NW	NW-SE	NE-SW
56	0.1066	0.1066	0.1066	0.1066	1.1744	0.7541	1.4394	1.3385	6	6	6	6
225	0.0266	0.0266	0.0266	0.0266	1.3182	0.8941	1.4165	1.3696	6	6	6	6
507	0.0118	0.0118	0.0118	0.0118	1.2861	0.8903	1.3635	1.3477	6	6	6	6
902	0.0067	0.0067	0.0067	0.0067	1.2728	0.9142	1.3215	1.3537	6	6	6	6
1408	0.0043	0.0043	0.0043	0.0043	1.281	1.0631	1.3261	1.3228	6	6	6	6
2028	0.003	0.003	0.003	0.003	1.3572	1.2088	1.3439	1.3267	6	6	6	6
2761	0.0022	0.0022	0.0022	0.0022	1.4197	1.3277	1.3777	1.3667	6	6	6	6
3605	0.0017	0.0017	0.0017	0.0017	1.4331	1.392	1.4221	1.4103	6	6	6	6
5633	0.0011	0.0011	0.0011	0.0011	1.4369	1.4369	1.4369	1.4369	6	6	6	6

Table 7.7 Estimates of 18 landscape metrics of LULC99 with different extents clipped from each of the four corners

Area (km^2)	Number of patches (*NP*)				Patch density (*PD*)				Largest patch index (*LPI*)			
	SW-NE	SE-NW	NW-SE	NE-SW	SW-NE	SE-NW	NW-SE	NE-SW	SW-NE	SE-NW	NW-SE	NE-SW
56	5118	2903	4578	4208	91	52	81	75	22	71	25	23
225	18329	17045	15968	15259	81	76	71	68	8	60	16	25
507	42660	37223	27514	33588	84	73	54	66	7	58	47	21
902	74288	71369	44430	57114	82	79	49	63	4	48	56	34
1408	106630	113215	70029	85542	76	80	50	61	6	34	56	40
2028	148470	153569	101889	122618	73	76	50	61	9	27	50	39
2761	193415	196303	151555	165792	70	71	55	60	22	20	47	36
3605	236647	242544	215503	221925	66	67	60	62	28	23	39	34
5633	374752	374752	374752	374752	67	67	67	67	30	30	30	30

Table 7.7 (Continued)

Area (km^2)	Landscape shape index (*LSI*)				Total edge (*TE*)				Edge density (*ED*)			
	SW-NE	SE-NW	NW-SE	NE-SW	SW-NE	SE-NW	NW-SE	NE-SW	SW-NE	SE-NW	NW-SE	NE-SW
56	34	21	31	34	997980	601680	905760	983100	177	107	161	175
225	66	57	57	58	3835440	3382320	3362700	3455700	170	150	149	153
507	99	82	66	85	8825400	7334220	5817030	7570890	174	145	115	149
902	132	118	80	109	15714420	14144490	9536070	12994860	174	157	106	144
1408	154	156	103	132	22990170	23235870	15317400	19644480	163	164	109	140
2028	179	180	129	158	32029050	32328540	23013000	28339470	158	159	114	140
2761	199	201	164	182	41574090	42083820	34260720	38024250	151	152	124	138
3605	215	220	202	209	51412650	52541160	48178200	49854600	143	148	134	138
5633	271	271	271	271	81224070	81224070	81224070	81224070	144	144	144	144

Table 7.7 (Continued)

Area (km^2)	Mean patch area (*MPA*)				Patch area standard deviation (*PASD*)				Patch area coeff of variation (*PACV*)			
	SW-NE	SE-NW	NW-SE	NE-SW	SW-NE	SE-NW	NW-SE	NE-SW	SW-NE	SE-NW	NW-SE	NE-SW
56	1.0993	1.938	1.2289	1.3370	20	74	27	25	1786	3820	2179	1682
225	1.2298	1.3224	1.4116	1.4772	22	104	35	52	1764	7897	2442	3539
507	1.1882	1.3617	1.8423	1.5091	26	151	146	82	2153	11124	7912	5454
902	1.2137	1.2633	2.0293	1.5786	24	164	240	138	2004	12961	11814	8741
1408	1.3207	1.2439	2.011	1.6463	43	145	297	195	3282	11688	14779	11855
2028	1.3656	1.3203	1.9899	1.6535	64	145	318	229	4670	10966	15989	13853
2761	1.4273	1.4063	1.8215	1.6651	146	165	333	251	10222	11755	18280	15042
3605	1.5234	1.4863	1.6728	1.6244	212	203	306	263	13903	13685	18307	16176
5633	1.5032	1.5032	1.5032	1.5032	257	257	257	257	17119	17119	17119	17119

Table 7.7 (Continued)

Area (km^2)	Total area (*TA*)				Area-weighted mean shape index (*AWMSI*)				Area-weighted mean fractal dimension index (*AWMFDI*)			
	SW-NE	SE-NW	NW-SE	NE-SW	SW-NE	SE-NW	NW-SE	NE-SW	SW-NE	SE-NW	NW-SE	NE-SW
56	5626	5626	5626	5626	7	11	7	8	1.2107	1.2607	1.2232	1.2313
225	22540	22540	22540	22540	6	25	8	11	1.2110	1.2988	1.2261	1.2501
507	50688	50688	50688	50688	8	31	15	16	1.2263	1.3088	1.2641	1.2717
902	90161	90161	90161	90161	8	36	24	27	1.2291	1.3049	1.289	1.2972
1408	140831	140831	140831	140831	10	32	30	33	1.2437	1.2962	1.2987	1.3056
2028	202753	202753	202753	202753	13	30	34	36	1.2545	1.2939	1.3030	1.3084
2761	276053	276053	276053	276053	22	31	40	36	1.2753	1.2986	1.3075	1.3060
3605	360498	360498	360498	360498	28	34	38	36	1.2890	1.3011	1.300	1.3026
5633	563323	563323	563323	563323	36	36	36	36	1.2972	1.2972	1.2972	1.2972

Table 7.7 (Continued)

Area (km^2)	Mean shape index (*MSI*)				Mean fractal dimension index (*MFDI*)				Contagion (*CONTAG*)			
	SW-NE	SE-NW	NW-SE	NE-SW	SW-NE	SE-NW	NW-SE	NE-SW	SW-NE	SE-NW	NW-SE	NE-SW
56	1.1115	1.0967	1.1073	1.1296	1.0222	1.0191	1.0215	1.0239	37	63	41	38
225	1.1240	1.0946	1.1108	1.1208	1.0236	1.0194	1.0216	1.0229	37	55	44	49
507	1.1153	1.0902	1.1074	1.1146	1.0222	1.0187	1.0215	1.0223	36	55	52	51
902	1.1154	1.0931	1.1052	1.1083	1.0218	1.0190	1.0215	1.0218	37	51	55	49
1408	1.1114	1.0959	1.1068	1.1080	1.0212	1.0194	1.0216	1.0216	38	45	55	51
2028	1.1084	1.0976	1.1070	1.1076	1.0209	1.0197	1.0214	1.0216	39	43	53	50
2761	1.1053	1.0992	1.1071	1.1074	1.0206	1.0199	1.0214	1.0215	41	42	50	47
3605	1.1049	1.1005	1.1074	1.1058	1.0207	1.0202	1.0213	1.0211	42	42	46	45
5633	1.1041	1.1041	1.1041	1.1041	1.0208	1.0208	1.0208	1.0208	42	42	42	42

Table 7.7 (Continued)

Area (km^2)	Patch richness density (*PRD*)				Shannon's diversity index (*SHDI*)				Patch richness (*PR*)			
	SW-NE	SE-NW	NW-SE	NE-SW	SW-NE	SE-NW	NW-SE	NE-SW	SW-NE	SE-NW	NW-SE	NE-SW
56	0.1066	0.0889	0.1066	0.0889	1.4057	0.7019	1.3235	1.2009	6	6	6	6
225	0.0266	0.0266	0.0266	0.0266	1.4284	0.9517	1.2695	1.1099	6	6	6	6
507	0.0118	0.0118	0.0118	0.0118	1.4465	0.9546	1.1261	1.0791	6	6	6	6
902	0.0067	0.0067	0.0067	0.0067	1.4310	1.0390	1.0536	1.1276	6	6	6	6
1408	0.0043	0.0043	0.0043	0.0043	1.4160	1.2010	1.0553	1.0867	6	6	6	6
2028	0.0030	0.0030	0.0030	0.0030	1.4002	1.2986	1.0856	1.1206	6	6	6	6
2761	0.0022	0.0022	0.0022	0.0022	1.3869	1.3462	1.1770	1.2247	6	6	6	6
3605	0.0017	0.0017	0.0017	0.0017	1.3613	1.3526	1.2615	1.2876	6	6	6	6
5633	0.0011	0.0011	0.0011	0.0011	1.3689	1.3689	1.3689	1.3689	6	6	6	6

ACKNOWLEDGEMENTS

I am very grateful to Professor Dr Paul L.G. Vlek of the Center for Development Research (ZEF), University of Bonn, Germany, and Professor Dr Benony K. Gordor of the University of Cape Coast (UCC), Ghana, for supervising this study. I thank them very much for their guidance and for finding time out of their busy schedules to read the draft of the thesis. Their comments and suggestions have helped to improve this final report.

Many thanks go to Professor Dr Soojin Park of the University of South Korea, Korea, who posed some of the challenges in this study. He was a member of my supervisory team until about half-way through the study when he was called to duty in his native country. I acknowledge, with gratitude, the contributions of Professor Dr Angela Kunoth of the Institute of Applied Mathematics, University of Bonn, Germany, who first introduced me to wavelet transforms which became one of the major tools in this research. I thank Dr. Ademola Braimoh for allowing me to use his data sets. I am thankful also to Dr. William Huber of ESRI Users' Forum (http://support.esri.com) who helped to write two short programs to solve Grid Aggregation Problems in ArcView. I am very grateful to Professor Dr van de Giesen and Drs Harald Kunstmann and Joseph Intsiful of the Glowa-Volta Project who read the initial draft and offered various pieces of advice. I also thank Ms Margaret Jend for translating the abstract into German.

I thank Professor Dr Frank K.A. Allotey of the Institute of Mathematical Sciences (IMS), Ghana, for his innovative idea of raising funds (both locally and abroad) to train and retained young mathematicians in Ghana, from which I am a beneficiary. I am particularly thankful to him for arranging collaboration between IMS, UCC and ZEF which pulled resources together to make this study come to fruition. To Professor Dr Nick van de Giesen, now of the Technical University of Delft, Netherlands, I say thank you to you for providing all the necessary tools and equipments for the study. To Dr Gunter Manske (coordinator, International Doctoral Studies Program for Development Research, ZEF) and his staff, Frau Sabine Aengenendt-Baer and her colleagues at the ZEFc secretariat, Mr. Ludger Hammer (Information Technology Center, ZEF) and his staff and Mr. Volker Merx (Librarian,

ZEF), I say many, many thanks to you all for the diverse ways you helped to make my study in Germany a success.

I thank the International Center for Theoretical Physics, Italy, for supporting the course work in Ghana and the Ghana government for granting me a three-year scholarship to conduct my research in Germany. I am grateful to Professor Dr Emmanuel Adow Obeng, Vice Chancellor, UCC, for granting me a three-year study leave and for all the provisions he made to ensure the success of the study. I thank Professors Vlek and van de Giesen for providing a three-month bridging stipend which made life a bit more bearable.

To Pastor Steve Gaultney, members of the Neighborhood Fellowship (Bonn-Nord) and the entire membership of the American Protestant Church with whom I worshipped during my stay in Bonn, I say thank you to you all for your prayers and fellowship. I acknowledge, with thanks, the helpful roles played by all friends in Bonn and elsewhere to make my study a success. I thank my parents for their love and support for all these years. Finally, I offer special thanks to my dear wife, Jane, for her love and support for me and also for taking good care of our beloved sons during my three-year stay in Germany. I thank my sons, Mawuli and Selasie Howard, for being good boys while I was away.

TO GOD BE THE GLORY, GREAT THINGS HE HATH DONE!